DAMPED FREE OSCILLATION OF MAGNETIZATION IN Ni-Fe THIN FILMS

Thesis by

Yoshitaka Suezawa

In Partial Fulfillment of the Requirements

For the Degree of

Doctor of Philosophy

California Institute of Technology

Pasadena, California

1976

(Submitted September 30, 1975)

D E D I C A T I O N

to

The late Mrs. Georgia L. Cassel

and

Mr. and Mrs. Floyd L. Humphrey

who

shared their lovely homes with me

in

Pasadena

and to

My Parents

who

sent me many encouragements

Acknowledgement

The author wishes to express his sincere gratitude for the kind and significant guidance received from Professor F. B. Humphrey throughout this research. He also wishes to express his many thanks to Professor C. H. Wilts for his help. Acknowledgement is also due to Professor R. V. Langmuir for valuable comments towards the accomplishment of this thesis. He wishes to thank O. G. Ramer for his friendly assistance in preparing the manuscript.

Financial support for this research was graciously received from the National Science Foundation of U.S.A. During the course of this research, the author gratefully received Graduate Research Assistantship, Graduate Teaching Assistantship and the Institute Scholarship.

ABSTRACT

Damped free oscillations of the magnetization have been clearly observed at the completion of 180° flux reversal along both the easy and the hard axis in Ni-Fe thin films. The flux component perpendicular to the applied pulse field was observed using a single turn pick-up loop around the film. The frequency of the oscillation was studied as a function of applied pulse field and compared with the results obtained by ferromagnetic resonance. The frequency of the damped free oscillation agreed quite well with that obtained by resonance when the frequency was measured after the oscillation had damped to small amplitude. The damping constant obtained from the decay of the oscillation agreed quite well with that obtained from the half-power linewidth of the resonance curve.

The Landau-Lifshitz equation proposed for the coherent rotation, using the value of the damping constant obtained by resonance, could describe the initial part of the magnetization reversal and the damped free oscillation in the films with low angular dispersion. Agreement between the experimental and the calculated transverse flux change for the entire waveform could not be obtained by using the value of damping constant obtained by resonance. The agreement was better at both higher applied field or lower anisotropy dispersion. The effect of eddy currents was negligible on the flux reversal but appeared as a slight increase of the damping constant obtained by resonance experiment.

TABLE OF CONTENTS

Chapter 1

INTRODUCTION

Magnetization reversal in ferromagnetic thin metallic films was extensively investigated in the mid 60's because of the prospective use of films as computer memory elements. Since then, the motivation for the application of the thin films for computer memory elements has faded away because of competition with other promising memory elements. The number of investigations of magnetization reversal has, therefore, considerably reduced. The main interest of the investigations that remain has shifted towards more fundamental and still unsolved problems.

One major unsolved problem involves the damping of the magnetization during a reversal. A possible way to investigate the damping is to analyze the reversal as a function of time. The analysis will be, however, formidably complicated unless the magnetization configuration is clearly known during the reversal. The fundamental simplicity of the coherent rotation provides this knowledge. A technical development in the observation of very high speed reversal signals offers a unique new opportunity to acquire a better understanding of the damping phenomena.

The Landau-Lifshitz dynamic equation has been widely recognized for its suitability in describing the coherent motion of magnetization in thin films. The occurrence of coherent magnetization reversal is, however, infrequent in actual films. Therefore, the description of magnetization reversal using the Landau-Lifshitz dynamic

equation has been always more or less qualitative. The applicability of the equation to the description of 180° flux reversals is carefully re-examined in Chapter 2. The departure of the actual magnetization reversal from the ideal coherent magnetization reversal was studied to understand the application of the equation to the 180° magnetization reversal. For this purpose, the effect of applied field, inhomogeneity of uniaxial anisotropy and eddy current loss on flux reversal waveforms was studied.

At the end of a 180° flux reversal, oscillation of the magnetization as it comes to the new equilibrium direction is predicted. This damped free oscillation has been observed and is discussed in Chapter 3. The direct comparison of the free oscillation with the resonance oscillation was possible. The comparison of the free oscillation frequency with the resonance frequency provided an insight into the role of magnetic fields of various origins during the reversal. A comparison was also made between the damping constant of the decay of free oscillation and that obtained from the half-power line width of the resonance curve. The comparison offered a unique method for better understanding of the damping associated with the motion of magnetization.

Chapter 2

COHERENT MAGNETIZATION REVERSAL

2.1 Introduction

2.1.1 Review of Dynamic Equations

To analyze magnetization reversal in ferromagnetic materials, it is desirable to describe the reversal by an equation whose parameters are simply related to measurable quantities and to the mechanism of reversal. Various dynamic equations have been proposed to analyze the motion of the magnetization and will be reviewed here in order to clarify their validity and applicability to the analyses of the reversal.

The measurable quantities for a typical flux reversal experiment are effects of total spins, but not separate effects of each spin. In the present experiment, a set of pick-up loops is used to detect the total flux change due to the motions of spins. When a dynamic equation is used, the interpretation of its solution is unavoidably ambiguous unless the configuration of the magnetization is known during the reversal. Even if a configuration is known, some complications may arise because of the mutual interactions of spins which generate effective internal fields, for example, a demagnetizing field due to divergence of magnetization and an exchange field, etc. These complications can be avoided, however, in two extreme cases. One is a case in which the interactions are strong enough to keep all the spins moving in unison, i.e., coherent rotation. In this case no effective field is

needed to be considered. The other is the case in which the mutual interactions are weak enough to be neglected.

An equation for the strong interaction case was proposed first by Landau and Lifshitz (1935). A similar equation was later proposed by Gilbert (1955). An equation for negligible interaction was proposed by Bloch for nuclear resonance theory (1946). Bloembergen (1950) found that Bloch's equation was applicable also for the strong interaction in a special case, i.e., ferromagnetic resonance. A generalized form of Landau-Lifshitz equation was proposed by Callen (1958). Some quantum mechanical considerations were given to relate this dynamic equation to reversal mechanisms. The effect of small fluctuations of spins was considered whereas their interactions are strong enough to be neglected in Landau-Lifshitz and Gilbert's equation.

The Landau-Lifshitz equation is given by

$$\frac{d\vec{M}}{dt} = -\gamma(\vec{M} \times \vec{H}) - \frac{\lambda}{M^2}\vec{M} \times (\vec{M} \times \vec{H}) \quad , \qquad (2\text{-}1)$$

where $\vec{M}$ is a magnetization vector, $\vec{H}$ is a magnetic field acting on $\vec{M}$, γ is the gyromagnetic ratio 1.76×10^7 [rad/sec-Oe] and λ is the adjustable scalar. Equation (2-1) is depicted in Fig. 2-1. The magnetization $\vec{M}$, the time derivative $\frac{dM}{dt}$, the first and second terms of Eq. (2-1) are vectorially shown in x, y, z coordinates as in Fig. 2-1a. The z-direction is chosen along the applied field $\vec{H}$. It can be seen from Fig. 2-1a that the vector $-\gamma(\vec{M} \times \vec{H}) \equiv \vec{T}_1$ is perpendicular to $\vec{M}$ and $\vec{H}$; and represents a component of the torque which causes a precession of $\vec{M}$ around $\vec{H}$. The vector $-(\lambda/M^2)\vec{M} \times (\vec{M} \times \vec{H}) \equiv \vec{T}_2$ is also perpendicular to $\vec{M}$ and is directed towards $\vec{H}$ in the plane determined by $\vec{M}$ and $\vec{H}$.

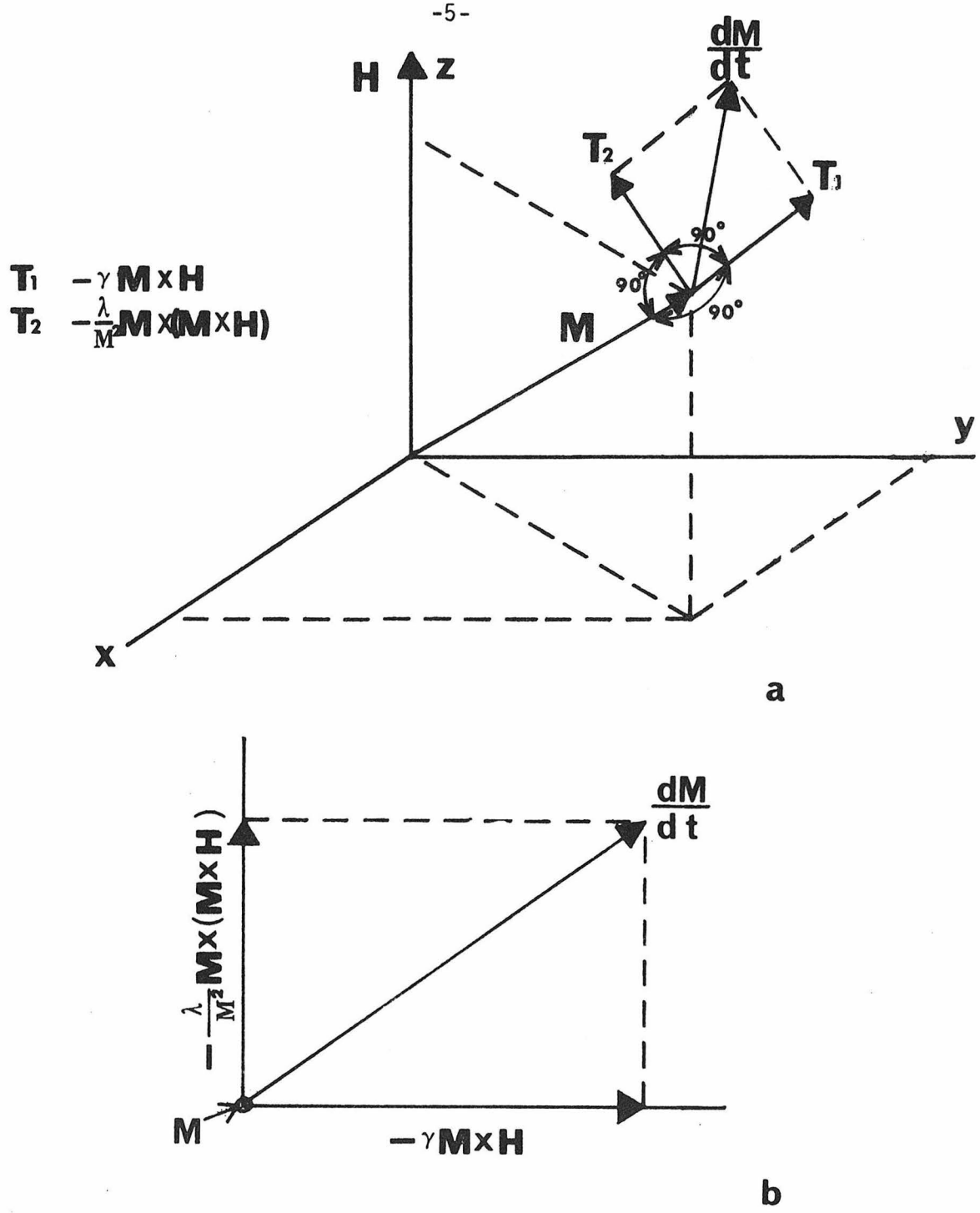

FIG.2-1 VECTORIAL REPRESENTATION
OF
LANDAU LIFSHITZ EQUATION

This vector represents a component of the torque which changes the direction of $\vec{M}$ towards $\vec{H}$. This directional change is called the relaxation of the magnetization. The second term was originally introduced to represent the damping which must cause the directional change of $\vec{M}$ towards its equilibrium direction along $\vec{H}$. This formulation is usually referred to as Landau-Lifshitz damping. The essential nature of Eq. (2-1) is shown in Fig. 2-1b, where a vector diagram of the equation is projected on a plane perpendicular to $\vec{M}$. The torques $\vec{T}_1$ and $\vec{T}_2$ are orthogonal and, therefore, are independent of each other. The independency causes an apparent difficulty as shown in Fig. 2-2, where the motions of the magnetizations are shown with λ as a parameter. From this figure, it can be seen that the relaxation of $\vec{M}$ speeds up as λ increases, while the precession keeps a constant angular frequency γH. Thus the reversal time decreases as λ increases.

Another formulation with, perhaps, more physical significance is the Gilbert equation. This equation is given by

$$\frac{d\vec{M}}{dt} = -\gamma(\vec{M} \times \vec{H}) + \frac{\alpha}{M}\vec{M} \times \frac{d\vec{M}}{dt} \quad , \qquad (2\text{-}2)$$

where α is an adjustable scalar. The first term of Eq. (2-2) is the same as in the Landau-Lifshitz equation. The major difference between the two formulations is in the introduction of the damping. In Eq. (2-2), the damping term (second term) represents a drag to the motion of magnetization. By rewriting Eq. (2-2) into the following form

$$\frac{d\vec{M}}{dt} = -\gamma\vec{M} \times [\vec{H} - \frac{\alpha}{M\gamma}\frac{d\vec{M}}{dt}] \quad , \qquad (2\text{-}3)$$

it is clear that $-\frac{\alpha}{M\gamma}\frac{d\vec{M}}{dt}$ represents an effective field opposite to the motion. The vectorial relationship between the terms in Eq. (2-2) is

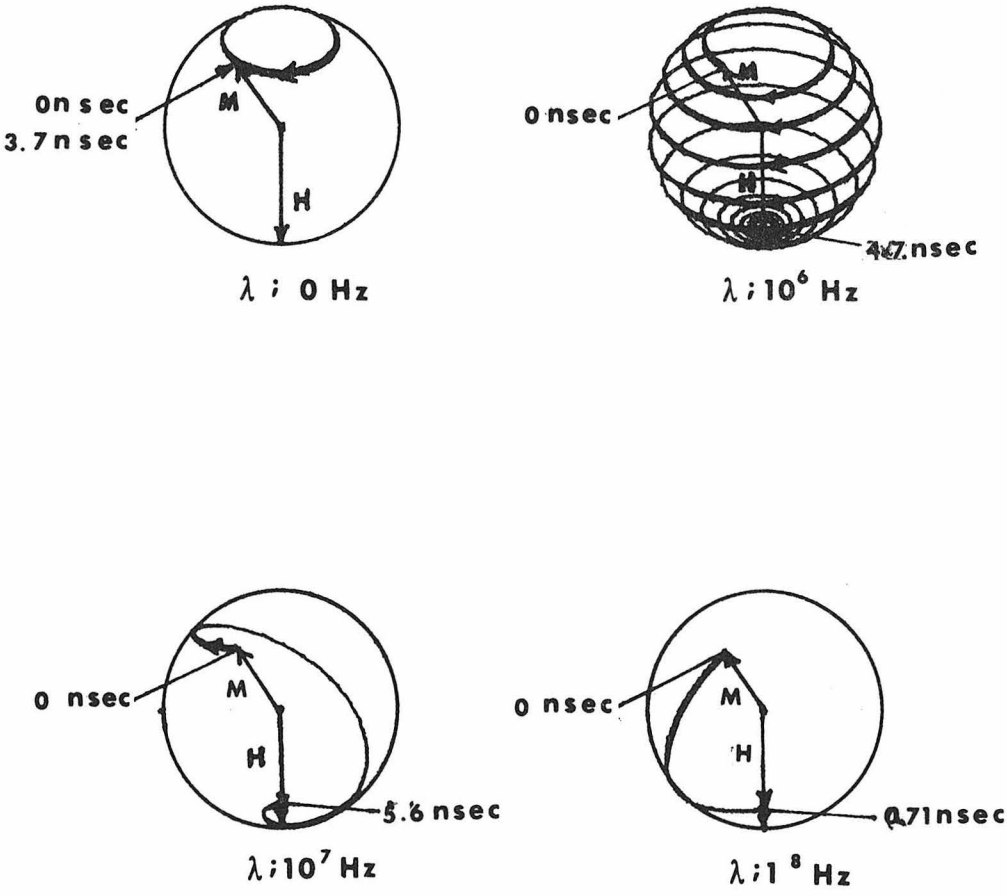

M	900	Gauss
γ	1.76×10^7	Rad Hz Oe^{-1}
H	100	Oe

FIG.2-2 MOTION OF MAGNETIZATION IN INFINITE MEDIUM

〈LANDAU LIFSHITZ EQUATION〉

shown in Fig. 2-3. The magnetization $\vec{M}$, the time derivative, $\frac{d\vec{M}}{dt}$, as well as the first and second terms of Eq. (2-2) are drawn vectorially in the Cartesian system. The z-direction was chosen along the applied field, $\vec{H}$. As before, the torque $\vec{T}_1$ is perpendicular to $\vec{M}$ and $\vec{H}$. In this case, however, the torque $\vec{T}_2$ is not in the plane determined by $\vec{M}$ and $\vec{H}$. This difference can be seen more conveniently in Fig. 2-3b, where the vector diagram is projected on a plane perpendicular to $\vec{M}$.

The motion of the magnetization during a reversal is shown in Fig. 2-4 for various values of the parameter α. When α is equal to zero, the magnetization precesses around the field with angular frequency γH without reversing. When α is small, the precession is still dominant, but a slow reversal occurs. When α is large, the motion of the magnetization is slow in every direction, therefore, both the precession and the reversal are slow. When α is equal to one, the reversal is the fastest.

The Gilbert and the Landau-Lifshitz equations are mathematically equivalent. Both equations have $d\vec{M}/dt$ in the plane perpendicular to $\vec{M}$, and the magnitude of $\vec{M}$ is conserved. This equivalence can be seen in Fig. 2-5, where the two equations are vectorially shown in the plane perpendicular to $\vec{M}$. The gyromagnetic ratio γ's for Landau-Lifshitz and Gilbert equations are subscripted by L and G, respectively. It can be seen from the geometrical considerations that

$$\gamma_L = \frac{\gamma_G}{1 + \alpha^2} \quad , \qquad (2\text{-}4)$$

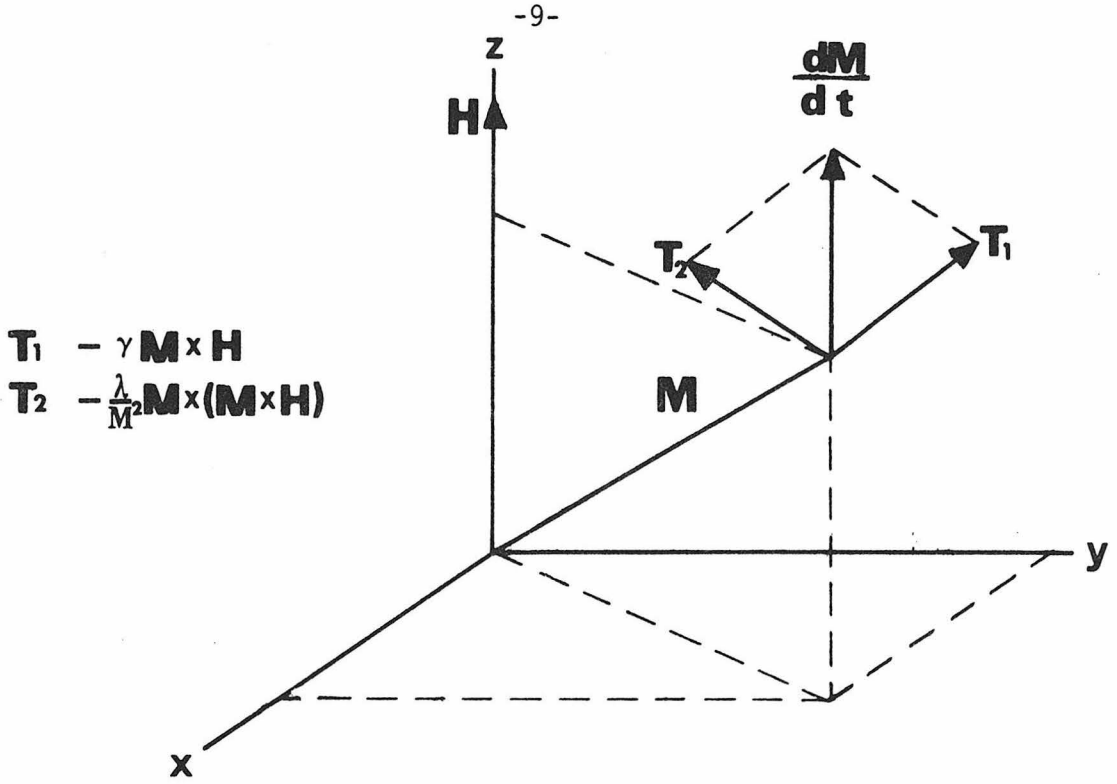

a

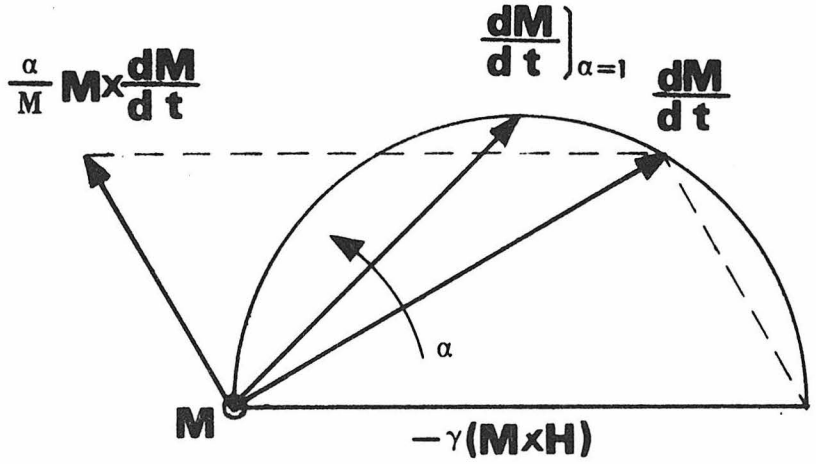

b

FIG. 2-3 VECTORIAL REPRESENTATION
OF
GILBERT EQUATION

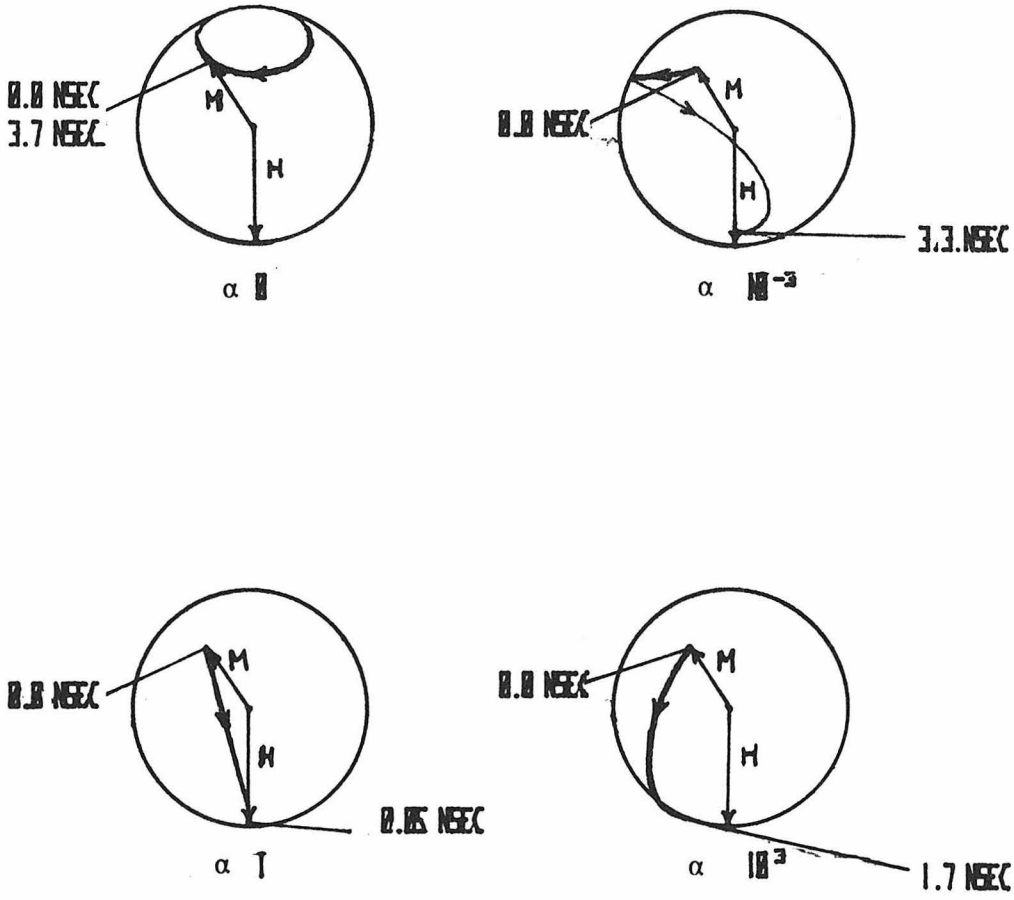

FIG.2-4 MOTION OF MAGNETIZATION IN INFINITE MEDIUM

〈GILBERT EQUATION〉

$$\lambda = \frac{M\gamma_G\alpha}{1 + \alpha^2} \quad , \qquad (2\text{-}5)$$

For usual magnetic materials, $\alpha << 1$. Therefore,

$$\gamma_L \sim \gamma_G \quad , \qquad (2\text{-}6)$$

and

$$\lambda \sim M\gamma_G\alpha \quad . \qquad (2\text{-}7)$$

In this case, there is no difference between the λ's and the damping parameters are simply related by a constant. The choice, therefore, can be made arbitrarily depending on the situation.

Another type of equation was introduced by Bloch (1946) in the theoretical analysis of the nuclear resonance, where the mutual interactions of spins are weak enough to be neglected. The same equation was later applied by Bloembergen (1950) to the analysis of ferromagnetic resonance where the mutual interactions of spins are strong. This so-called Bloch-Bloembergen equation is:

$$\left(\frac{d\vec{M}}{dt}\right)_{x,y} = -\gamma(\vec{M} \times \vec{H})_{x,y} - \frac{\vec{M}_{x,y}}{T_2} \quad , \qquad (2\text{-}8)$$

$$\left(\frac{d\vec{M}}{dt}\right)_{z} = -\gamma(\vec{M} \times \vec{H})_{z} - \frac{\vec{M}_z - \vec{M}_o}{T_1} \quad , \qquad (2\text{-}9)$$

or

$$\frac{d\vec{M}}{dt} = -\gamma(\vec{M} \times \vec{H}) - \frac{\vec{M}_{x,y}}{T_2} - \frac{\vec{M}_z - \vec{M}_o}{T_1} \quad , \qquad (2\text{-}10)$$

where the subscripts x, y, z are used to describe the vector components in the Cartesian system. The z axis is along the applied field. The parameters T_1 and T_2 represent the longitudinal and transverse

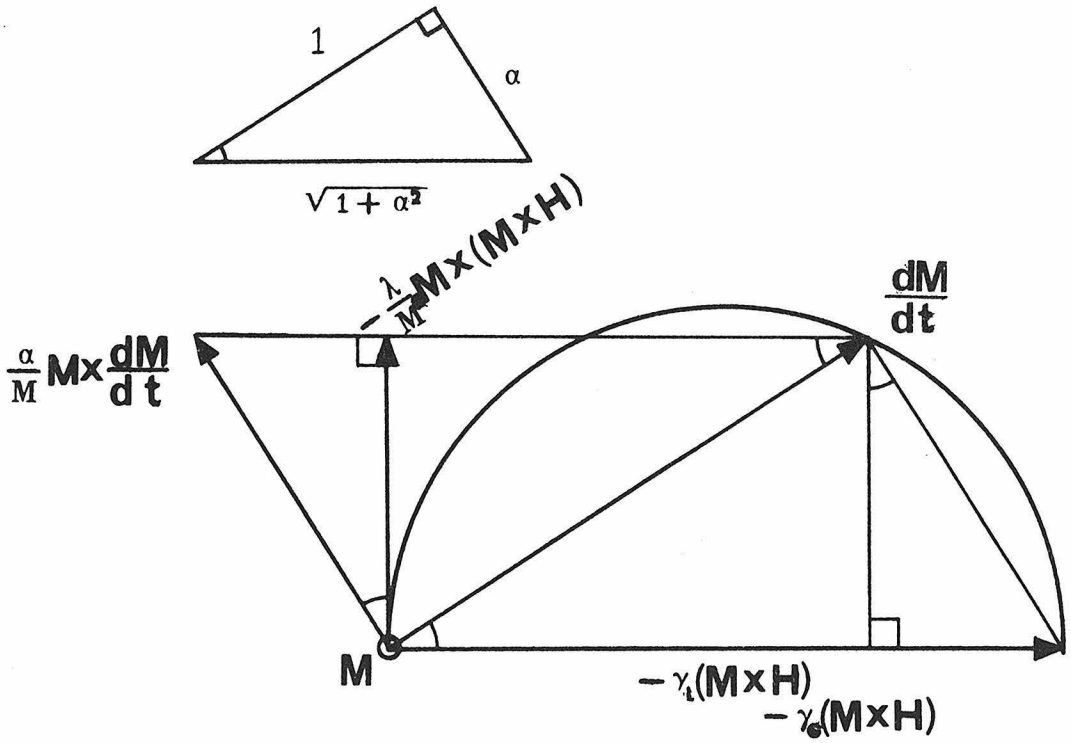

FIG.2-5 EQUIVALENCE BETWEEN
LANDAU-LIFSHITZ EQUATION
AND
GILBERT EQUATION

relaxation time, respectively, and M_o is the saturation magnetization at equilibrium.

A vectorial representation of the Bloch-Bloembergen equation (2-10) is shown in Fig. 2-6. The vectors $\vec{M}$, $\frac{d\vec{M}}{dt}$ and the three terms of Eq. (2-10) are shown. The vector $-\gamma(\vec{M} \times \vec{H})$ represents the torque causing the precession of the magnetization around the field as in the previous case. The vectors $\vec{M}_{x,y}/T_2$ and $(\vec{M}_z-\vec{M}_o)/T_1$ represent the torques causing the relaxation of $\vec{M}$ towards the applied field. The essential difference of this equation from the Landau-Lifshitz or the Gilbert equation is that the vector $\frac{d\vec{M}}{dt}$ has a component along $\vec{M}$, indicating the magnitude of $\vec{M}$ changes with time. Therefore, $\vec{M}$ is not conserved.

It might seem strange that the Bloch equation, which is based on the assumption of negligible mutual interactions of spins, can be applied to ferromagnetic resonance. However, the Bloch equation is equivalent to the Landau-Lifshitz equation if the deviation of the magnetization $\vec{M}$ from its equilibrium $\vec{M}_o$ is small. The terms of the Bloch-Bloembergen equation are shown in Fig. 2-7 for the case where $\vec{M}$ is very close to $\vec{M}_o$. In this case,

$$-\frac{\vec{M}_{x,y}}{T_z} \sim -\frac{\lambda}{M^2}\vec{M} \times (\vec{M} \times \vec{H}) \quad , \qquad (2\text{-}11)$$

and

$$-\left|\frac{\vec{M}_z - \vec{M}_o}{T_1}\right| \sim 0 \quad , \qquad (2\text{-}12)$$

Therefore, the Bloch-Bloembergen equation can be used in the analysis of ferromagnetic resonance where the magnetization is almost aligned along its equilibrium direction and yet is not appropriate for the large angle magnetization reversals under consideration here.

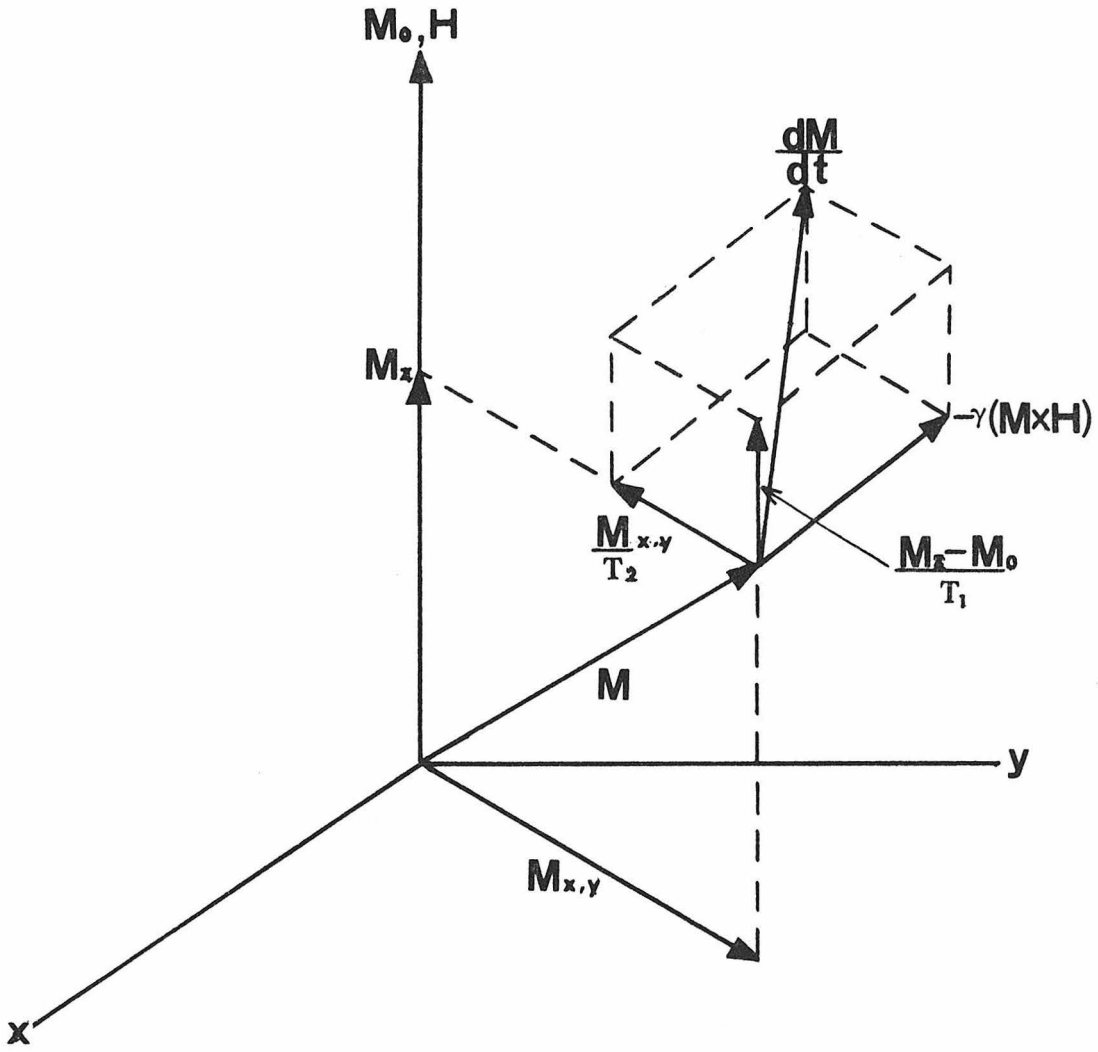

FIG.2-6 VECTORIAL REPRESENTATION
OF
BLOCH-BLOEMBERGEN
EQUATION

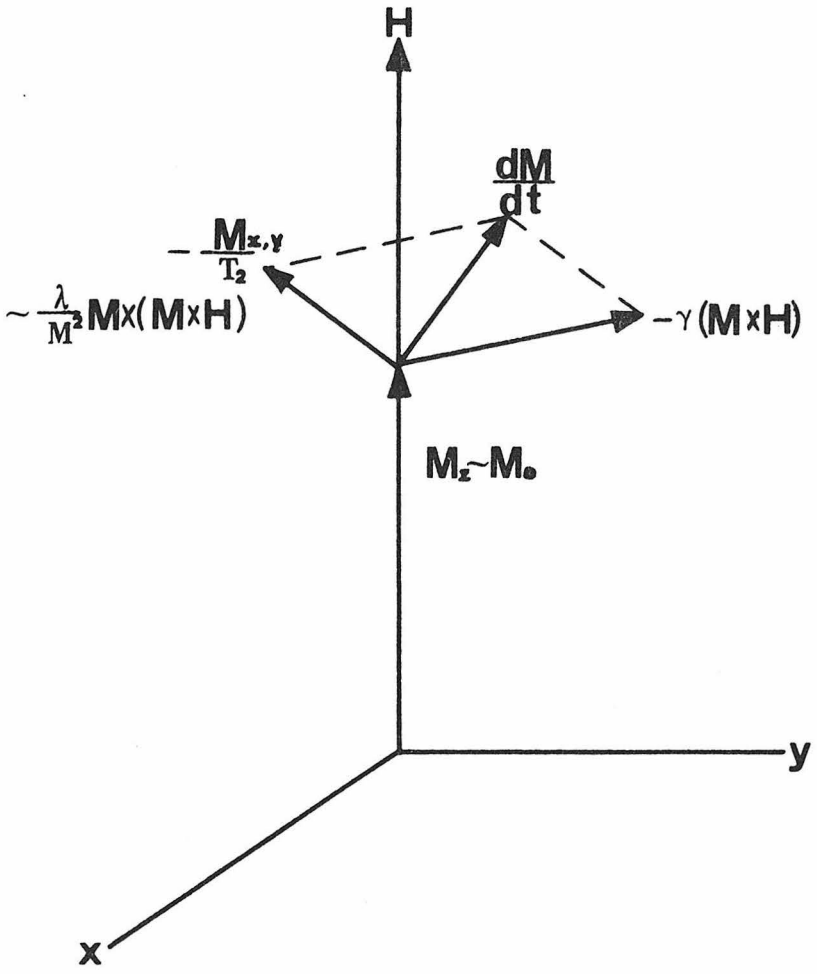

FIG.2-7 EQUIVALENCE BETWEEN
LANDAU-LIFSHITZ
AND
BLOCH-BLOEMBERGEN
EQUATIONS

Callen (1958) proposed a very general equation:

$$\frac{d\vec{M}}{dt} = \alpha\vec{M} - \gamma(\vec{M} \times \vec{H}) - \lambda\vec{M} \times \vec{M} \times \vec{H} \quad , \qquad (2\text{-}13)$$

where α, γ and λ are all adjustable scalar parameters. The three terms of this equation represent three mutually orthogonal components of the motion. The second and third terms are of the same form as in the Landau-Lifshitz equation but $\vec{M}$ is not conserved in magnitude as can be seen in the first term. He related α, γ and λ to the intrinsic properties of the material, the strength of the applied field, and the state of the spin system. For the special case where $\alpha = 0$, $\vec{M}$ is conserved. Therefore, it might be expected that his equation could be used for the coherent magnetization reversal. Unfortunately, the analysis has been made only for the case where $\vec{M}$ is near its equilibrium, to avoid a complication due to the couplings between the uniform mode of spin wave to other modes. The condition that $\vec{M}$ is near its equilibrium is apparently not appropriate for the magnetization reversal. For this reason, Eq. (2-13) cannot be used in the present case, where $\vec{M}$ rotates away from its equilibrium.

In analyzing a flux reversal in thin ferromagnetic films, a complication arises because of the existence of the demagnetizing field and the effective field due to a uniaxial anisotropy. The magnetic field exerted on the magnetization is the sum of the externally applied field, the demagnetizing field and the field due to the anisotropy. For thin films, a good approximation is that the demagnetizing field is perpendicular to the film plane, because a typical thickness to diameter ratio is 10^{-5}. The demagnetizing field is given by

$$\vec{H}_m = -4\pi\vec{M}_n \quad , \quad (2\text{-}14)$$

where the z-direction is along the film normal. An expression for effective field due to the anisotropy is derived in Sec. 2.1.2 and is given by

$$\vec{H}_a = H_k \frac{M_x}{M} \quad , \quad (2\text{-}15)$$

$$\text{or} \quad = (H_k \cos\phi) \quad , \quad (2\text{-}16)$$

where $H_k = 2K/M$. The x and y directions are along the easy and hard axes respectively and $\vec{i}$ and $\vec{j}$ are the respective unit vectors.

Because of the film geometry, it is possible to simplify the problem by separating the motion into two orthogonal directions. An example is shown in Fig. 2-8 for the Landau-Lifshitz equation. The terms of Eq. (2-1) are shown in the Cartesian system. The x, y, and z axes are chosen along the easy axis, the hard axis and the normal to the film plane, respectively. The sum of the applied field, $\vec{H}_s$ $(= \vec{H}_{sx} + \vec{H}_{sy})$, and the field due to the anisotropy, $\vec{H}_a$, is shown by the vector $\vec{H}$ $(=\vec{H}_x + \vec{H}_y)$. The initial precession of $\vec{M}$ around $\vec{H}$ creates a strong demagnetizing field $-4\pi\vec{M}_z$. (The vector $\vec{M}_z$ is not shown to emphasize that $\vec{M}$ is almost in the film plane.) The torque due to the field $\vec{H}$ is $-\gamma(\vec{M} \times \vec{H})$ and is shown by the vector 1. The vector $-\gamma(\vec{M} \times \vec{H})$ is perpendicular to $\vec{M}$ and almost perpendicular to the x,y plane. The torque due to the demagnetizing field $-4\pi M_z$ is $\gamma(\vec{M} \times 4\pi\vec{M}_z)$ and is shown by the vector 2. The vector $\gamma(\vec{M} \times 4\pi\vec{M}_z)$ is also perpendicular to M and lies almost in the x,y plane. The damping terms $-(\lambda/M^2)\vec{M} \times (\vec{M} \times \vec{H})$ and $(\lambda/M^2)\vec{M} \times (\vec{M} \times 4\pi\vec{M}_z)$ are shown by the

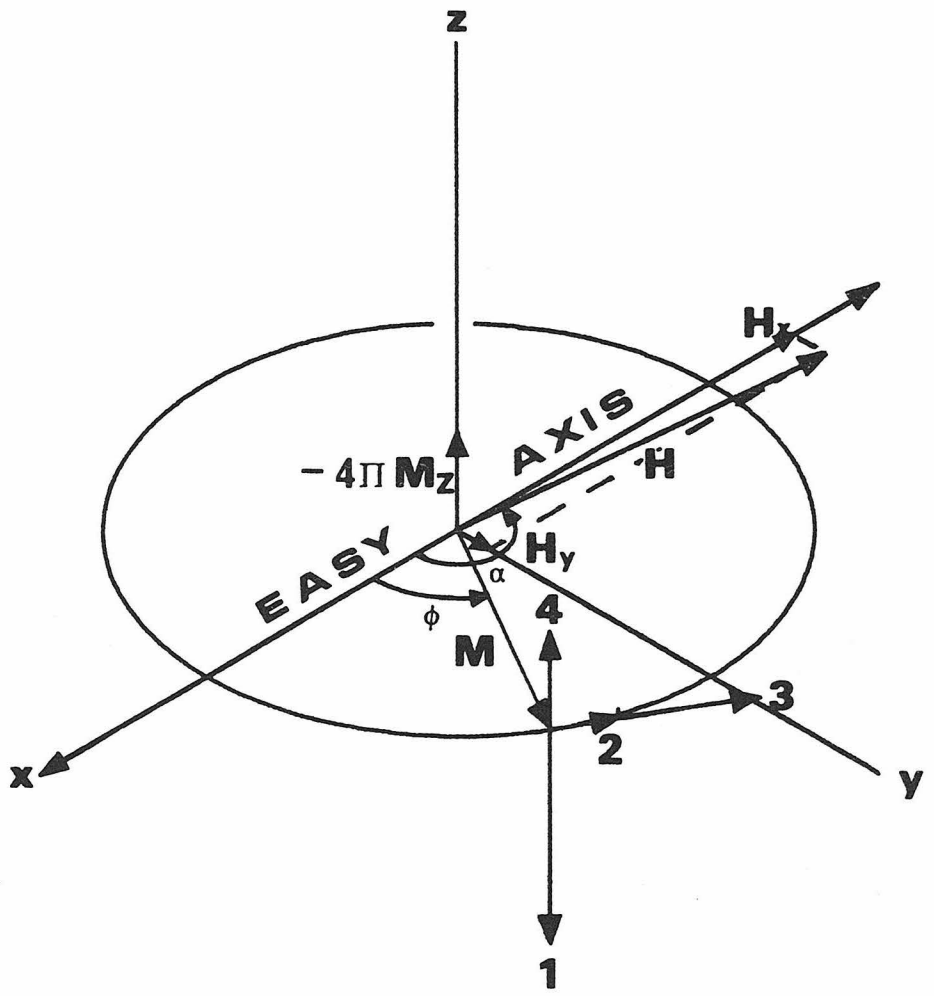

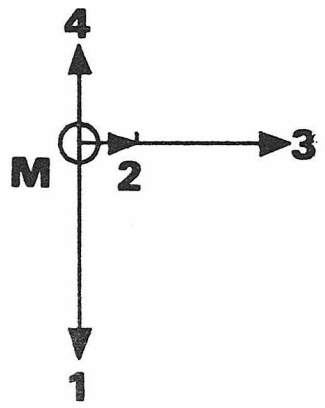

1 $-\gamma \mathbf{M}\times\mathbf{H}$
2 $-\lambda/M^2\,\mathbf{M}\times(\mathbf{M}\times\mathbf{H})$
3 $\gamma \mathbf{M}\times 4\Pi\mathbf{M}_z$
4 $\lambda/M^2\mathbf{M}\times(\mathbf{M}\times 4\Pi\mathbf{M}_z)$

FIG. 2-8 APPLICATION OF LANDAU-LIFSHITZ EQUATION TO MOTION OF MAGNETIZATION IN FERROMAGNETIC THIN FILM

vectors 3 and 4. The vector $-(\lambda/M^2)\vec{M} \times (\vec{M} \times \vec{H})$, 3, lies almost in the x,y plane and parallel to the vector $\gamma(\vec{M} \times 4\pi\vec{M}_z)$, 2. The vector $(\lambda/M^2)\vec{M} \times (\vec{M} \times 4\pi\vec{M}_z)$, 4, is almost perpendicular to the x,y plane and antiparallel to the vector $-\gamma(\vec{M} \times \vec{H})$, 1.

From Fig. 2-9, one obtains

$$\left(\frac{d\vec{M}}{dt}\right)_{xy} = -\gamma(\vec{M} \times 4\pi\vec{M}_z) - \frac{\lambda}{M^2}\vec{M} \times [\vec{M} \times (\vec{H}_x + \vec{H}_y)] \quad , \qquad (2\text{-}17)$$

$$\left(\frac{d\vec{M}}{dt}\right)_{z} = \gamma\vec{M}_x(\vec{H}_x + \vec{H}_y) - \frac{\lambda}{M^2}\vec{M} \times (\vec{M} \times 4\pi\vec{M}_z) \quad , \qquad (2\text{-}18)$$

thus,

$$\dot{M\phi} = -4\pi\gamma M \sin\theta - \lambda(H_x \cos\phi + H_y \sin\phi) \quad , \qquad (2\text{-}19)$$

$$\dot{M\theta} = \gamma M(H_x \cos\phi + H_y \sin\phi) - 4\pi\lambda M \sin\theta \quad . \qquad (2\text{-}20)$$

Where ϕ is the rotation angle of the magnetization from the easy axis and θ is that from the film plane. Equations (2-19) and (2-20) can be solved for ϕ and θ as:

$$\ddot{\phi} + 4\pi\lambda\dot{\phi} + 4\pi\gamma^2 M[H_k \sin\phi \cos\phi - H_{sx} \sin\phi + H_{sy} \cos\phi] = 0, \qquad (2\text{-}21)$$

$$\theta = -\frac{1}{4\pi\gamma}\dot{\phi} \quad . \qquad (2\text{-}22)$$

when $\sin\theta \sim \theta$ and $\gamma M \gg \lambda H$. These equations were previously obtained by Smith (1958) using a different analysis. For the present investigation, Eq. (2-21) is generally most convenient, because it contains only the angle of the rotation. It was solved digitally using a HP9820 calculator for various values of H_k, λ and H_{sx}.

2.1.2 Ferromagnetic Thin Films and Magnetization Reversal

Thin films of Ni-Fe were first prepared by Blois (1955) by vacuum evaporation. He also showed that an in-plane uniaxial anisotropy was induced when a film was evaporated with a magnetic field in the plane of the film. Ever since, Ni-Fe thin films have been of interest and investigated by many workers in the field. The two unique characteristics of films, the extreme geometry and the uniaxial anisotropy, have been the principal reasons for their popularity.

Because of the film geometry (the diameter to thickness ratio of $\sim 10^5$), the magnetization lies in the film plane for most circumstances. The demagnetizing field normal to the film plane is huge. It is $-4\pi M \sin\theta$ when the magnetization, M, rises from the film plane by θ degrees. For example, in the case of 83 Ni-17 Fe film, the demagnetizing field of about 190 Oe is generated when the magnetization rises only 1 degree from the film surface. Therefore, the magnetization lies in the film plane unless a large magnetic field is applied normal to the film surface.

The uniaxial anisotropy can be described by a free energy of the magnetization system;

$$E = K \sin^2 \phi \quad , \qquad (2\text{-}23)$$

where K is a constant called the anisotropy constant and ϕ is the angle of the magnetization rotation from the easy axis. The axis of the minimum energy is developed along the direction of the field during the evaporation. The magnetization lies along this axis in the absence of an external field. The axis is called the easy axis, and the axis perpendicular to it is called the hard axis.

The torque, $\vec{T}$, exerted on the magnetization, $\vec{M}$, due to the anisotropy, is given by

$$\vec{T} = -\frac{\partial E}{\partial \phi}\vec{n} = -2K \sin\phi \cos\phi\vec{n} = -(\frac{2K}{M}\cos\phi)\sin\phi\vec{n}, \quad (2\text{-}24)$$

where $\vec{n}$ is a unit vector normal to the film plane. On the other hand, without the anisotropy, the torque exerted on the magnetization by a field, $\vec{H}$, is given by

$$\vec{T} = -\vec{M} \times \vec{H} = -MH \sin\phi\vec{n} \quad . \quad (2\text{-}25)$$

where ϕ is the angle of the magnetization rotation from the field. Comparing the above two expressions, it can be said that $(2K/M)\cos\phi$ in Eq. (2-24) has the same role as the magnetic field applied along the easy axis. Therefore, $(2K/M)\cos\phi$ can be regarded as an effective field due to the anisotropy for the magnetization directed at an angle, ϕ, from the easy axis. For the magnetization in the vicinity of the easy axis, the effective field is equal to $2K/M$, called an anisotropy field and denoted by H_K.

The spins in a real single domain film are not parallel to each other because of various inhomogeneities in the film. The possible causes of the microscopic fluctuations in the spin alignment are local fluctuations of anisotropy, local magnetostriction, local strain, non-uniform distribution of magnetocrystalline anisotropy in polycrystalline film, etc. Anisotropy dispersion has been widely used as a measure of magnetic inhomogeneities in thin films. The concept of anisotropy dispersion is based on the assumption that the film is composed of many noninteractive microscopic regions of ideal single domains, each with its own uniaxial anisotropy of different magnitude

and axial direction. Uniaxial anisotropy observed macroscopically is considered to be the average effect of the anisotropy of these microscopic domains. Both magnitude and angular dispersion of the anisotropy has been considered. The magnitude dispersion, Δ_{90}, is defined in such a way that 90% of the film area possesses anisotropy field within $\pm \Delta_{90} H_K$ of H_K. The angular dispersion, α_{90}, is defined in such a way that 90% of the film area possesses anisotropy axis within $\pm \alpha_{90}$ degrees of the macroscopic easy axis. The physical interpretation of the anisotropy dispersion is not clear since mutual interactions between the ideal single domains are totally ignored. The use of anisotropy dispersion, with a clear specification of the measuring method, is still a useful practical measure to specify film inhomogeneities.

The occurrence of coherent magnetization reversal in real thin films is infrequent. A reason is the nonparallel distribution of spins. Two effects of the nonparallel distribution can be considered. One is the nonuniformity of the torques exerted on the spins (Frumkin 1972). The nonuniformity causes a different speed for a different spin. Another effect is the additional internal fields, i.e., the demagnetizing field due to the divergence of magnetization and the effective field due to the exchange effect (Harte, 1964, 1967; Stein, 1965, 1966). This internal field is spatially dependent, imposing a different torque on each spin. Therefore, a difference in the speeds of the spin rotations results.

2.1.3 Review of Previous Investigations

—— Reversal Mechanisms ——

The coherent rotation mode was first proposed by Conger and Essig (1956) for the magnetization reversal in ferromagnetic thin films. The idea was based on the concept that the only possible domain structure for films thinner than 4000 Å is a single domain. The single domain concept was based on a calculation done by Kittel (1946) in which he assumed a fixed wall structure in an isotropic material. It was later shown that neither condition held for these thin films so that the single domain concept was wrong. Further, Conger and Essig's experiment was considerably limited by the response time of the equipment.

Two modes of the reversal were recognized by Olson and Pohm (1958). One was the domain wall motion and the other was the (coherent) rotation mode. Their experiment was to reverse the magnetization from a saturated state near the easy axis to the other by applying a pulse field oppositely directed. They also applied a small constant bias field along the hard axis. The inverse of the reversal time was plotted against the pulse field with bias field as a parameter. The resultant curve had a nonlinear region for low pulse fields and a linear region for higher fields. The nonlinear region was not affected by the bias field; whereas, the linear region was. Since the domain wall motion should not be affected by the bias field perpendicular to the wall, the nonlinear region was identified as the domain wall motion region. The linear region was identified as the rotational region.

The switching waveforms had two parts: an initial spike corres-

ponding to the magnetization rotation and a long tail corresponding to the domain wall motion. However, with an applied field just above the onset of the rotational mode, the waveform showed a deviation from what was theoretically expected of the rotational mode. The deviation was attributed to the inhomogeneity of the film.

Deviation from coherent rotation was clearly shown by Humphrey (1958), experimentally. He proposed a new reversal mechanism, i.e., noncoherent rotation mode, to account for the deviation. The two orthogonal flux components (parallel and perpendicular to the pulse field) were observed simultaneously. If the reversal is due to a coherent rotation, the perpendicular component should reach a maximum when the other is half changed.However, his experiment showed no such result. It was proposed that the magnetization starts to rotate coherently, but that the magnetization then loses its coherency, and the reversal is completed by a noncoherent rotation mode.

Coherent magnetization rotation was analyzed by Smith (1958) using Eq. (2-23). The limitation of the viscous-flow approximation ($d^2\phi/dt^2 = 0$; ϕ being the rotation angle of the magnetization) was shown. The approximate solution agreed with the exact solution only when the switching time was longer than 10 nsec. The exact solution showed the oscillatory nature of the coherent magnetization rotation. This oscillation of the magnetization was, however, not observed because of the insufficient time resolution of his apparatus.

Three mechanisms of the magnetization reversal were proposed by Humphrey and Gyorgy (1959) for thin films and toroids. The inverse switching time vs. applied field curve was observed to have three

regions. The nonlinear region for just above the coercive force of the film was attributed to the domain wall motion; the steep linear region for the drive field much higher than the rotational threshold field was attributed to the coherent rotation and the intermediate linear region of the lower slope was attributed to noncoherent rotation.

Fast flux reversal of reversal time about 1 nsec. was observed by Dietrich, et al (1960). Using a sampling oscilloscope, their apparatus had a response time of 0.35 nsec. The reversal was claimed to be of a coherent rotation mode. The magnetization oscillation predicted by Smith was observed. The damping constant λ was calculated from the decay time of the oscillation and was shown to agree with the damping constant calculated from in-plane resonance experiment. Detailed systematic investigation of the oscillation was, however, not made at that time.

The transition from a coherent to a noncoherent rotation mode was investigated by Stein (1965, 1966). The flux component parallel to the pulse field was plotted against the perpendicular component during the reversal. The resultant locus simulates the motion of the magnetization. When the applied field was much higher than the calculated rotational threshold, the locus was a semicircle, indicating a coherent rotation. When the applied field was just above the threshold, the locus deviated from a circle. This deviation indicated a transition from an initial coherent rotation mode to a noncoherent rotation mode.

Stein proposed a model for the noncoherent rotation mode
The model is based on the assumption that the direction of

the magnetization fluctuates periodically along one direction taken in the film plane. According to the model (Fig. 2-9), the portion which rotates ahead of the average magnetization speeds up when the latter passes through its minimum torque direction. On the other hand, the portion which rotates behind the average magnetization slows down. The difference in the speeds intensifies the fluctuation and results in regions of stripes in which the direction of the magnetization changes periodically along a direction perpendicular to the stripes. The divergence of the magnetization creates internal fields and the rotation of the magnetization is slowed down. The boundaries between the stripes then move with a speed much faster than the normal domain wall motion, and the reversal is completed.

Harte also proposed a model for the noncoherent rotation (1965). The model is also based on a spatial fluctuation of the magnetization. The fluctuation was treated as spin waves expanded along one direction taken in the film plane. The average magnetization was assumed to rotate much faster than the spin waves can rearrange themselves. In other words, the initial pattern of the magnetization distribution was assumed not to follow the rotation of the average magnetization. According to this model, a reaction torque is exerted on the average magnetization as it rotates. As this torque retards a further rotation, the spin waves rearrange themselves. The torque is then relaxed, and the rotation resumes. The reversal is completed by an oscillatory rotation due to a continuation of the retardation and the relaxation.

Conclusive photographic observations of dynamic magnetization

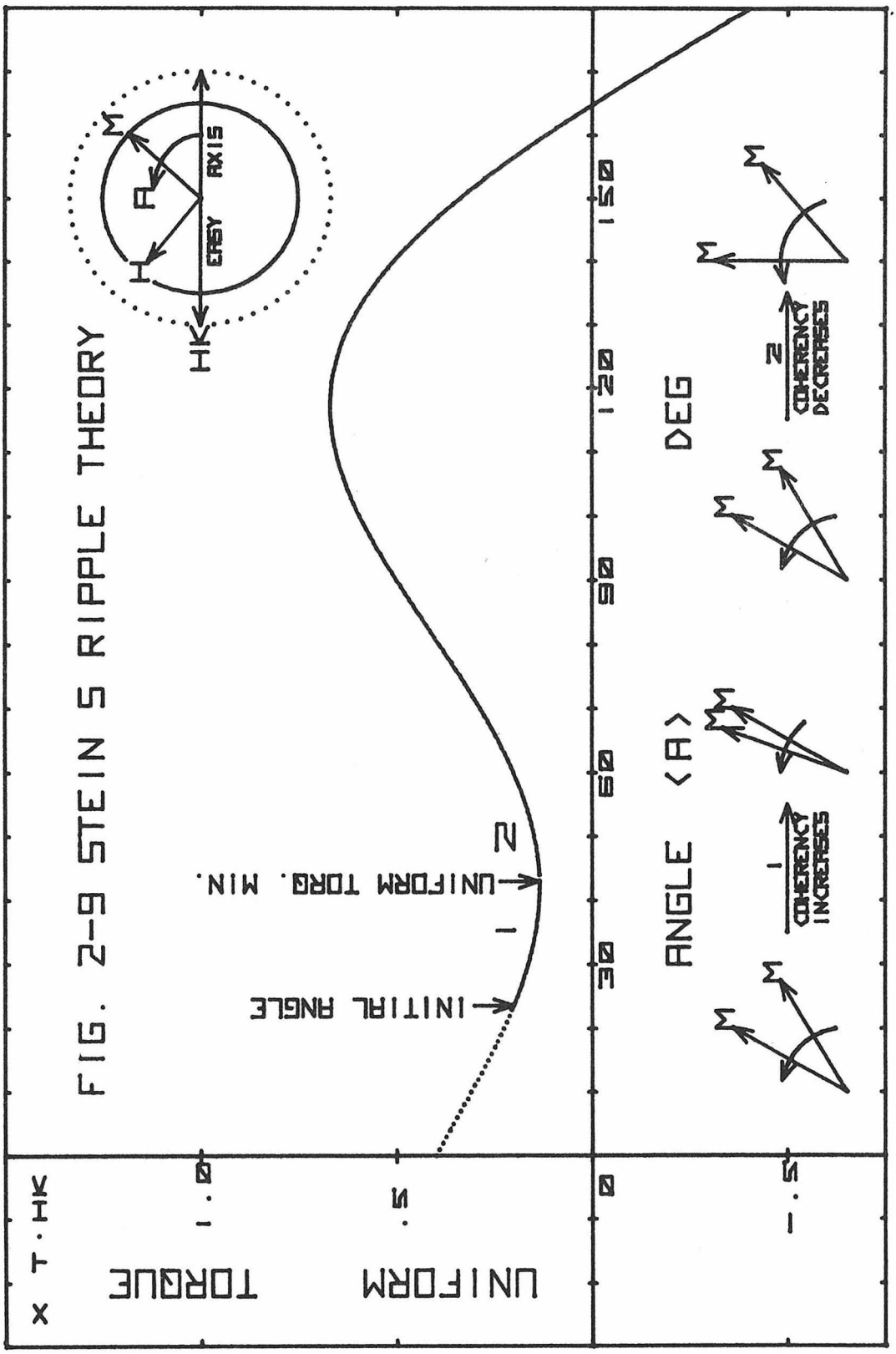
FIG. 2-9 STEIN 5 RIPPLE THEORY
TORQUE
UNIFORM
X T·HK
1.0
.5
0
-.5
INITIAL ANGLE
UNIFORM TORQ. MIN.
1
2
30
60
90
120
150
ANGLE <A>
DEG
1
COHERENCY INCREASES
2
COHERENCY DECREASES
M
A
H
HK
EASY AXIS

configuration during the high speed magnetization reversal were made in a series of experiments done by Kryder and Humphrey (1969-1972). The Kerr magneto-optic effect was used for the observations. The direct observations of the dynamic magnetization configuration eliminated the ambiguities inherent to the pick-up loop method used by previous investigators (Hearn, 1964; Sakurai, et al, 1966; Hoper, 1967; Telesnin et al, 1966, etc.). Five mechanisms of the reversal were found. These were: (1) domain wall motion, (2) diffuse boundary propagation, (3) noncoherent rotation, (4) nucleation and subsequent reversal of partially reversed regions, and (5) coherent rotation. The diffuse boundary is a poorly defined, jagged, and diffuse boundary separating regions of anti-parallel magnetization. The boundary lies transverse to the easy axis. The direction of the propagation is quite different from the normal domain wall motion. The speed of the propagation is one to three orders of magnitude faster than domain wall motion. The noncoherent rotation occurs with transverse bias fields. Initially, the magnetization rotates coherently. As the magnetization rotates 5°~20° beyond the minimum torque direction discussed by Stein, a stripe pattern of dark and bright regions appears on the photograph, indicating a periodic change of the magnetization direction. With fields just above the threshold for the coherent rotation, regions of reversed magnetization nucleate throughout the stripes, and the reversal is completed. With larger fields, the rotation of the magnetization slows down, and the stripes disappear as the reversal is completed. The nucleation and subsequent reversal of partially reversed regions occurs with zero or small transverse bias fields. The

magnetization reverses on small (0.01 mm^2) regions sequentially in time. For very large pulse fields with transverse bias fields, coherent rotation was proposed.

The identification of the coherent rotation mode is based on the observation that the photograph of the film surface darkened uniformly during the 10 nsec. rise time of the pulse field. However, the magnetization configuration could not be observed during the coherent rotation, because the 10 nsec. exposure time is of the order of the reversal time. Although the observations were consistent with the coherent rotation idea, the lack of time resolution left the reversal mechanism in this region uncertain.

2.2 Experimental Method

2.2.1 Apparatus

2.2.1.1 Schematic Diagram

The experimental setup used for the present investigation is schematically shown in Fig. 2-10. The transmission line pulse generator (PG) generates a step pulse voltage at a repetition rate of 60 Hz. The rise time, the maximum pulse length and the maximum amplitude are 0.23 nsec., 1.7 μsec. and 2.5 KV, respectively. The pulse goes through the transmission line system, including a stripline section (SL), and is terminated in the characteristic impedance of 50 Ω (Ro). Between the stripline and the ground plane, a uniform magnetic field pulse with maximum amplitude of 13 Oe is generated.

The thin film under investigation is placed in the center of the stripline section. The magnetization reversal is detected by a single turn pickup loop (PL), closely surrounding the film. The induced voltage is detected by a sampling oscilloscope (SS) of rise time less than 25 psec. High frequency (0.2~1 GHz) disturbances are subtracted after the sampling. The subtraction is made electronically by a differential amplifier (A) with an integrater. The noise free integrated signal is recorded on an X-Y recorder (XY).

2.2.1.2 Transmission Line Pulse Generator

The transmission line pulse generator is schematically shown in Fig. 2-10b. The regulated 0~5 KV power supply (V) charges a coaxial cable (RG-17A/U) of length 170 m through a resister (R) of 97.4 KΩ. The cable is discharged at 60 Hz through a relay (RL). The pulse voltage is equal to half the charging voltage, and the length is

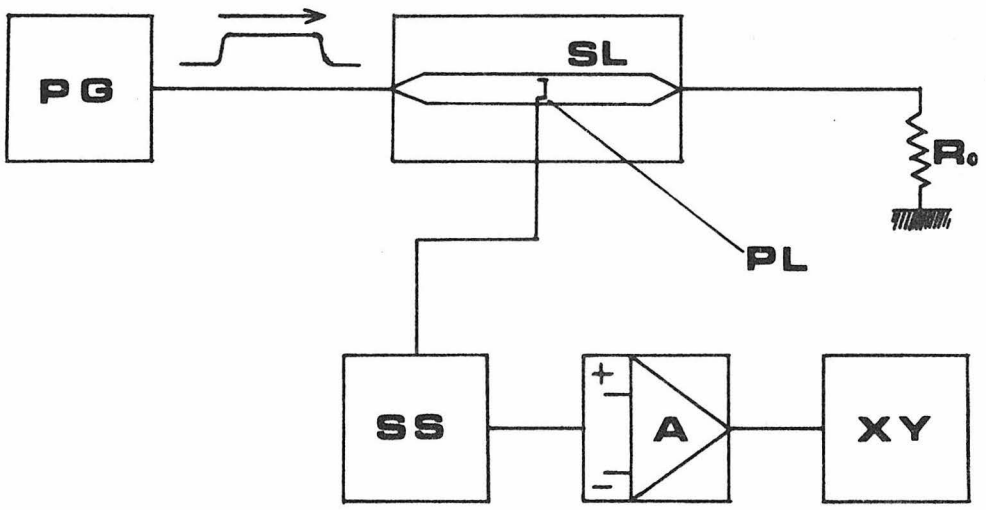

PG TRANSMISSION LINE PULSE GENERATOR
SL STRIP LINE
R TERMINAL RESISTOR 50 OHM
PL PICK-UP LOOP
SS SAMPLING OSCILLOSCOPE
A DIFFERENTIAL AMPLIFIER
XY XY RECORDER

FIG.2-10a APPARATUS

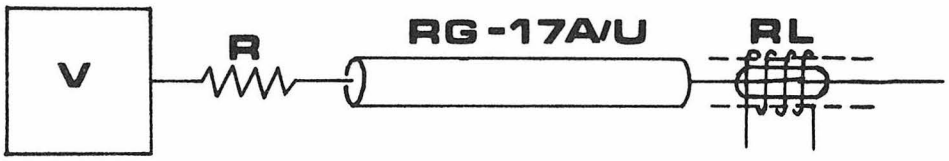

V REGULATED POWER SUPPLY
R REGISTER 97.4 OHM
RG-17A/U COAXIAL CABLE
RL RELAY WITH MERCURY WETTED CONTACTS

FIG.2-10b TRANSMISSION LINE PULSE GENERATOR

twice the time required for wave propagation through the charging cable. The value of the charging resister should be chosen between the two limiting values. The maximum value is determined by the charging time constant. The time constant should be small, so that jitter of the relay closing time will not cause a fluctuation in the charged voltage. The minimum value is determined by the maximum current which will allow the relay to open. For the relays used here, this current is a few hundred milliamperes.

2.2.1.3 Relay

The relay has mercury wetted contacts and is sealed in a glass capsule with hydrogen at about ten atmospheres pressure. The use of mercury contacts prevents multi-contacting due to the bouncing of the reeds. Because of the high pressure hydrogen, the contacts can hold a high voltage gradient and the high gas mobility helps the heat dissipation. The relay can be mounted in a coaxial holder. This mounting enables a connection to a coaxial cable with the minimum mismatch. A relay of this type was invented by Brown and Pollard (1947). Garwin (1950) applied it to the transmission line pulse generator and claimed the rise time of 0.2 nsec. at a pulse voltage of 10 V. The voltage of 10 kV can be applied to the relay, if the surface of the glass capsule is covered with Corona dope (Red-X Corona Dope, Walso Electronics Mfg. Co., Los Angeles, California) (Humphrey, 1967).

2.2.1.4 Stripline

Stripline geometry is particularly suitable for the investigation of high speed flux reversal in thin films. The thin film can be placed under the stripline so that the uniform magnetic field can be

applied parallel to the film surface. The stripline of length, L = 234 mm, width, W = 27 mm, thickness, t = 1.27 mm and separation from the ground plane, d = 4.37 mm was used in the present investigation (Fig. 2-10c). The ends of the stripline have a wedge shape allowing a smooth transition to a coaxial line. The characteristic impedance, Z_o, and the floating capacitance between the stripline and the ground plane, C_F, are given as

$$Z_o = \frac{188.3}{\sqrt{\varepsilon_r}\left(\frac{W}{2d} + \frac{C_f'}{0.0855\ \varepsilon_r}\right)} \quad [\Omega] \quad , \qquad (2\text{-}26)$$

and

$$C_f' = \frac{0.0855\ \varepsilon_r}{\pi}\left[\frac{2}{1 - t/2d}\ln\left(\frac{1}{1 - t/2d} + 1\right) - \left(\frac{1}{1 - t/2d} - 1\right)\ln\left(\frac{1}{(1 - t/d)^2} - 1\right)\right] \quad [pf/cm] \quad , \qquad (2\text{-}27)$$

where ε_r is the relative dielectric constant of the substance between the stripline and the ground plane (Cohn, 1954). In this investigation, ε_r = 1 for air. For the geometry given above, the characteristic impedance Z_o is 50.8 Ω. A satisfactory match with coaxial cable RG-8AU (Z_o = 50 Ω) or RG-8V (Z_o = 52 Ω) is obtained.

2.2.1.5 Pickup Loop

The cross sectional view of the pickup loop is shown in Fig. 2-10d. The loop is a single thin wire (#40) surrounding the film. One end is grounded so that the electrostatic coupling is minimized. The other

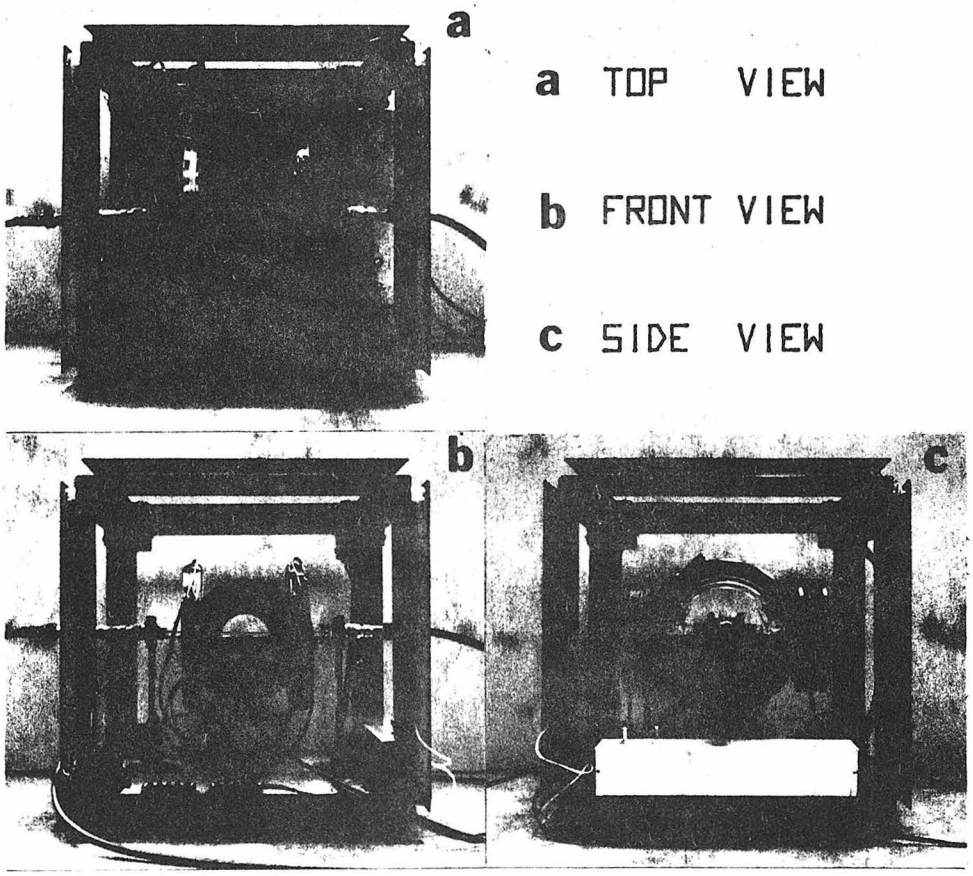

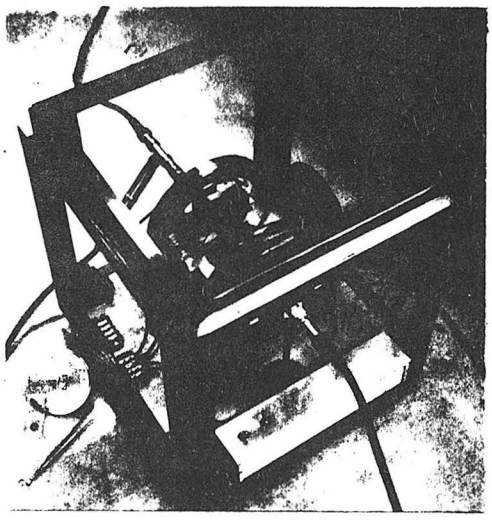

FIG. 2-10C STRIP LINE AND COILS

end is connected to the GR type 874. The capacitive coupling with the stripline is shielded by a brass tube (outer diameter 0.6 mm, inner diameter 0.4 mm). The tube is cut at the center to prevent inductive shielding. The loop and the connector are mounted on the rotatable part of the ground plane. The direction of the loop can be adjusted to prevent inductive coupling to the magnetic field pulse.

2.2.1.5 Noise Subtracter and Integrator

The disturbances to the signal are mainly due to inductive and capacitive coupling between the pickup loop and the field pulse. Both the directional adjustment and the shielding of the loop are used to reduce this coupling. However, some coupling remains even with these precautions. The residual disturbing signal has the same order of magnitude as the desired signal. The disturbing signal is repetitive at 60 Hz. Therefore, it can be automatically subtracted from the disturbed signal. The disturbing signal itself is detected by applying the pulse field after the film is saturated. The disturbing signal and the disturbed signal are alternately sampled by the sampling oscilloscope. The respective outputs are connected to the plus and the minus inputs of a differential amplifier (Analog Device Co., 143A) through a relay. With a capacitive feedback, the output of the amplifier is the noise free integrated signal (Fig. 2-10e).

2.2.1.6 Calibration of Magnetic Field Pulse

The magnetic field pulse, Hp, is related to the charging voltage, V, of the transmission line pulse generator as:

$$Hp = GV \quad , \qquad (2\text{-}28)$$

where G is a constant determined by the stripline geometry. The

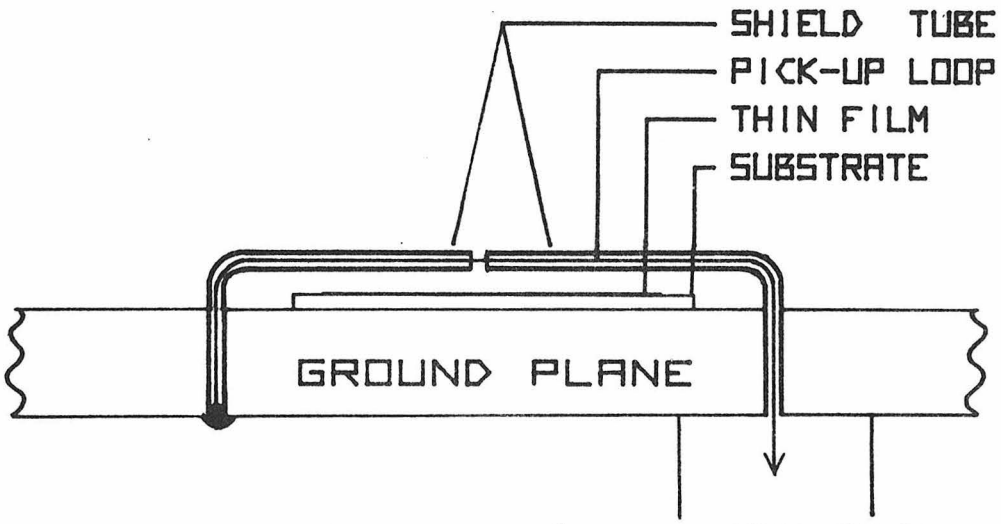

FIG. 2-10d GR 874
PICK-UP LOOP

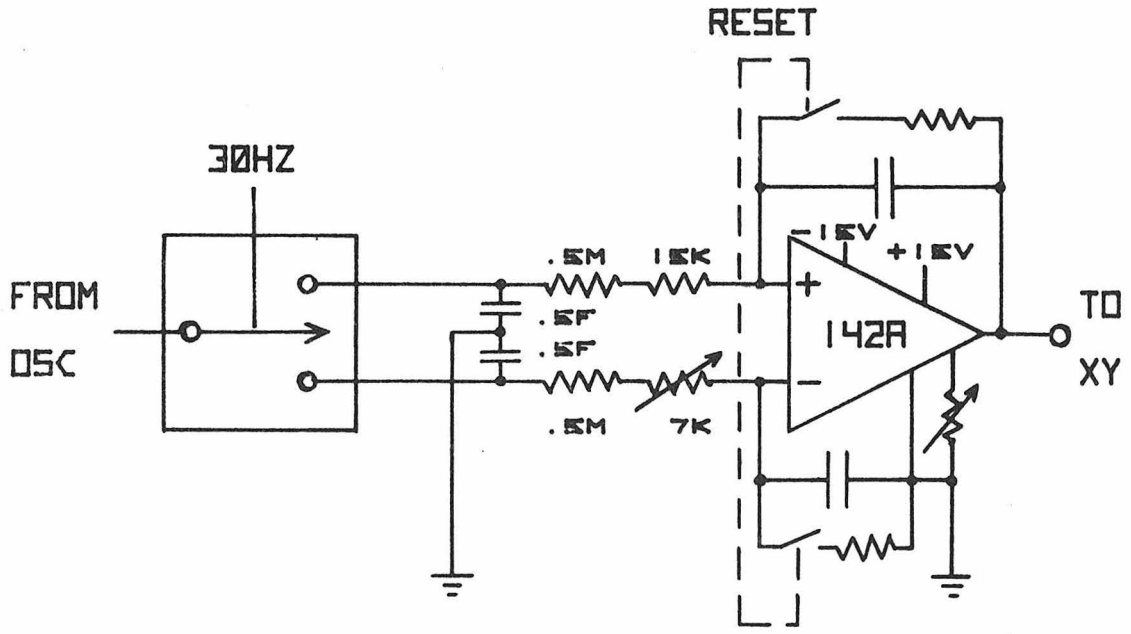

FIG. 2-10e
NOISE SUBTRACTER
AND INTEGRATOR

method proposed by Tatsumoto, et al (1963) gives the value of G. The method utilizes magnetization reversal. When a bias field, ΔHb, is added opposite to the field pulse, the latter must be increased by ΔHp to restore the zero bias waveform. Since

$$\Delta Hb = \Delta Hp = G\Delta V \quad , \qquad (2\text{-}29)$$

G can be obtained by the slope of a ΔHb vs ΔV curve. This method is simple and accurate. The constant is 2.6 Oe/KV for the present investigation.

2.2.2 Measurement of Quasi-Static Quantities

The fundamental quantities for the description of thin ferromagnetic films are the saturation magnetization, Ms, uniaxial anisotropy constant, K, anisotropy field, Hk, coercive force, Hc, magnitude dispersion of anisotropy, Δ_{90}, angular dispersion of anisotropy, α_{90}. They can be measured by using a hysteresis loop tracer and ferromagnetic resonance spectrometer.

The coercive force can be measured from a hysteresis loop for a magnetic field applied along the easy axis. Typical theoretical and actual loops are shown in Fig. 2-11a and b, respectively. For both cases, the component of the magnetization is measured along the applied field and plotted against the field. For an ideal single domain film with an anisotropy field of Hk, the loop is rectangular showing discrete jumps at ±Hk (Fig. 2-11a); in this case, Hc = Hk because the reversal occurs by coherent rotation. For a typical film, Hc < Hk because domain wall motion occurs before coherent rotation (Fig. 2-11b). Although the loop deviates from a rectangle, the coercive force is easily read on the horizontal axis.

The anisotropy field can be measured from a hysteresis loop for a magnetic field applied along the hard axis. Typical theoretical and actual loops are shown in Fig. 2-11c and d, respectively. For both cases, the component of the magnetization is measured along the applied field and plotted against the field. For an ideal single domain film, the loop is closed and saturates at ±Hk (Fig. 2-11c). For a typical film, the loop is slightly open, and the saturation field is not sharply defined (Fig. 2-11d). For this reason, it is usual to obtain

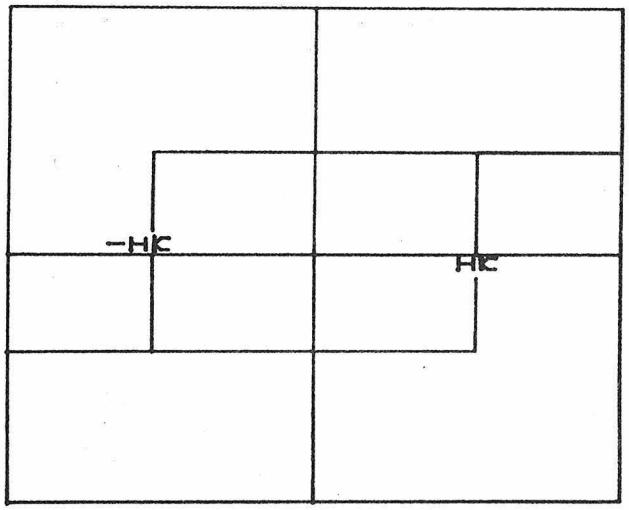

a IDEAL FILM

HC = HK

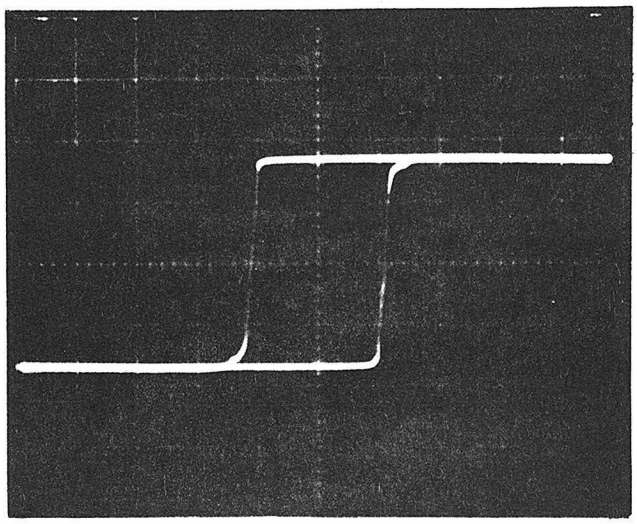

b REAL FILM

HC 2.2 〈OE〉

HOR. 2 〈OE/DIV〉
VER. 0.4〈V/DIV〉

FIG.2-11
MEASURMENT OF COERCIVE FORCE
- EASY AXIS HYSTERESIS LOOP -

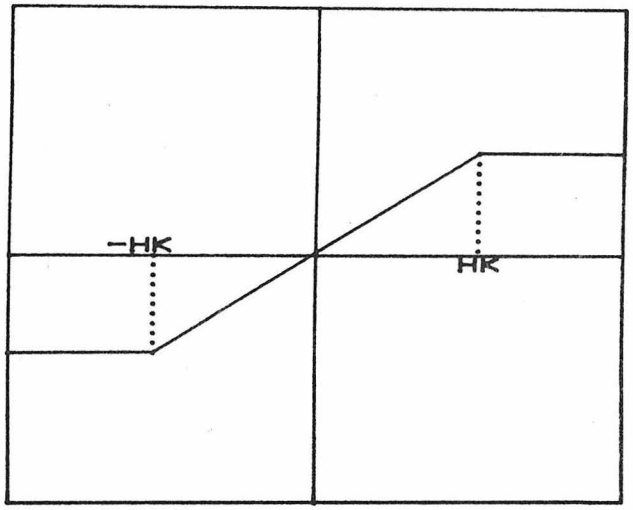

c IDEAL FILM

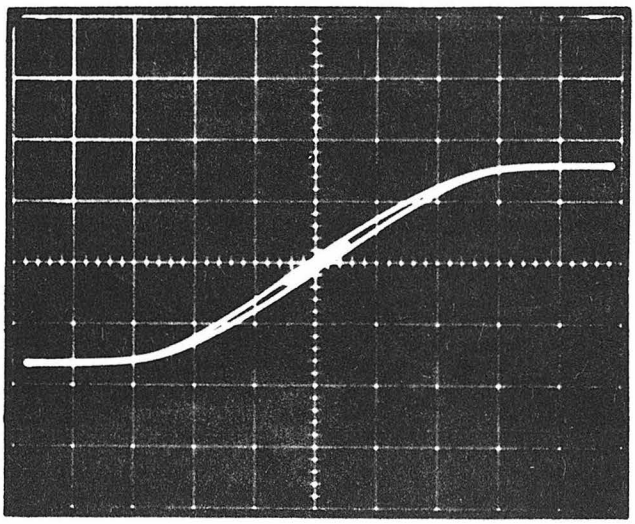

d

REAL FILM

HK 2.7 〈OE〉

HOR. 1 〈OE/DIV〉
VER. Ø.4〈V/DIV〉

FIG.2-11
MEASURMENT OF ANISOTROPY FIELD
- HARD AXIS HYSTERESIS LOOP -

Hk from the intersection of the saturation level and the extrapolation of a minor loop (the little closed loop at the origin shown in Fig. 2-11d).

The anisotropy field can be directly obtained by the following method proposed by Kobelev (1962). The drive field is applied 45° from the easy axis. The component of the magnetization is measured perpendicularly to the field. The resultant hysteresis loop has a shape shown in Fig. 2-11e. A constant field is then applied perpendicularly to the drive field and is increased until a certain portion of the loop becomes flat as shown in Fig. 2-11f. The constant field required is Hk/2.

The concept of the dispersion is based on the assumption that the film is composed of microscopic regions of single domains. The interaction between these regions is ignored. Therefore, the measured value of the dispersion depends on the measuring method except for films with infinitesimal dispersions. The specification of the method is important.

Two methods of measuring the angular dispersion were proposed by Crowther (1956). Both methods utilize the hysteresis loop for a magnetic field applied along the hard axis. The component of the magnetization is observed along the direction perpendicular to the field, rather than parallel. For real films, no magnetization component is observed in this direction. In the "crossed loop" method, the film is rotated in either direction, so that some magnetization component can be observed. At some angle, the maximum of the loop will be 90% of the saturation value. This angle is defined as α_{90}. In

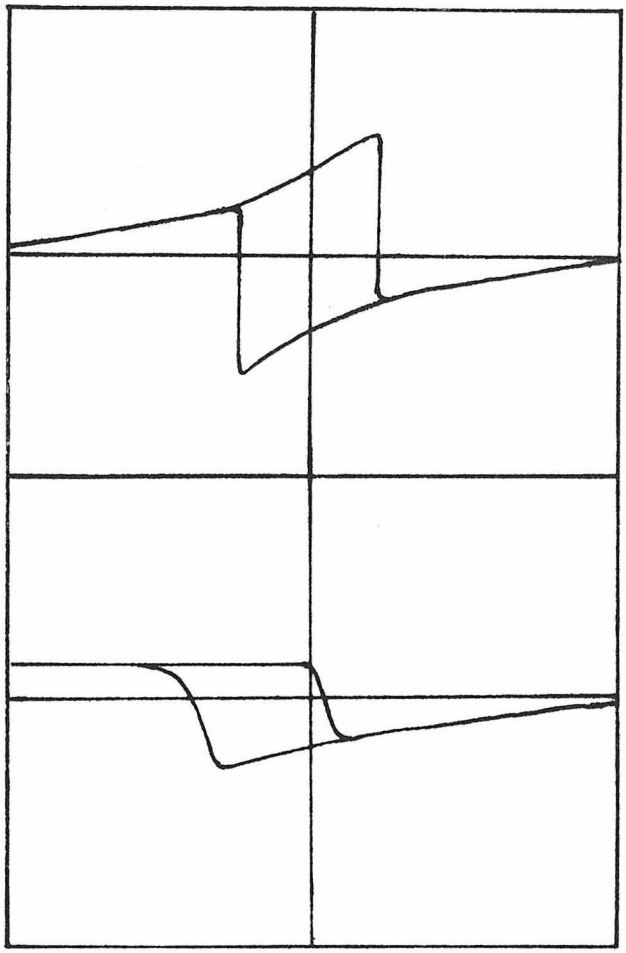

EASY AXIS
HYSTERESIS LOOP

(OBSERVED
PERPENDICULAR
TO ALTERNATE
FIELD)

WITH CONST FIELD
OF HK/2 APPLIED
PERPENDICULAR TO
ALTERNATE FIELD

FIG. 2-11
MEASUREMENT OF ANISOTROPY FIELD
- KOBELEV METHOD -

the other method, a bias field is applied perpendicularly to the driving field. At some value, $H\alpha_{90}$, of the bias field, the maximum of the loop will be 90% of the saturation value. The dispersion is then,

$$\alpha_{90} = \sin^{-1}\frac{H\alpha_{90}}{H_k} \quad , \qquad (2\text{-}30)$$

The value of $Ms\gamma^2$ is obtained by the in-plane resonance method. In this method, a constant magnetic field is applied in the film plane. A microwave magnetic field is also applied in the film plane, but perpendicularly to the constant field. The magnetization processes around the constant field. At resonance, the constant field, H, and the frequency, f, satisfies:

$$f^2 = \frac{Ms\gamma^2}{\pi}(H \pm Hk) \quad , \qquad (2\text{-}31)$$

where + or - corresponds to the constant field being along the easy or the hard axis, respectively (Sec. 3.1.2). The slope of the f^2 vs. H curve gives the value of $Ms\gamma^2$. The value of Ms can be also obtained if the value of γ is known. The anisotropy field can also be obtained from the intersection of the curve with the field axis. The coercive force can be obtained by observing a discrete change in the resonance curve for the easy axis. A typical resonance curve is shown in Fig. 2-12, where the microwave power absorbed in the film is plotted against the driving field. It can be seen that the jumps occur at $\pm Hc$, where one curve is transferred to the other. These are symmetrical about the vertical axis. A further reference should be made to Sec. 3.2.2.

FIG.2-12
RESONANCE
<EASY AXIS
POWER <NORMALIZED BY PMAX>
APPLIED FIELD <NORMALIZED BY HK>
F²≡<My²/π²><H5+HK>
HC
F²≡<My²/π²><H5+HK>
HC

2.2.3 Sample

The Ni-Fe films used in this work were 1 cm diameter disks of ~1200Å thick. They were vacuum-evaporated at 10^{-7} Torr, from Ni-Fe alloys onto heated glass substrates. Since films of various anisotropy fields and dispersions were desired, the substrate temperatures from 35°C to 300°C were used. Various melt compositions from 81 Ni-19 Fe to 88 Ni-12Fe were also used.

The anisotropy field as a function of substrate temperature is shown in Fig. 2-13 with the melt composition as a parameter. The anisotropy field is a decreasing function of the substrate temperature and ranges from 1.6 Oe to 5.9 Oe. It decreases with increasing Ni % (except for the two data points). This temperature characteristic of the anisotropy field is the same as obtained by Wilts (1966).

The anisotropy dispersion (α_{90}) as a function of substrate temperature is shown in Fig. 2-14 with the melt composition as a parameter. The anisotropy dispersion ranges from 1.7° to 9.8° and is minimum around 200°C. It increases with increasing Ni % (except for two data points).

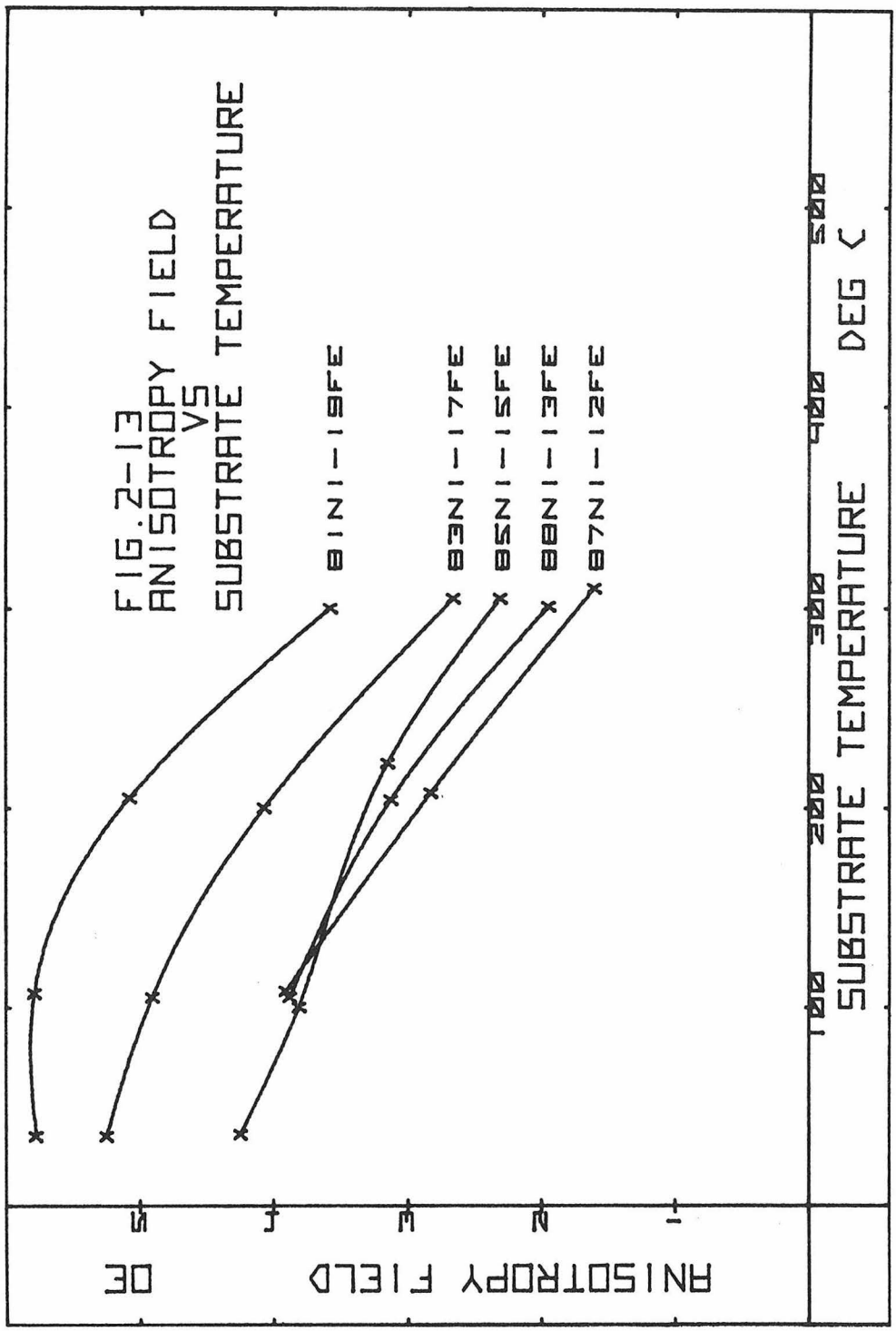
FIG.2-13
ANISOTROPY FIELD
VS
SUBSTRATE TEMPERATURE
B1N1-19FE
B3N1-17FE
B5N1-15FE
B8N1-13FE
B7N1-12FE
ANISOTROPY FIELD OE
SUBSTRATE TEMPERATURE DEG C
100
200
300
400
500
1
2
3
4
5

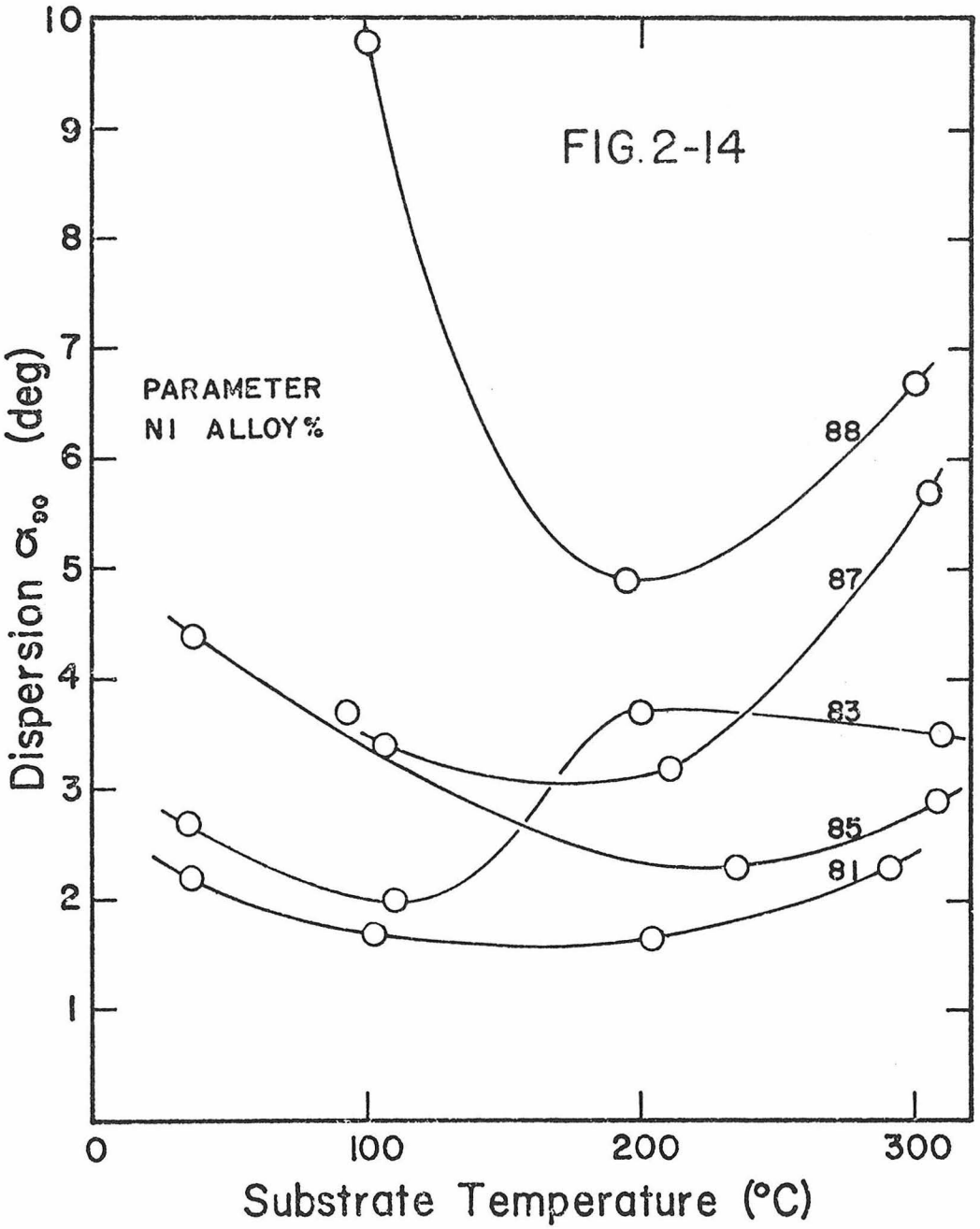
FIG. 2-14
PARAMETER
NI ALLOY%
88
87
83
85
81
Dispersion σ_{90} (deg)
Substrate Temperature (°C)
0
100
200
300
1
2
3
4
5
6
7
8
9
10

2.3 Results and Discussion

2.3.1 Transverse Flux Waveform

Typical transverse flux as a function of time is shown in Fig. 2-15 on an arbitrary scale with the applied field as a parameter. The waveforms are those for the sample 18-19-4 with an anisotropy field of 2.7 Oe, a coercive force of 2.2 Oe, and an anisotropy angular dispersion of 3.5°. The alloy composition is 83 Ni-17 Fe wt.% and the substrate temperature during the evaporation was 300°C. The waveforms for pulse fields of 0.5 H_k, 0.77 H_k, H_k and 2.0 H_k applied along the easy axis are shown by the broken lines A, B, C and D, respectively. A bias field, $H_\perp$, of 0.1 H_k was applied along the hard axis to make an initial angle of 6° ($\sin^{-1} H_\perp/H_k$) between the magnetization and the easy axis. This is to insure a uniform rotation of the magnetization. The corresponding theoretical waveforms were calculated using the dynamic equation (2-21), with λ = 0.15 GHz. The waveforms are shown by the dotted lines A', B', C' and D', respectively, for the above pulse fields.

Below the threshold field, reversal does not occur as indicated by the waveform A. Here the applied field (H_s = 0.5 H_k) is smaller than the threshold field 0.7 H_k. According to the coherent rotation theory, the magnetization should rotate from its initial angle of 6° to the new equilibrium at 12° ($\sim H_\perp/(H_k-H_s)$). However, the observed waveform A is composed of two parts; the first part indicating coherent rotation and the second part indicating a slower flux change. The experimental and theoretical waveforms A and A' agree during the first 1 nsec until the observed flux reaches the equilibrium theoretically

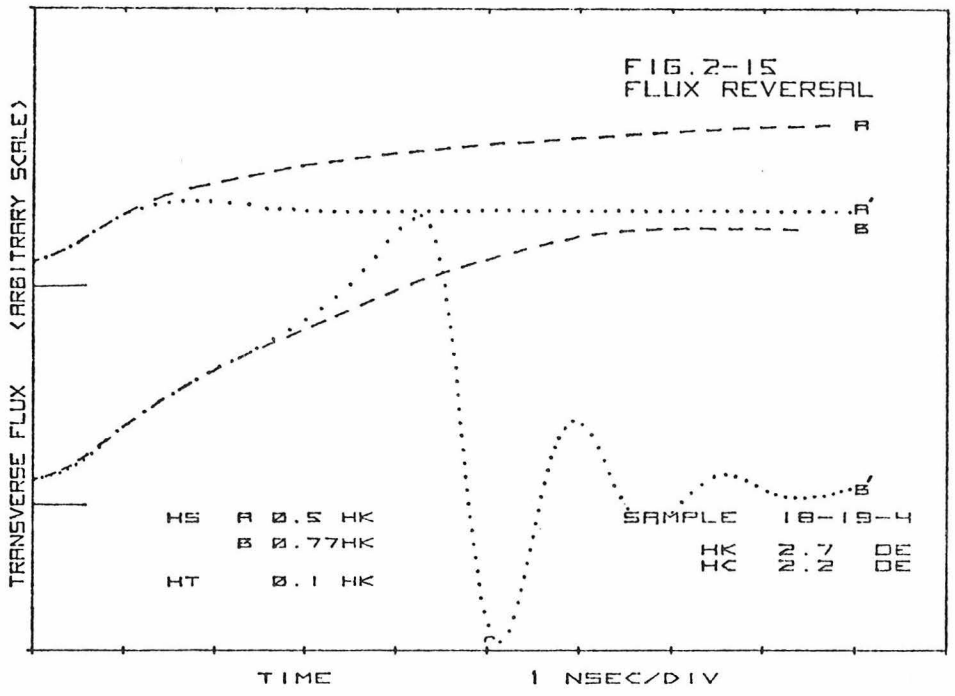
FIG. 2-15
FLUX REVERSAL
A
A'
B
B'
TRANSVERSE FLUX (ARBITRARY SCALE)
HS A 0.5 HK
B 0.77HK
HT 0.1 HK
SAMPLE 18-19-4
HK 2.7 OE
HC 2.2 OE
TIME
1 NSEC/DIV

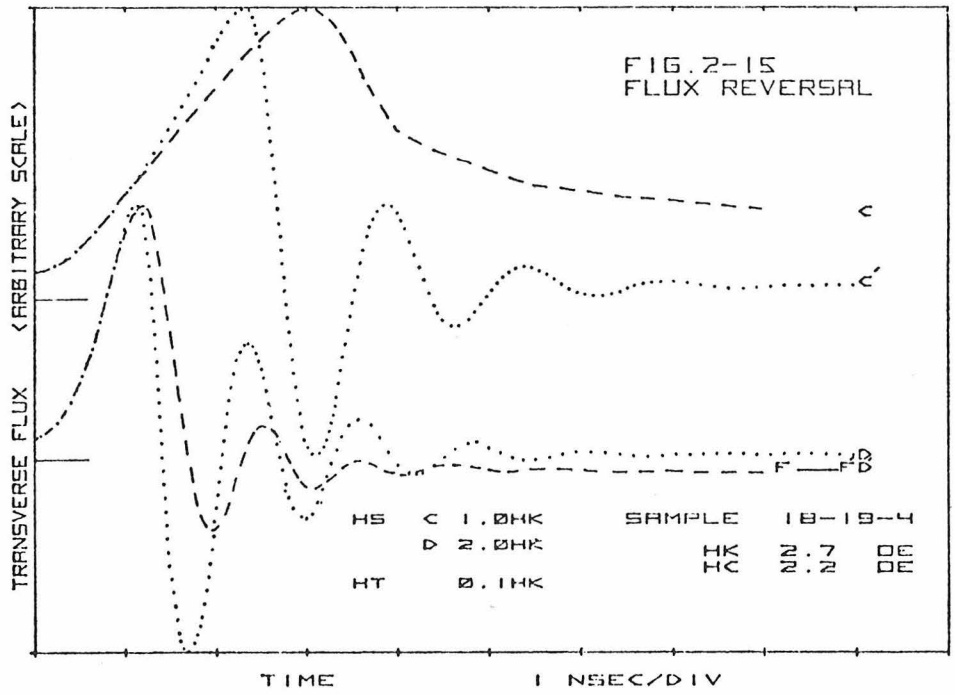
FIG. 2-15
FLUX REVERSAL
C
C'
D
D'
F
F'
TRANSVERSE FLUX (ARBITRARY SCALE)
HS C 1.0HK
D 2.0HK
HT 0.1HK
SAMPLE 18-19-4
HK 2.7 OE
HC 2.2 OE
TIME
1 NSEC/DIV

expected. After the transverse flux reaches the equilibrium, the experimental curve still continues to increase, but the speed of the flux change is much slower than the initial change. This slow change is apparently not due to coherent rotation.

Above the threshold field, flux reversal occurs as shown by the waveforms B, C and D. Each waveform has a maximum, indicating that the magnetization rotates beyond the hard axis. When the applied field is about 10% higher than the threshold field ($H_s = 0.77\ H_k$), the transverse flux reaches its maximum at about 7 nsec as shown by the solid line B. Comparing the theoretical waveform B' and the experimental waveform B, it can be seen that these two waveforms agree for the first 2 nsec. It is clear that coherent rotation is occurring during this period and that Eq. (2-21) describes the initial period. At about 2 nsec, however, the slope of the waveform B decreases abruptly, indicating a sudden retardation of the rotation. The waveform B', however, does not show such an abrupt change. The discrepancy between the waveforms B and B' is quite large after this abrupt change. This change can be interpreted as an occurrence of noncoherent rotation.

When the applied pulse field is equal to the anisotropy field, the transverse flux reaches a maximum about 3 nsec after the start of the reversal (curve C). The experimental and calculated waveforms C and C' agree again for the period of the first 1 nsec, indicating coherent rotation.

When the applied pulse field is increased to 2 H_k, the transverse flux reaches its maximum at about 1 nsec after the start of the

reversal (curve D). Note, the switching speed becomes much faster. An oscillation can be seen around the final flux level (the horizontal line F - F') and lasts for about four cycles and decays exponentially.

2.3.2 Effect of Transverse Bias Field

The effect of the transverse bias field on the flux reversal can be seen in Fig. 2-16. The transverse flux waveform of the sample 18-19-4 is shown with the bias field as a parameter. The pulse field of 2 H_k was applied along the easy axis in all cases. Transverse bias fields, 0.03 H_k, 0.06 H_k, 0.1 H_k, 0.2 H_k and 0.5 H_k, were applied along the hard axis. The respective waveforms are shown by the curves A, B, C, D and E.

When the transverse bias field is small, as in the case $H_\perp$ = 0.03 H_k, the transverse wave forms are composed of two parts; the initial part with a rapid increase and the following part with a slow increase. As the transverse bias field increases, the flux changes faster, and the oscillation begins to appear as in the case of $H_\perp$ = 0.06 H_k. It can be seen that the waveform maximum increases as the transverse bias increases. This indicates that the entire region of the sample has not been rotating, but an increasing amount begins to rotate. As the transverse bias field increases from 0.1 H_k to 0.5 H_k, the flux changes faster and the oscillation becomes clearer. The frequency of the oscillation is almost independent of the transverse bias field. In this case the waveform maximum decreases as the transverse bias field increases since the total rotational angle decreases.

2.3.3 The Effect of Anisotropy Dispersion on the Transverse Flux Waveform

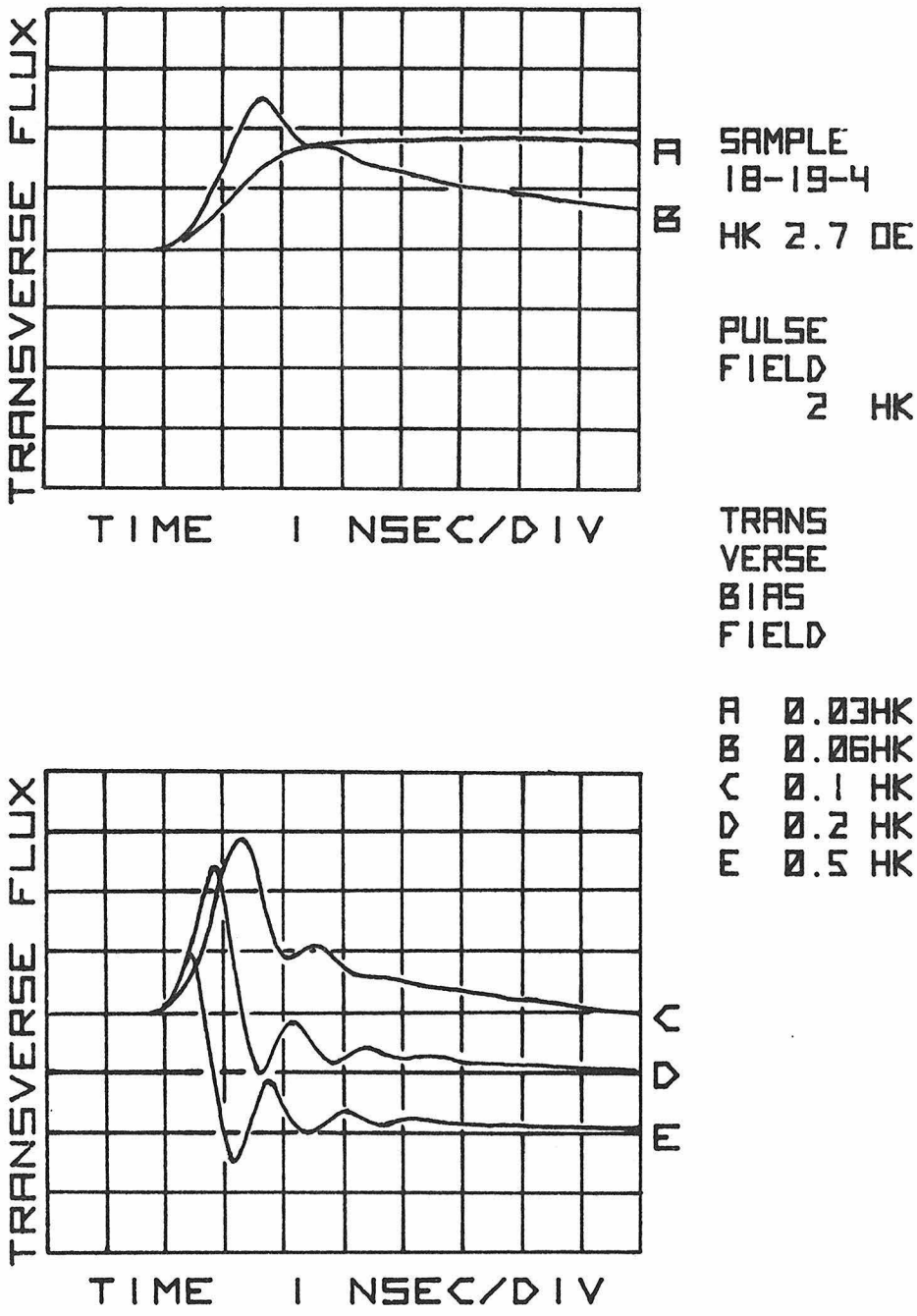

FIG. 2-16 EFFECT OF TRANSVERSE BIAS FIELD

The effect of anisotropy dispersion (α_{90}) on the transverse flux waveform can be seen in Fig. 2-17. The waveforms of the samples 19-29-7 and 18-19-16 are the curves A and B, respectively. A pulse field of 2 H_k along the easy axis and a transverse bias field of 0.1 H_k are applied. The dispersion for samples 19-29-7 and 18-19-16 is 1.9° and 2.6°, respectively. The anisotropy field for both samples is about 5.0 Oe.

The effect of the dispersion appears most critically in the reversal speed and the oscillation. The waveform A shows a faster reversal than B, therefore, the smaller the dispersion, the faster the reversal. The reversal times for sample 19-29-7 and 18-19-16 are 0.64 nsec and 1.0 nsec, respectively. Also, it can be seen that the waveform A shows the oscillation with larger amplitude and more periods than B, indicating a smaller damping.

The effect of angular dispersion on the reversal speed is more obvious for a sample with large dispersion. The transverse flux waveforms of sample 19-13-7 and sample 19-13-3 are shown in Fig. 2-18 by curves A and B, respectively. The respective dispersion is 3.0° and 5.7°. Both samples have anisotropy field of about 3.0 Oe. The pulse field of 3 H_k and transverse bias field of 0.1 H_k were used for both cases. Waveform B shows a much slower reversal than A; again, the smaller the dispersion, the faster the reversal. Note that the time scale for curve B is 5 times longer than that for curve A. The reversal time for sample 19-13-7 is 2.3 nsec, whereas, that for sample 19-13-3 is 48.5 nsec. A slight oscillation can be seen on curve A as the transverse flux decreases towards its final level,

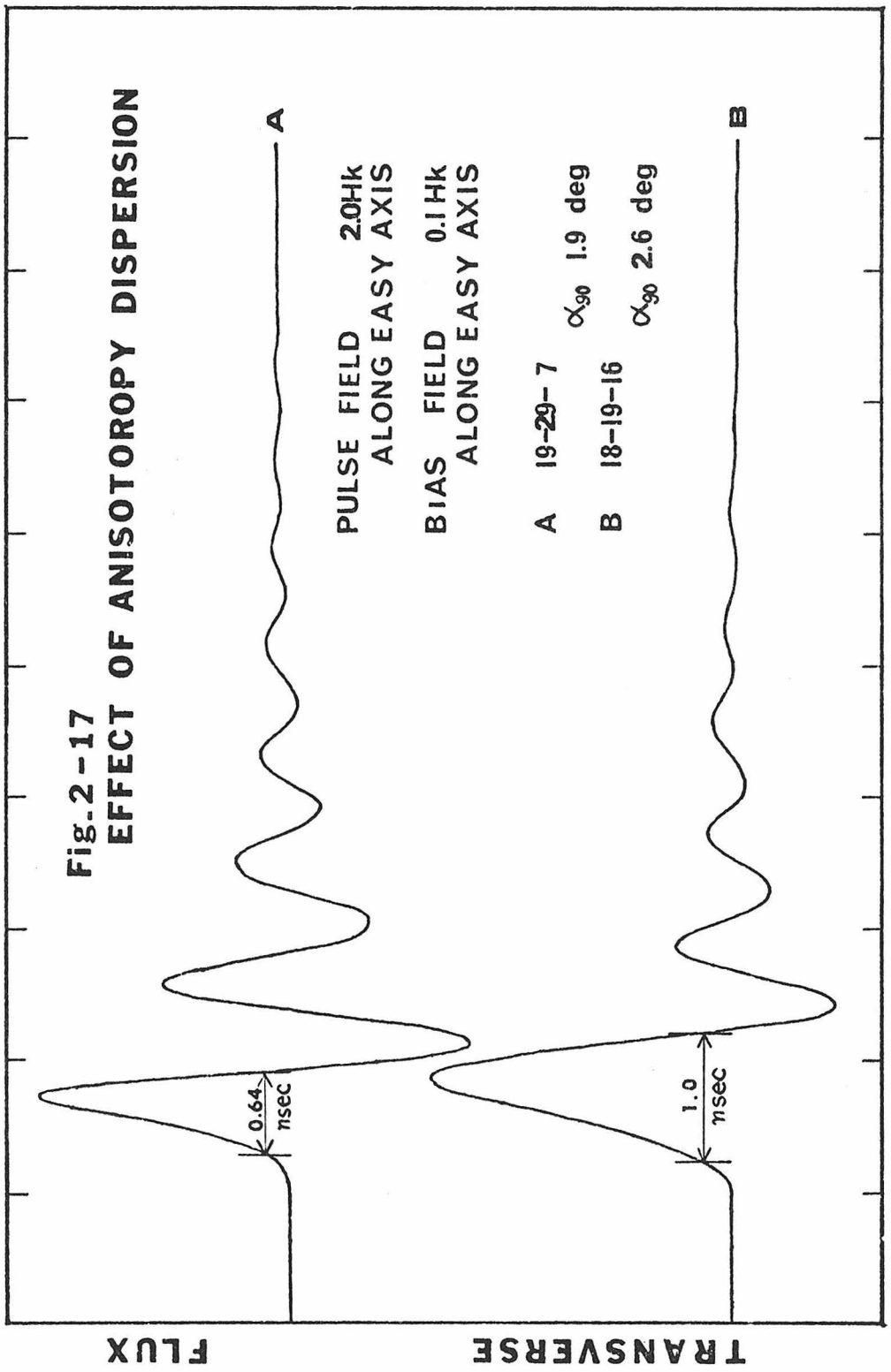
Fig. 2-17
EFFECT OF ANISOTOROPY DISPERSION
A
B
PULSE FIELD 2.0Hk
ALONG EASY AXIS
BIAS FIELD 0.1Hk
ALONG EASY AXIS
A 19-29- 7 α_{90} 1.9 deg
B 18-19-16 α_{90} 2.6 deg
0.64 nsec
1.0 nsec
FLUX
TRANSVERSE
T I M E
1 nsec/div

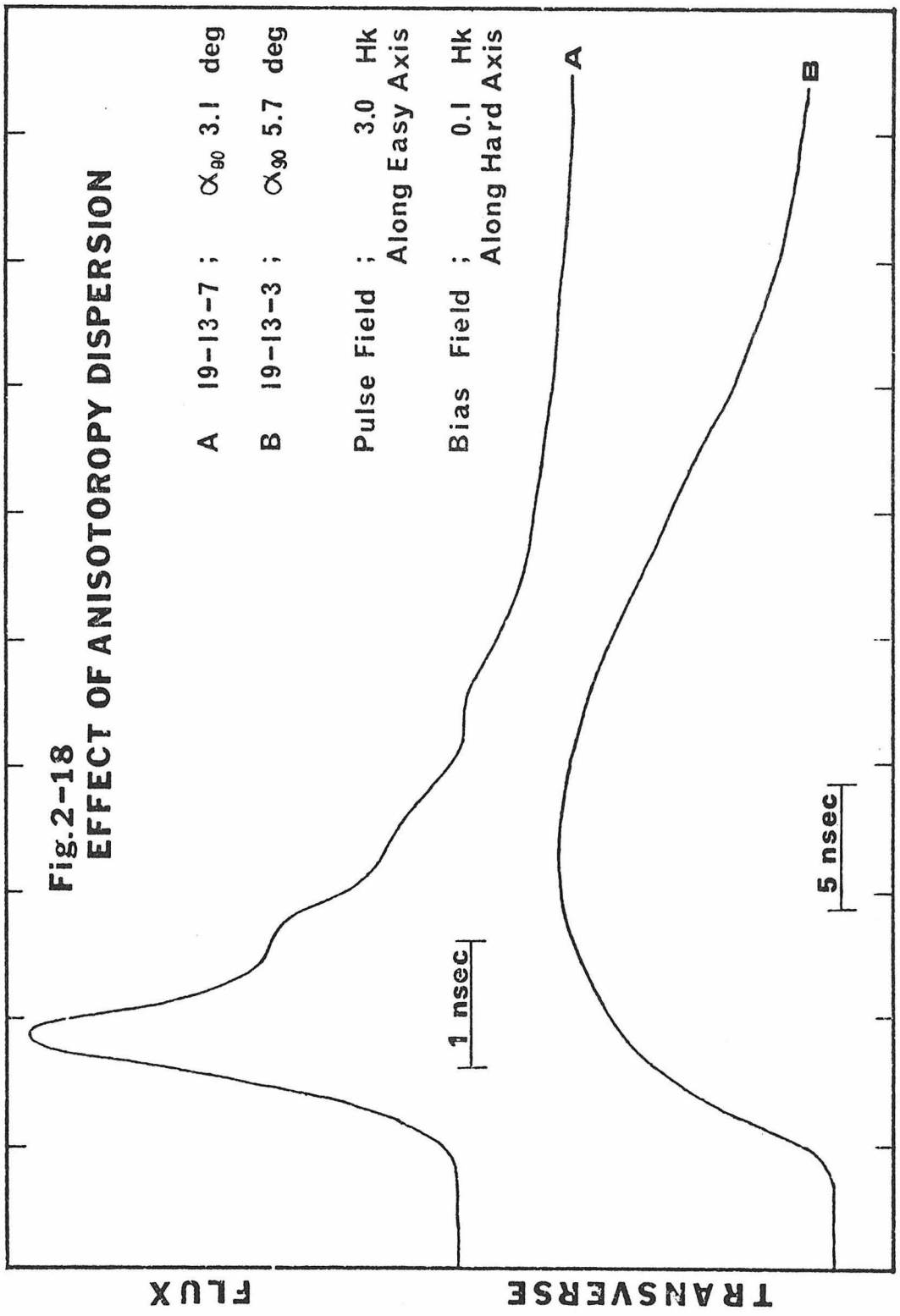
Fig.2-18
EFFECT OF ANISOTOROPY DISPERSION
A 19-13-7 ; α_{90} 3.1 deg
B 19-13-3 ; α_{90} 5.7 deg
Pulse Field ; 3.0 Hk
Along Easy Axis
Bias Field ; 0.1 Hk
Along Hard Axis
A
B
1 nsec
5 nsec
FLUX
TRANSVERSE
T I M E

whereas no hint of an oscillation is apparent in curve B. It is clear that the angular dispersion is critically affecting the reversal.

The effect of the dispersion is most conveniently summarized using the inverse switching time vs. applied field curve ($1/\tau - H_s$). The switching time, τ, is defined as the time interval between the 10% values of the maximum flux. The shape of the $1/\tau - H_s$ curve calculated according to equation (2-21) depends on the five quantities, M, γ, H_k, λ and the transverse bias field $H_\perp$. Therefore, the direct comparison of the $1/\tau - H_s$ curves for the various samples is somewhat difficult. To avoid this complication, Eq. (2-21) was normalized as follows, i.e.,

$$\frac{d^2\phi}{d\tau^2} + 4\pi\lambda' \frac{d\phi}{d\tau} + 4\pi^2(\sin\phi\cos\phi - h_s \sin\phi - h_\perp \cos\phi) = 0 \quad , \qquad (2\text{-}32)$$

where

$$\tau = t\sqrt{\frac{M\gamma^2}{\pi} H_k} = tf_k$$

$$\lambda' = \lambda/\sqrt{\frac{M\gamma^2}{\pi} H_k} = \lambda/f_k \quad , \qquad (2\text{-}33)$$

$$h_s = H_s/H_k$$

$$h_\perp = H_\perp/H_k$$

The normalizing factor $\sqrt{\frac{M\gamma^2}{\pi} H_k} = f_k$ is the natural resonance frequency. It can be seen from the Eq. (2-32) that the normalized

$1/\tau$ - h_s curve for a given value of $h_\perp$ can be determined only if the normalized values of the damping parameter λ' are specified. Therefore, the comparison of the $1/\tau$ - H_s curves for the various samples becomes easier.

The normalized $1/\tau$ - h_s curves for samples 19-29-7, 18-19-16, and 19-13-7 are shown in Fig. 2-19 by curves 1, 2, and 3, respectively. The anisotropy dispersion, α_{90}, for these samples are 1.9, 2.6 and 3.1 degr., respectively. The normalized inverse switching time is an increasing function of the normalized applied field. The average slope of the $1/\tau$ - h_s curve decreases with increasing dispersion, indicating that the sample with larger dispersion reverses slower.

2.3.4 The Effect of Pick-up Loop Frequency Response on the Transverse Flux Waveform

The frequency-response of the pick-up loop was examined in an attempt to clarify the cause of the discrepancies between the experimental and calculated transverse flux waveforms. The frequency response was obtained by detecting the voltage induced in it by a microwave voltage and the induced voltage were measured by a sampling oscilloscope with a rise time less than 25 psec. The frequency response of the pick-up loop can be most conveniently seen by the analogy with a high frequency filter. The normalized induced voltage divided by the frequency is plotted as a function of frequency in Fig. 2-20. The corner frequency of 1.4 GHz can be seen. Transverse flux waveforms were calculated assuming that the pick-up loop is in series with an R-C filter of time constant 0.7 nsec (= 1/1.4 GHz) as shown

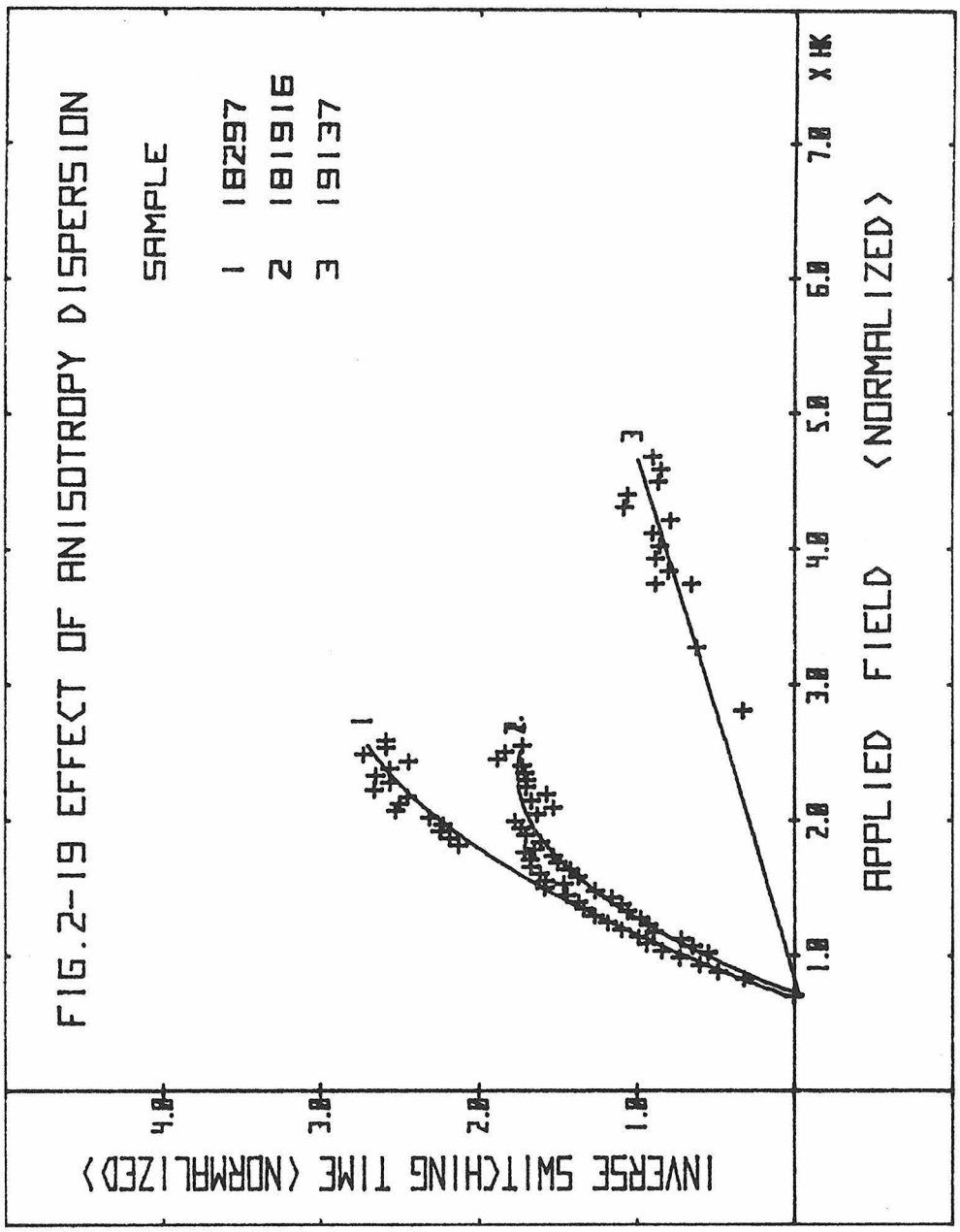
FIG.2-19 EFFECT OF ANISOTROPY DISPERSION
SAMPLE
1 18297
2 181916
3 19137
INVERSE SWITCHING TIME (NORMALIZED)
APPLIED FIELD (NORMALIZED)
X HK
1.0
2.0
3.0
4.0
5.0
6.0
7.0

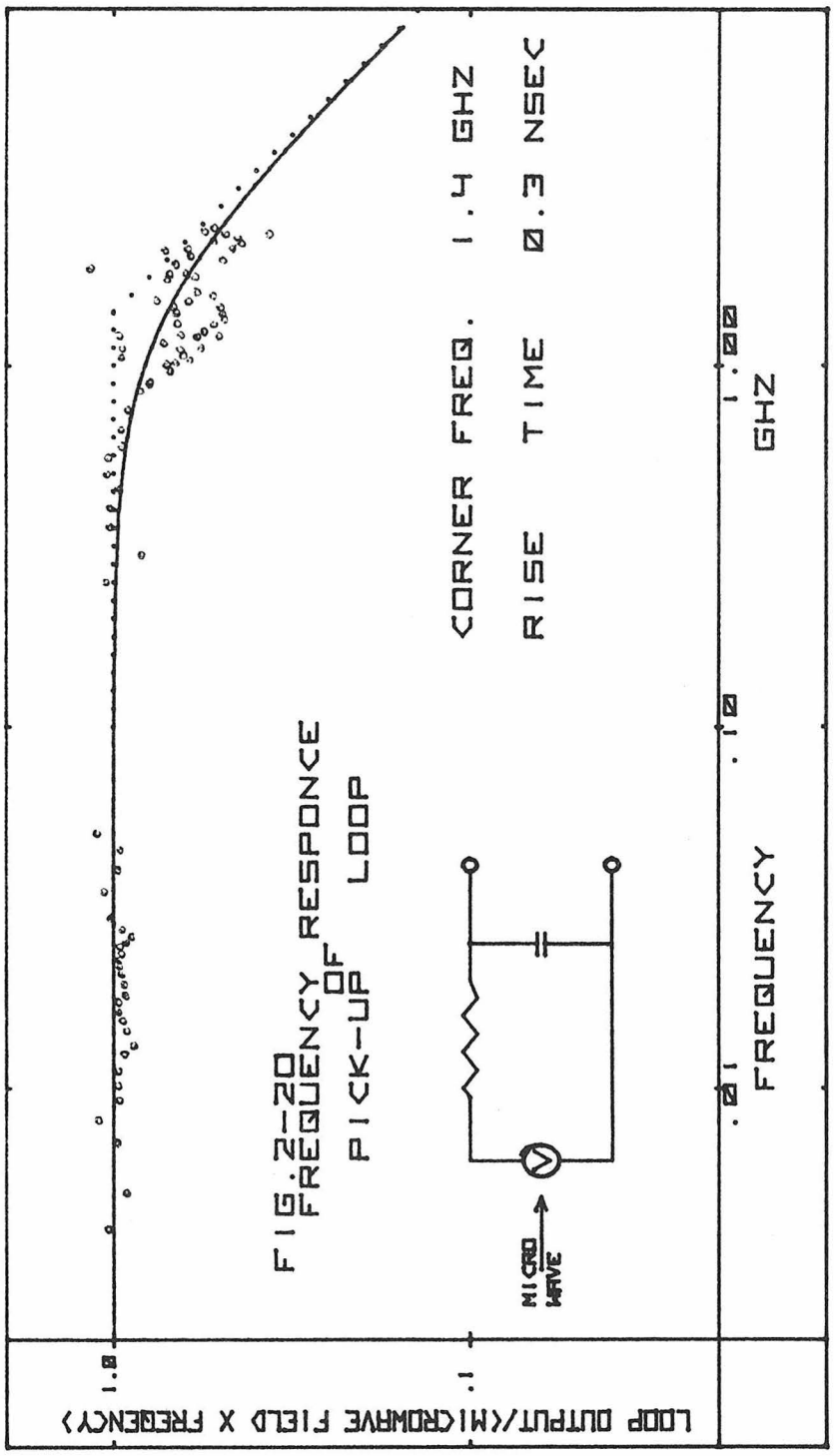

FIG. 2-20
FREQUENCY RESPONCE OF PICK-UP LOOP

in Fig. 2-20. Typical examples of the calculated waveform are shown in Fig. 2-21 for the same sample 18-19-4 that was discussed in the previous section. The waveforms for a pulse field of 1.4 H_k and 2.9 H_k are shown in Fig. 2-21 a and b, respectively. The transverse bias field of 0.1 H_k was applied in each reversal.

For the applied field of 1.4 H_k, a recognizable resemblance exists between the experimental and calculated transverse flux waveforms, shown respectively by the broken and dotted lines in Fig. 2-21a. Both experimental and calculated waveforms are characterized by a damped oscillation during the approach to the final level. However, the quantitative agreement between the experimental and calculated waveform is poor. The switching time determined by the calculated waveform is 2.1 nsec; whereas, the actual switching time is 4.9 nsec.

For the applied field of 2.9 H_k, improved agreement was again obtained between the experimental and calculated transverse flux waveforms as shown respectively by the broken and dotted lines in Fig. 2-21b. The amplitude of the damped oscillation of the calculated waveform is nearly equal to that of the experimental waveform; whereas, the waveform calculated without considering the pick-up loop frequency response showed a damped oscillation of exceedingly large amplitude. The quantitative agreement between the experimental and calculated waveforms is still unsatisfactory.

2.3.5 Thickness Dependence of Transverse Flux Waveform

The thickness dependence of the transverse flux waveform was investigated using 83 Ni-17 Fe films of various thickness from 351 Å to 1867 Å. The melt composition of 83 Ni-17 Fe wt.% was chosen to

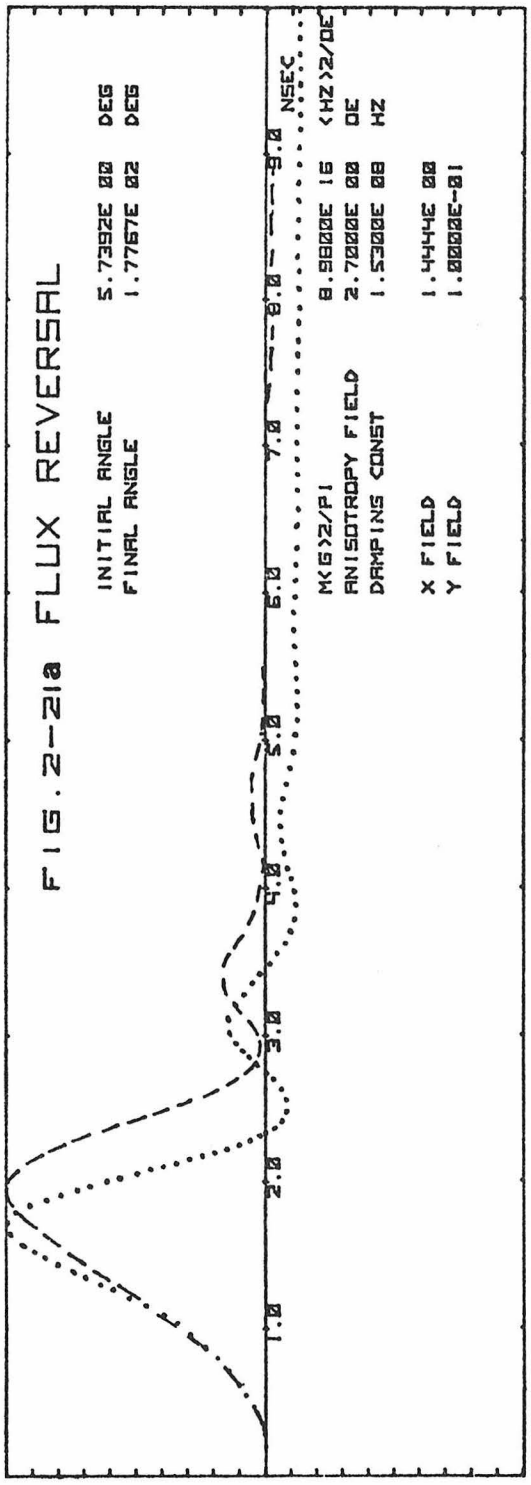
FIG. 2-21a FLUX REVERSAL
INITIAL ANGLE 5.7392E 00 DEG
FINAL ANGLE 1.7767E 02 DEG
MG*2/PI 8.9800E 15 <HZ**2/OE
ANISOTROPY FIELD 2.7000E 00 OE
DAMPING CONST 1.5300E 08 HZ
X FIELD 1.4444E 00
Y FIELD 1.0000E-01
1.0
2.0
3.0
4.0
5.0
6.0
7.0
8.0
9.0
NSEC

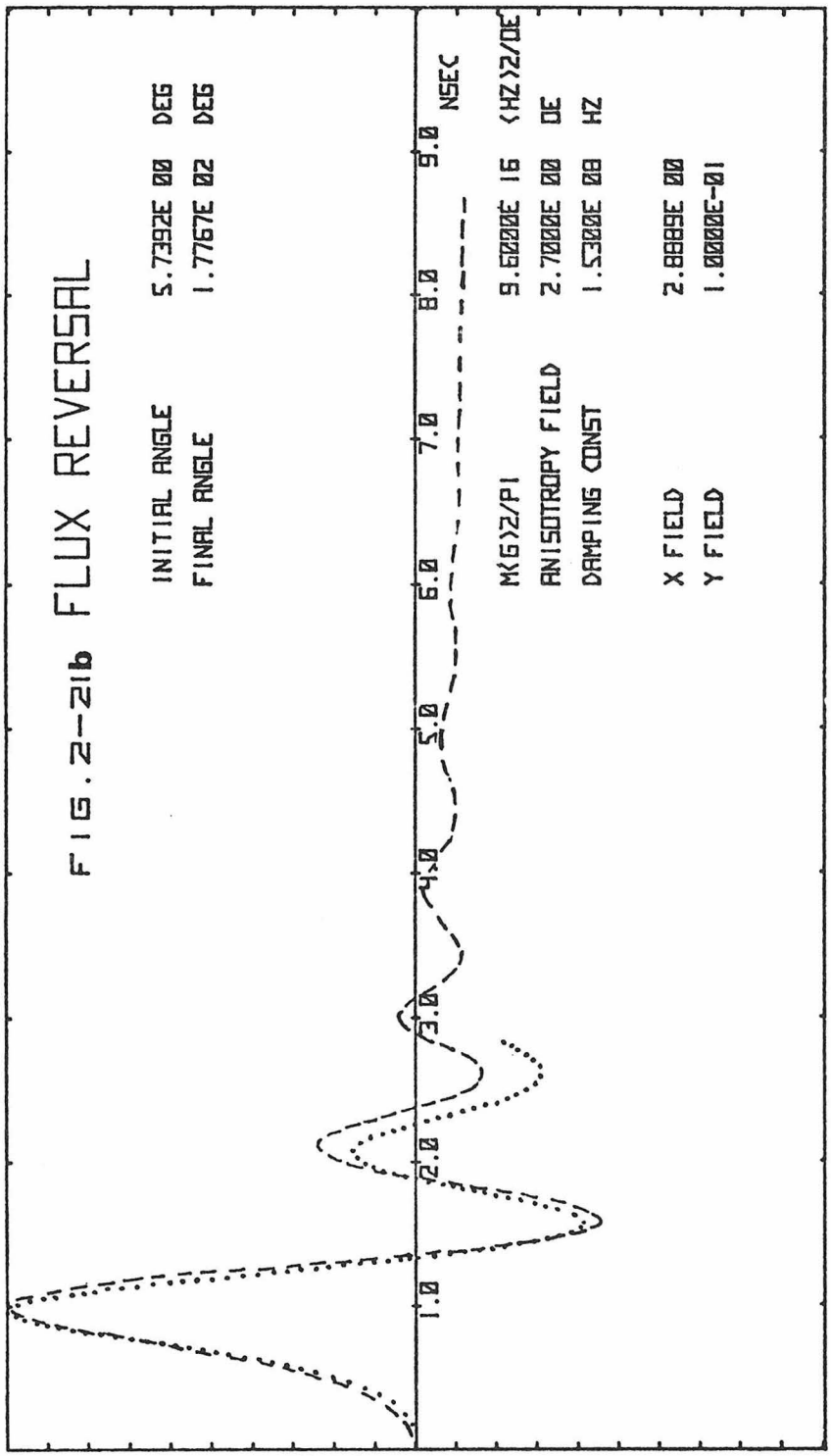
FIG. 2-21b FLUX REVERSAL
INITIAL ANGLE 5.7392E 00 DEG
FINAL ANGLE 1.7767E 02 DEG
1.0
2.0
3.0
4.0
5.0
6.0
7.0
8.0
9.0
NSEC
M(G)2/PI 9.6000E 15 (HZ)2/OE
ANISOTROPY FIELD 2.7000E 00 OE
DAMPING CONST 1.5300E 08 HZ
X FIELD 2.8888E 00
Y FIELD 1.0000E-01

avoid possible complications arising from the magnetostrictive effect commonly observed at other compositions. The films were evaporated in vacuum of 10^{-7} Torr onto glass substrates heated at 200°C. The substrate temperature of 200°C was chosen to obtain small values of anisotropy dispersion. The film thickness, the anisotropy field, the coercive force, the angular dispersion, and the damping constant, are listed for each film in Table 2-1. The damping constant was obtained by ferromagnetic resonance.

No.	Sample Code	t[Å]	H_k[Oe]	H_c[Oe]	α_{90}[deg]	λ[GHz]
A	38-31- 3	351	5.4	2.0	1.0	0.117
B	38-30- 3	640	5.6	1.7	1.1	0.127
C	38-31- 7	955	5.6	2.5	2.0	0.129
D	38-30- 7	1228	5.7	1.9	1.3	0.140
E	38-30-11	1832	5.5	1.4	3.3	0.162
F	38-31-11	1867	5.1	2.0	4.4	0.242

Table 2-1

The damping constant is shown as a function of film thickness in Fig. 2-22. It can be seen that the damping constant increases with thickness. The increase is superimposed on a constant part of 0.116 GHz considered to be the intrinsic damping constant. The thickness dependent part can be attributed to the eddy current damping due to the motion of magnetization. This part is given by

$$\lambda_{edd}(t) = \frac{(4\pi M)^2 \gamma^2}{12\rho} \times 10^{-26}\, t^2 \quad , \qquad (2\text{-}34)$$

where M is the saturation magnetization in Oe, γ is the gyromagnetic ratio, 1.76×10^7 [rad-Oe^{-1}-sec^{-1}], t is the film thickness in Å and

ρ is the resistivity in $\mu\Omega$-cm. A uniform distribution of the magnetization across the film thickness was assumed (Smith 1963). The resistivity is also a function of thickness and can be given by

$$\rho(t) = \rho_0 \left\{ 1 - \frac{3\, l_0}{t} \int_0^{\pi/2} [1 - \exp(-t/l_0 \cos\theta)] \sin^3\theta \cos\theta \, d\theta \right\}^{-1} , \quad (2\text{-}35)$$

where ρ_0 is the intrinsic resistivity and l_0 is the mean free path of electrons, assuming diffuse scattering of electrons at film surfaces (Fuchs, 1938). Using the values of ρ_0 = 26 $\mu\Omega$-cm, l_0 = 225 Å, and the intrinsic damping constant of 0.116 GHz, the damping constant was calculated as a function of thickness and is shown by the solid line in Fig. 2-22. The use of 26 $\mu\Omega$-cm for polycrystalline Ni-Fe film is reasonable considering that the resistivity of a single crystal Ni-Fe film is 14 $\mu\Omega$-cm (Mayadas, et al., 1974). The experimental data points were well fitted by the calculated curve. The slow increase in damping is due to the effect of eddy currents. The abrupt change shown by the experimental point at 1867 Å is in agreement with the abrupt increase in dispersion discussed later.

The thickness dependence of the transverse flux waveform can be understood by comparing the experimental waveform with the calculated waveform. The waveforms for samples A and E are shown in Fig. 2-23 a and b, respectively, where the experimental waveforms are shown by the broken lines and those calculated are shown by the dotted lines. All the waveforms are for the pulse field of $2H_k$ applied along the easy axis and the transverse bias field of 0.1 H_k. The calculations were made using Eq. (2-21) with the value of λ obtained by

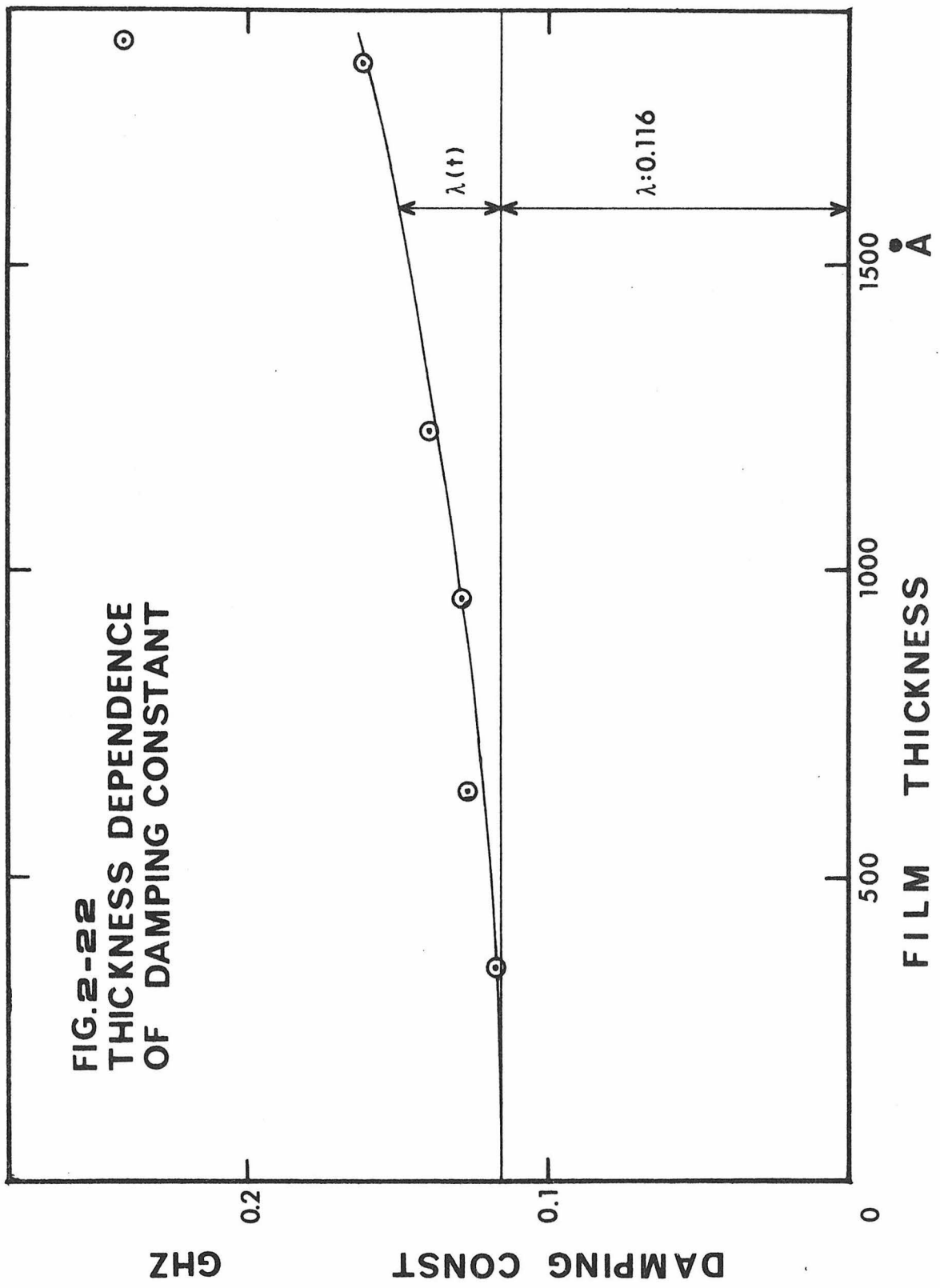
FIG.2-22
THICKNESS DEPENDENCE
OF DAMPING CONSTANT
DAMPING CONST GHZ
0.2
0.1
0
500
1000
1500
Å
FILM THICKNESS
λ(t)
λ:0.116

resonance. The effect of a finite frequency response for the pick-up loop was included. For thickness 351 Å, the experimental waveform, A, and the calculated waveform, A', agree well as can be seen in Fig. 2-23a. Similar agreement was also found for thickness 640, 955 and 1228 Å. For thickness 1832 Å, however, the agreement is poor as can be seen in Fig. 2-23b, where the calculated waveform, E', shows a clear oscillation and the experimental waveform, E, shows no trace of oscillation. It is interesting to note that this discrepancy can be correlated to the abrupt increase of anisotropy dispersion. The angular dispersion as a function of film thickness is shown in Fig. 2-24. It can be seen that the dispersion increases slowly until about 1200 Å and then increases abruptly. It is in this region where the large discrepancy is seen. The use of Eq. (2-21) tacitly assumes coherent rotation. Therefore, it is strongly suggested that the large dispersion inhibits coherent rotation. Hence, it is not surprising that the agreement for the 1832 Å point is poor.

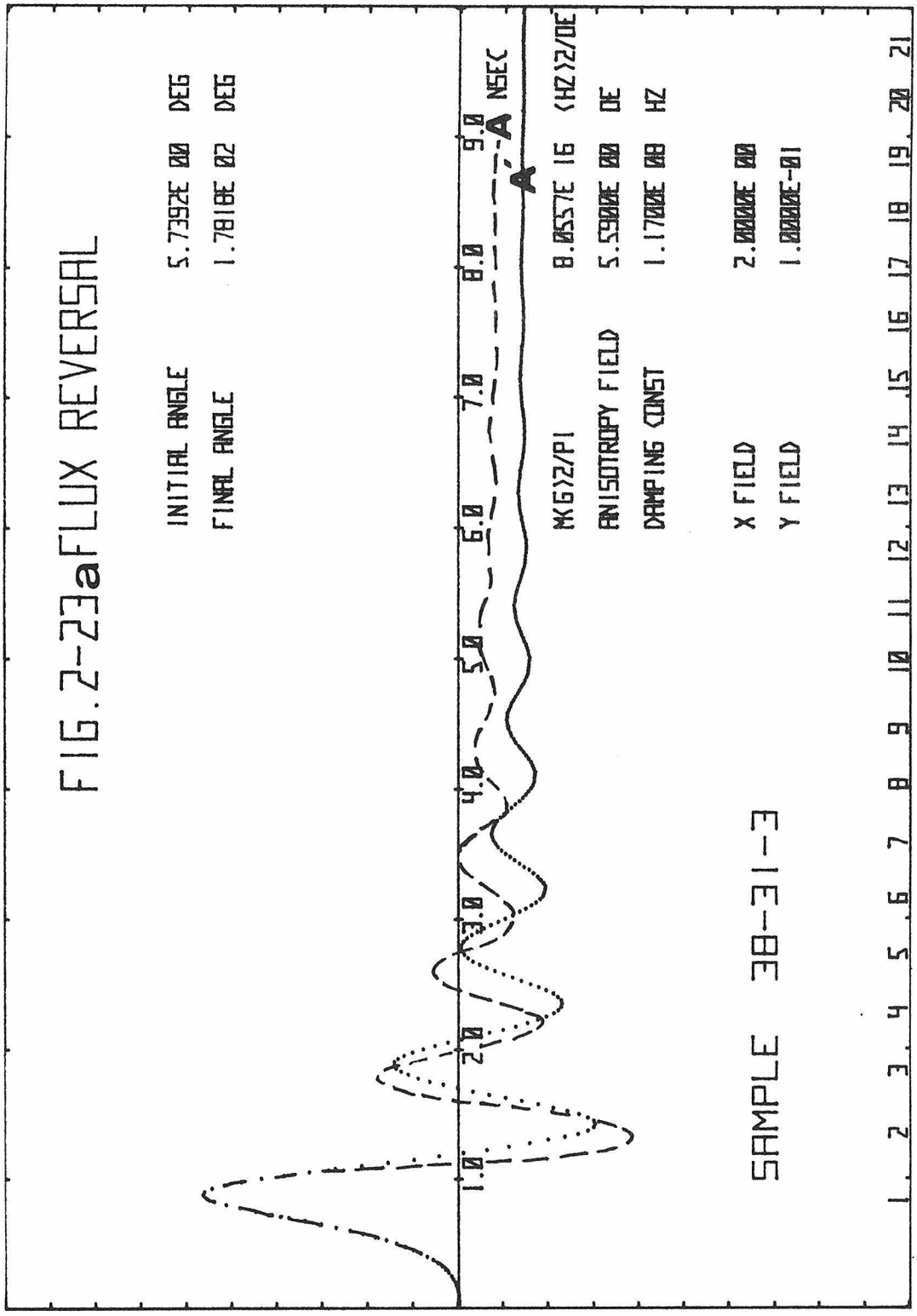
FIG. 2-23a FLUX REVERSAL
INITIAL ANGLE 5.73926 00 DEG
FINAL ANGLE 1.78186 02 DEG
A
A' NSEC
MG)2/PI 8.05576 16 (HZ)2/OE
ANISOTROPY FIELD 5.53006 00 OE
DAMPING CONST 1.17006 00 HZ
X FIELD 2.00006 00
Y FIELD 1.00006-01
SAMPLE 38-31-3

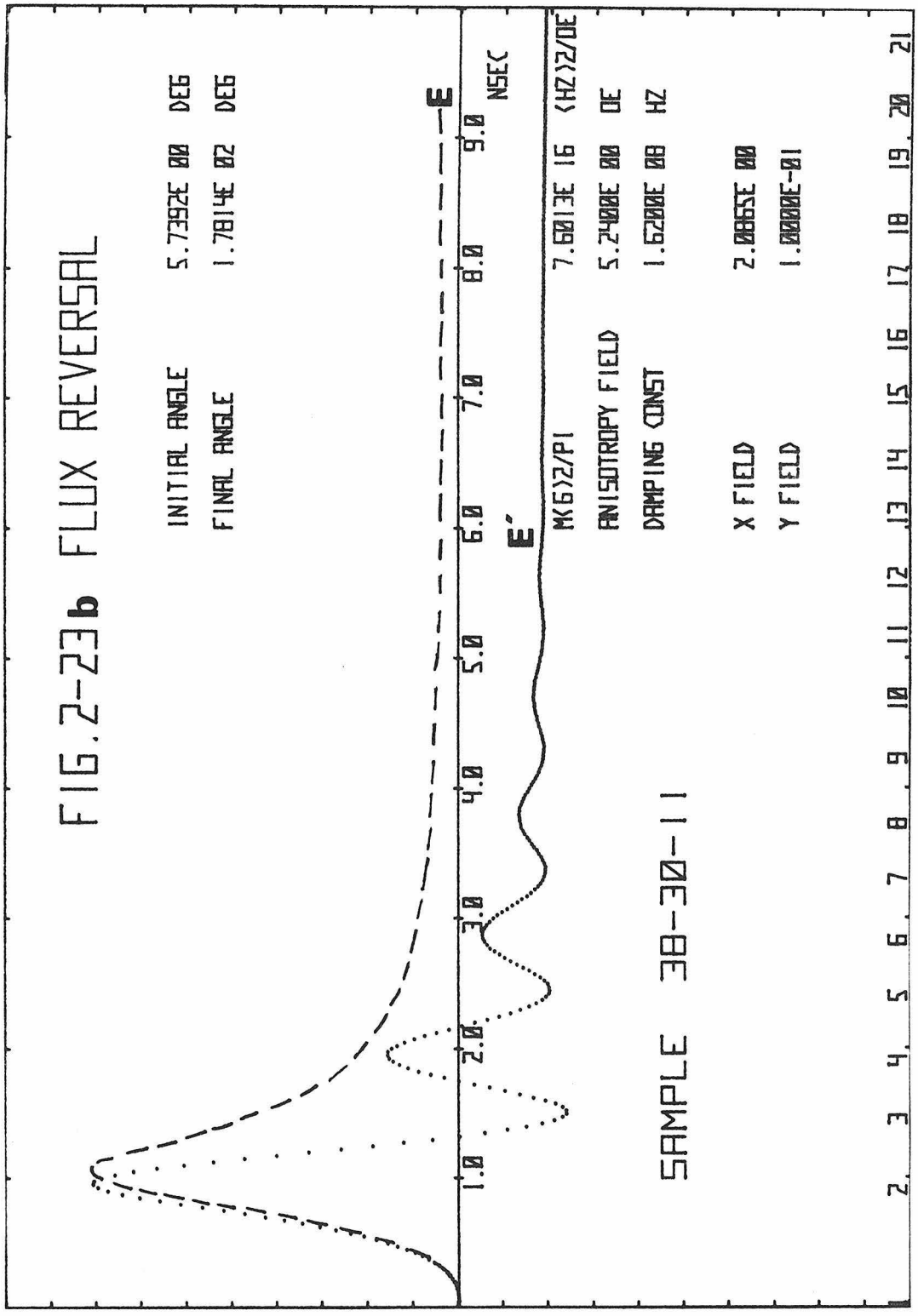
FIG.2-23b FLUX REVERSAL
INITIAL ANGLE 5.73925 00 DEG
FINAL ANGLE 1.78145 02 DEG
E
E'
NSEC
MG)2/PI 7.6013E 16 (HZ)2/OE
ANISOTROPY FIELD 5.2400E 00 OE
DAMPING CONST 1.6200E 00 HZ
X FIELD 2.0855E 00
Y FIELD 1.0000E-01
SAMPLE 38-30-11

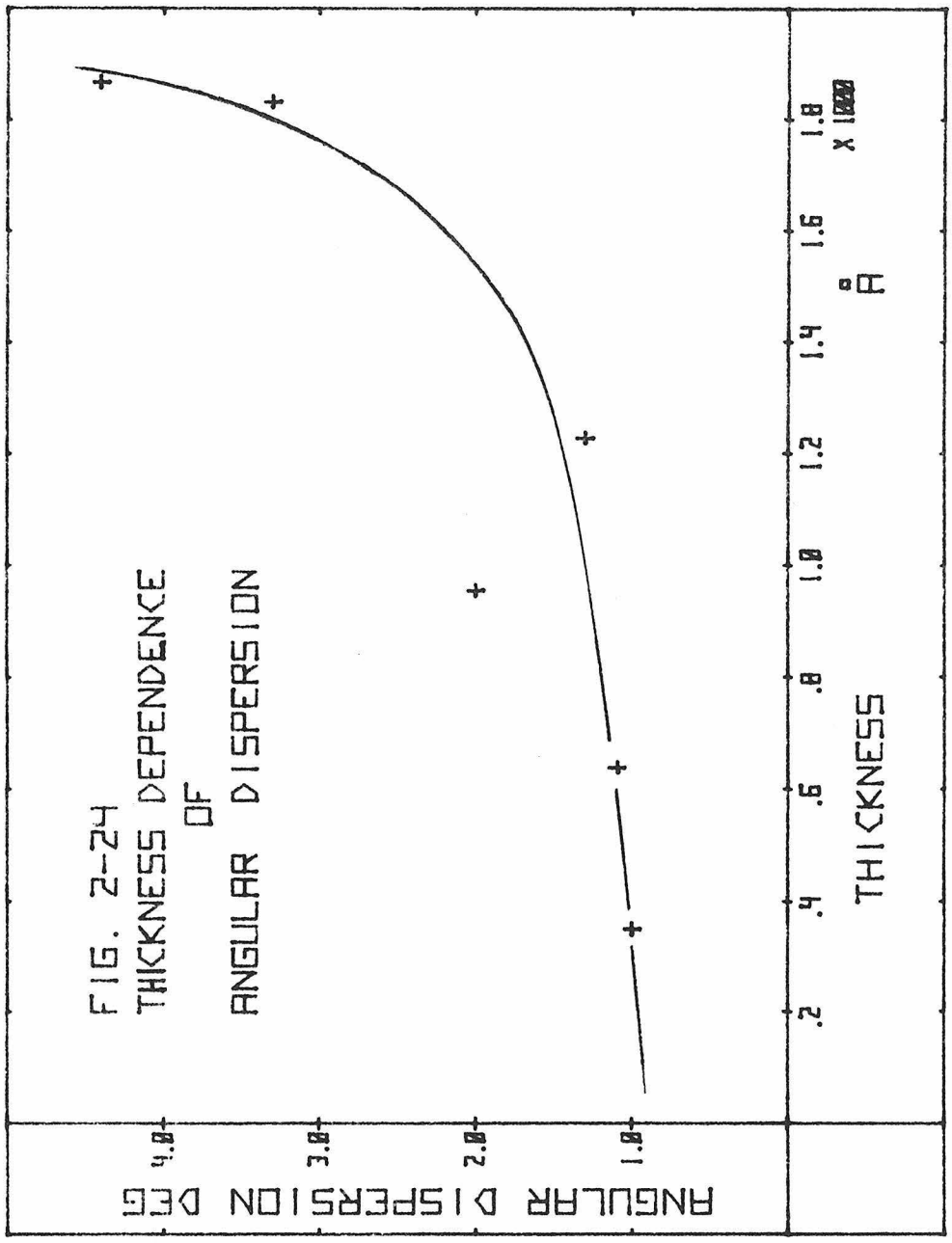
FIG. 2-24
THICKNESS DEPENDENCE
OF
ANGULAR DISPERSION
ANGULAR DISPERSION DEG
4.0
3.0
2.0
1.0
.2
.4
.6
.8
1.0
1.2
1.4
1.6
1.8
THICKNESS
A

2.2.5 Summary

For applied fields much larger than the coherent rotation threshold field and with small dispersions (α_{90}), the transverse flux waveform can be described by Eq. (2-21). If the frequency response of the pick-up loop is considered, the description is better. For these fields, the damped free oscillation can be clearly seen. For fields near the threshold, the experimental waveform indicates a slower reversal than the calculated waveform. For smaller fields, the differences increase considerably. Dispersion has a critical effect on the reversal; the larger dispersion films show slower reversals and no oscillation. Eddy currents have only a slight effect on the damping and no effect on the waveforms.

Chapter 3

DAMPED FREE OSCILLATION OF THE MAGNETIZATION IN Ni-Fe THIN FILMS

3.1 Introduction

3.1.1 General

Free oscillation of the magnetization can be excited in Ni-Fe films when the direction of magnetization is suddenly changed by the application of a magnetic field pulse. The magnetization oscillates around its new equilibrium direction approaching it exponentially with time. A typical example is the oscillation at the completion of 180° flux reversal. Damped free oscillation can be investigated by detecting the voltage induced in a pick-up loop around the film. The frequency of the oscillation is related to the total effective field. This field is composed of the pulse and bias fields, the effective field due to the anisotropy and the demagnetizing field normal to the film plane. The exponential decay of the oscillation is a measure of how fast the oscillating spin system can release its energy. Therefore, the damping constant, for example λ in the Landau-Lifshitz equation, can be determined from the decay of the oscillation.

Steady state oscillation can be excited around a constant field when a microwave field is applied perpendicularly to it. For the in-plane resonance, both fields are applied in the film plane. At resonance, the frequency is determined by the applied field, the effective field due to the anisotropy and the demagnetizing field normal to the film plane. The damping constant is determined by the resonance linewidth.

Comparison of the frequencies of damped free and forced oscillations should lead to a better understanding of the contribution of the applied field, the effective field due to the anisotropy, and the demagnetizing field. Comparison of the damping constants should lead to a better understanding of the damping mechanism, since the amplitudes of those oscillations are quite different.

3.1.2 Theory

To analyze the free oscillation and the in-plane resonance, the dynamic equation of the magnetization

$$\frac{d^2\phi}{dt^2} + 4\pi\lambda \frac{d\phi}{dt} + 4\pi\gamma^2 MH_k(\sin\phi\cos\phi - h_s\sin\phi + h_\perp\cos\phi) = 0 \quad , \qquad (2\text{-}21)$$

derived in the previous chapter will be used.

This equation was derived from the Landau-Lifshitz equation, assuming the conservation of magnetization. Damped free oscillation of the magnetization at the completion of a 180° flux reversal should be due to coherent rotation since the pulse and transverse bias fields are applied uniformly over the film surface and therefore uniformly over all spins. The oscillation of magnetization in the in-plane resonance experiment should be also due to coherent oscillation since the constant and transverse microwave fields are applied uniformly over the film surface. Therefore, Eq. (2-21) is applicable to the analysis of both damped free oscillation and resonant oscillation.

Equation (2-21) can be linearized in the vicinity of a given reference direction. The direction of magnetization is expressed by

$$\phi = \phi_o + \delta \quad , \qquad (3\text{-}1)$$

where ϕ_o is the reference direction, and δ is the deviation from the reference angle and $\delta << 1$. Equation (2-21) then becomes

$$\frac{d^2\delta}{dt^2} + 4\pi\lambda \frac{d\delta}{dt} + 4\pi\gamma^2 MH_k(\cos 2\phi_o + h_s \cos\phi_o + h_\perp \sin \phi_o)\, \delta$$

$$= 4\pi\gamma^2 MH_k(\sin \phi_o \cos \phi_o + h_s \sin \phi_o - h_\perp \cos \phi_o) \quad . \qquad (3\text{-}2)$$

Thus Eq. (2-21) is in a more convenient form to be applied to various cases of oscillation.

Damped free oscillation at the completion of 180° flux reversal can be analyzed by Eq. (3-2) after the oscillation amplitude becomes small. For the oscillation after the reversal along the easy axis, the solution is:

$$\delta(t) = \delta(o) \frac{\sqrt{\omega^2 + (4\pi\lambda)^2}}{\omega} e^{-2\pi\lambda t} \sin(\omega t + \alpha) \sim$$

$$\delta(o) e^{-2\pi\lambda t} \sin(\omega t + \alpha) \quad , \qquad (3\text{-}3)$$

where

$$\omega^2 = 4\pi\gamma^2 MH_k(1 + |h_s|) - (2\pi\lambda)^2 \quad , \qquad (3\text{-}4)$$

and

$$\sin \alpha = \frac{\omega}{\sqrt{\omega^2 + (2\pi\lambda)^2}} \sim 1 \quad ,$$

with

$$h_s = \text{const.}, \qquad h_\perp << 1, \qquad \text{and} \qquad \phi_o = \pi$$

This solution indicates that the magnetization oscillates around its equilibrium direction, and that the oscillation decays exponentially. It is thus possible to calculate analytically the frequency and the damping constant from the damped free oscillation.

For the oscillation after the reversal along the hard axis, the solution is:

$$\delta(t) = \delta(0)\frac{\sqrt{\omega^2 + (2\pi\lambda)^2}}{\omega} e^{-2\pi\lambda t} \sin(\omega t + \alpha) \sim \delta(0) e^{-2\pi\lambda t} \sin(\omega t + \alpha) \quad , \qquad (3\text{-}5)$$

where

$$\omega^2 = 4\pi\gamma^2 M H_k (|h_s| - 1) - (2\pi\lambda)^2 \quad , \qquad (3\text{-}6)$$

and

$$\sin\alpha = \frac{\omega}{\sqrt{\omega^2 + (2\pi\lambda)^2}} \sim 1$$

In-plane resonance oscillation can also be analyzed by Eq. (3-2). For the oscillation around the easy axis, Eq. (3-2) becomes

$$\frac{d^2\delta}{dt^2} + 4\pi\lambda \frac{d\delta}{dt} + 4\pi\gamma^2 M H_k (1 + h_s)\delta = -4\pi\gamma^2 M H_k h_\perp \quad , \qquad (3\text{-}7)$$

where the reference angle ϕ_o is taken as $\phi_o = 0$. The steady state solution of the above equation is given by

$$\delta = \frac{4\pi\gamma^2 M H_k}{[-\omega^2 + j4\pi\lambda\omega + 4\pi\gamma^2 M H_k (1 + h_s)]} h_\perp \quad . \qquad (3\text{-}8)$$

If the oscillation is detected by a pick-up loop whose plane is aligned in parallel with the constant field, the power generated in the loop is:

$$P = \frac{K^2 h_o{}^2 M^2}{2Z_o} \cdot \frac{(4\pi\gamma^2 M H_k \omega \cos \phi_o)^2}{(\omega_o{}^2 - \omega^2)^2 + (4\pi\lambda\omega)^2}$$

$$= P_{max} \cdot \frac{1}{1 + (\frac{\omega_o}{4\pi\lambda})^2 (\frac{\omega}{\omega_o} - \frac{\omega_o}{\omega})^2} \quad , \qquad (3\text{-}9)$$

where

$$\omega_o{}^2 = \gamma^2 4\pi M(H_s + H_k) \quad , \qquad (3\text{-}10)$$

- K is a coupling constant between the magnetic flux and the pick-up loop,
- h_o is the peak value of the microwave field,
- Z_o is the characteristic impedance of the transmission line,

and

- ω is the angular frequency of the microwave field.

Similar equations can be obtained for the field applied along the hard axis; in this case, $+H_k$ must be replaced by $-H_k$.

The normalized power is plotted as a function of the applied field for a fixed ω in Fig. 3-1. It can be seen that the power is maximum when the condition $\omega_o = \omega$ is satisfied. In Fig. 3-2, the

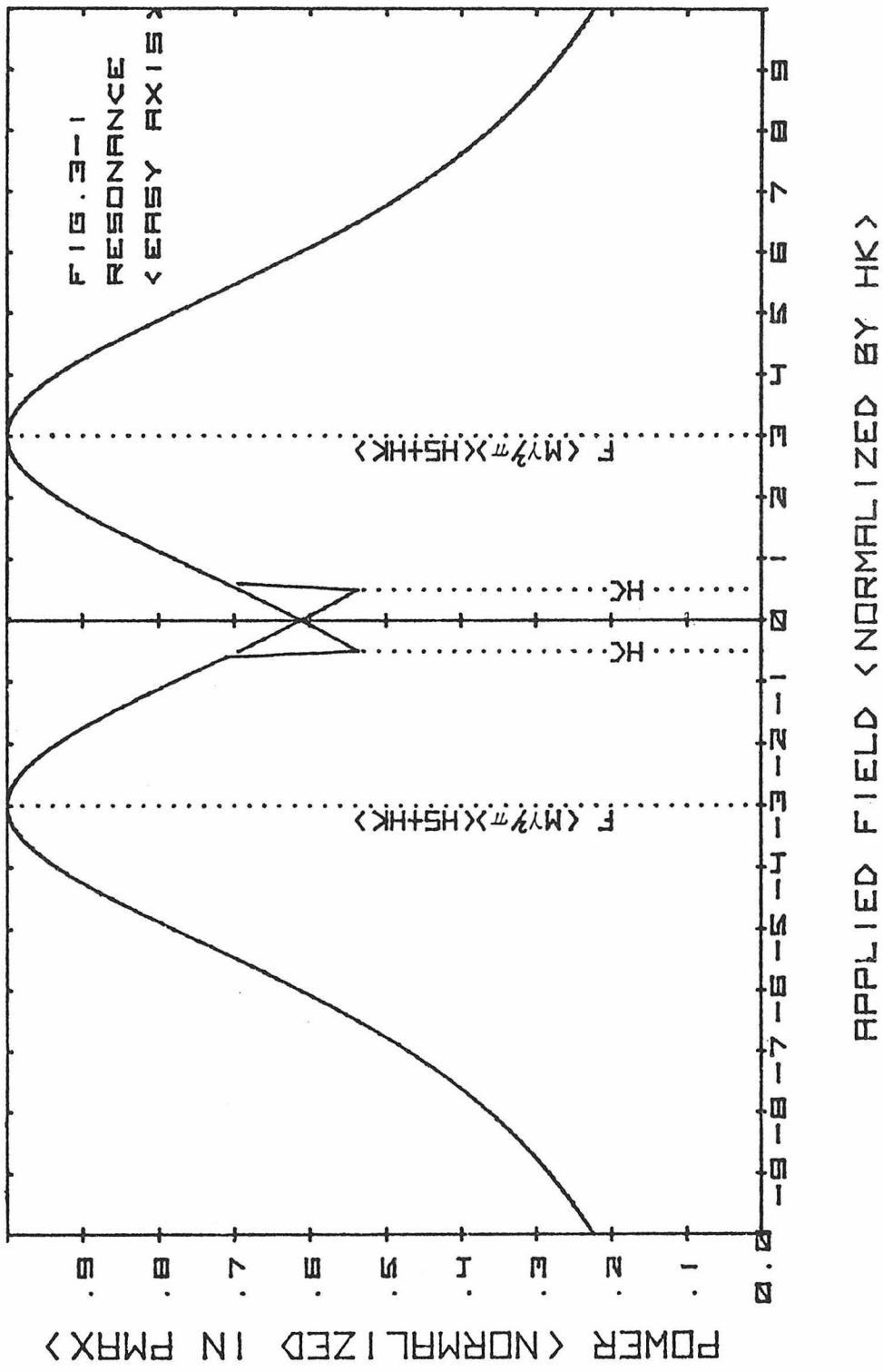
FIG.3-1
RESONANCE
<EASY AXIS>
F <MγγπX><HS+HK>
HC
HC
F <MγγπX><HS+HK>
POWER <NORMALIZED IN PMAX>
APPLIED FIELD <NORMALIZED BY HK>

normalized power is plotted as a function of the applied field with frequency as a parameter. It can be seen that the resonant peak shifts quadratically to higher fields as the frequency increases.

The damping constant can be calculated from the resonance curve. According to the Eq. (3-9), the half power points are given by

$$\frac{1}{1 + \left(\frac{\omega_o}{4\pi\lambda}\right)^2 \left(\frac{\omega}{\omega_o} - \frac{\omega_o}{\omega}\right)^2} = \frac{1}{2}$$

The half power linewidth ΔH_s is

$$\Delta H_s = \frac{\Delta(\omega_o^2)}{4\pi\gamma^2 M} = \frac{2\omega}{\gamma^2 M}\lambda \quad . \qquad (3\text{-}11)$$

or in terms of damping

$$\lambda = \frac{\gamma^2 M}{2\omega}\Delta H_s \quad . \qquad (3\text{-}12)$$

With the damping constant λ as a parameter, the in-plane resonance curve is shown in Fig. 3-3. It can be seen that the half power linewidth increases linearly as the damping constant increases.

It has been shown that the frequency and damping of the damped free and forced resonance oscillations can be described by the same equation by assuming that both oscillations are due to coherent rotation. In fact, the frequency of both oscillations show the same quadratic relationship with applied field. The damping of these

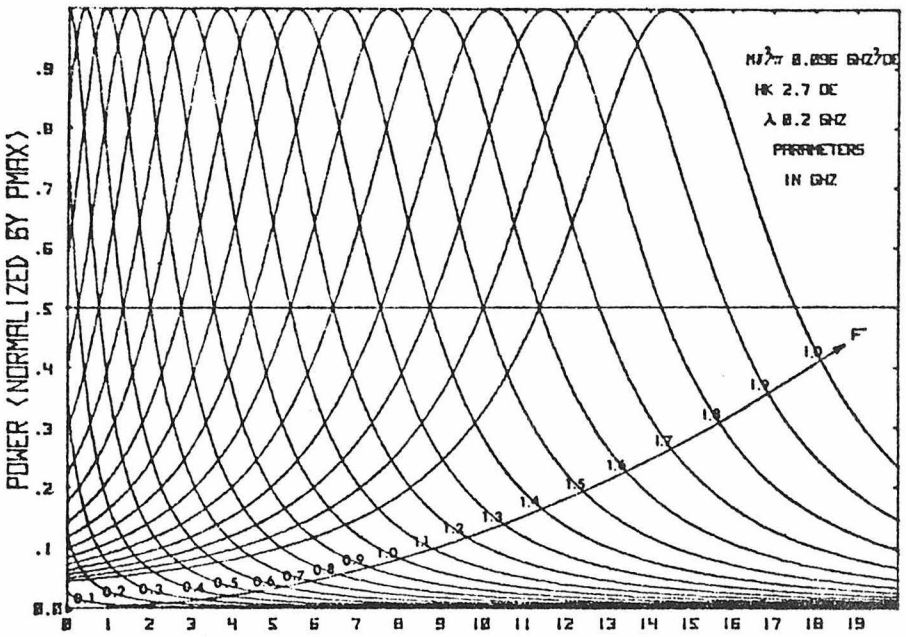

FIG.3-2 RESONANCE (ALONG EASY AXIS)

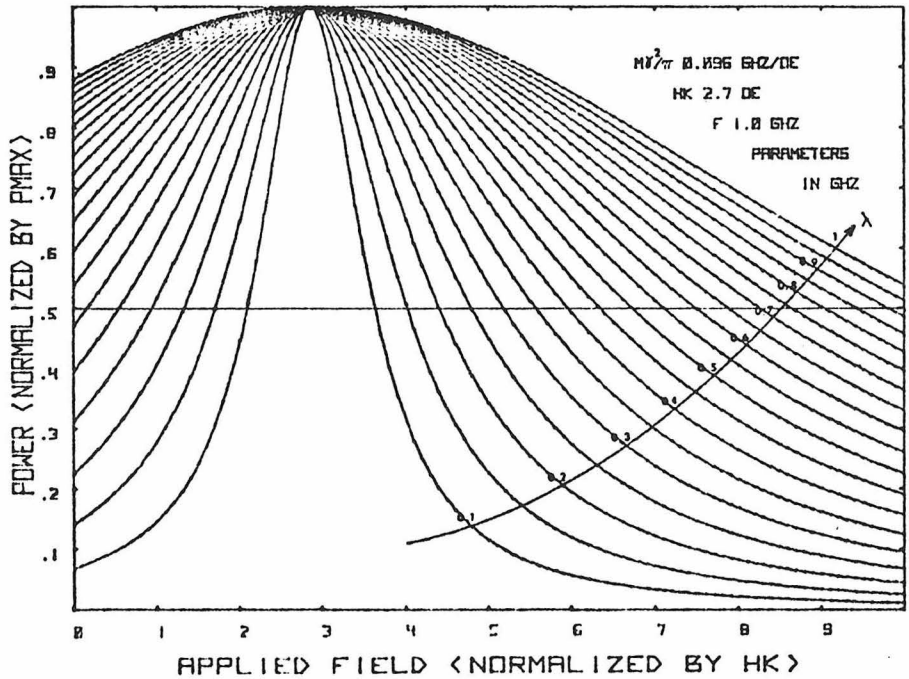

FIG.3-3 RESONANCE (ALONG EASY AXIS)

oscillations can be described using the same constant λ.

3.1.3 Previous Investigations

Oscillation of the magnetization in Ni-Fe films at the completion of a 180° reversal along the easy axis was predicted by Smith (1958, Sec. 2.1.3.1). Observation of the oscillation was, however, beyond the experimental capability of the time. The first experimental observation was made by Dietrich, Proebster and Wolf (1960) in conjunction with a study of other aspects of reversal. They suggested, in passing, that the oscillation was ferromagnetic resonance excited by the driving field pulse (Sec. 2.1.3.1).

The first systematic study of free oscillation was small angle oscillation by Wolf (1960-1961). The oscillation was excited around a constant magnetic field by applying a small field pulse perpendicular to the constant field. The investigation compared this oscillation with in-plane resonance, i.e., forced steady state oscillation. The results of this study are summarized in Fig. 3-4. Oscillation frequency (squared) is shown as a function of applied field in Fig. 3-4a for the oscillation along both the easy and hard axis. The corresponding curves for the resonance are also shown. The results were analyzed on a basis of Eq. (2-21); and the general agreement with the theory was good. However, two difficulties with the theory were noticed. First, for the oscillations along the easy axis, the slope of the f^2-H_s curve for the free oscillation does not agree with that for resonance. Secondly, the f^2-H_s curve for the free oscillation along the hard axis does not intersect at $+H_k$, which it should according to Eq. (2-21). Unfortunately, the seriousness of these difficulties was uncertain, because the observation was at the limit of the accuracy. The damp-

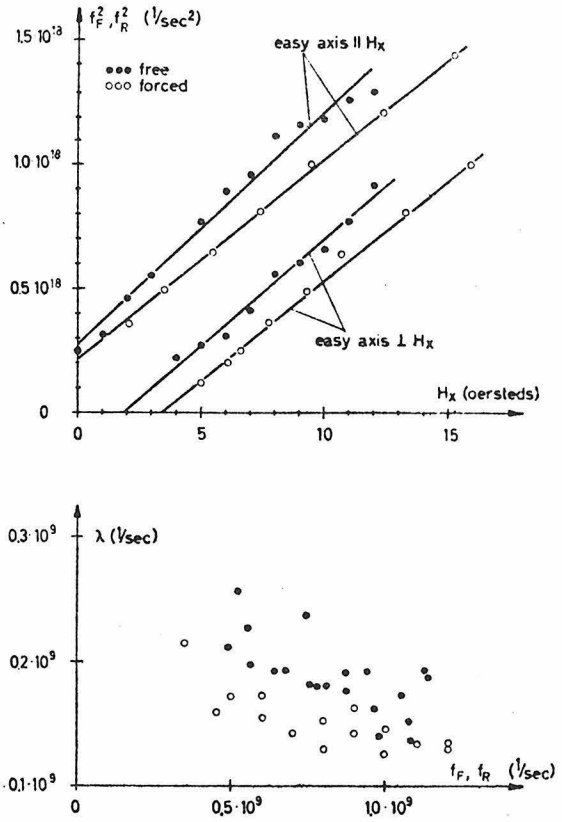

(a) Frequency f_F of free oscillations and resonance frequency f_R of ferromagnetic resonance as a function of the dc field H_x and two orientations of the easy axis. Film 230 *B*3, 1180 *A* thick, H_k=3.0 oe, H_o=1.8 oe. (b) Damping factor λ obtained from free oscillations and ferromagnetic resonance as a function of the oscillation frequency f_F and the resonance frequency f_R, respectively.

Fig. 3-4 (after Wolf)

ing parameter was calculated from the decay of the oscillation and was compared with that obtained from in-plane resonance. The damping parameter is shown in Fig. 3-4b as a function of the frequency. The parameter is a decreasing function of the frequency for both the free oscillation and the resonance. This characteristic is similar to those obtained for resonance (Smith, 1958; Hasty and Boudreaux, 1961). As to the value of the damping parameter, Eq. (2-21) predicts the same value for both the free oscillation and the resonance. With an error of 30~50%, the experimental results agree with this prediction. The small angle free oscillation was also studied by Hearn (1964). His results are quite similar to Wolf's.

Free oscillation was observed also at the completion of 90° switching (Hearn,1964). The experiment was to reorient the magnetization from the easy axis to the hard axis. The result was analyzed by using Eq. (2-21). The qualitative agreement with the theory was good. He did, however, have typically 25% discrepancies in the observed frequencies.

Free oscillation at the completion of 180° reversal was investigated for the first time in detail by Suezawa and Humphrey (1972). The oscillation was observed both along the easy and the hard axis. The f^2 vs. H curves were similar to those obtained for the small angle oscillation, but better agreement was found between the free oscillation and resonance. The damping parameter obtained from the decay of the free oscillation was in good agreement with that obtain from resonance. The accuracy for their method is better than other methods, since the oscillation is observed for many cycles. It was

pointed out that the measurement was to be made after the oscillation amplitude becomes small.

3.2 Experimental Method

3.2.1 The Damped Free Oscillation

3.2.1.1 The Observation of the Damped Free Oscillation

For the observation of free oscillation at the completion of 180° magnetization reversal, the experimental arrangement is the same as that used for the 180° magnetization reversal experiment (Sec. 2.2.1). If the reversal is along the easy axis, the film is first saturated in one easy direction. A small bias field is applied along the hard axis so that the magnetization is in equilibrium at a small angle from the easy axis. The magnetic field pulse is then applied along the other easy direction. The magnetization, therefore, reverses towards a new equilibrium, and oscillation can be observed as it approaches this new equilibrium. For reversal along the hard axis, a constant magnetic field of magnitude larger than H_k is applied along a hard direction. A small bias magnetic field is also applied along the easy axis so that the magnetization is initially at an angle from the hard direction. The magnetic field pulse is then applied along the other hard direction. The magnetization then reverses towards a new equilibrium and oscillation can be observed as it approaches this new equilibrium. Since the oscillation can be most sensitively detected normal to the field pulse, the transverse flux waveforms are observed. The pick-up loop is aligned along the easy or the hard axis to detect the oscillation along the respective axis.

3.2.1.2 The Period Measurement and the Frequency Calculation.

The frequency of the damped free oscillation is obtained directly from the transverse flux waveform. The oscillation can be expressed by;

$$\delta(t) = \delta_0 e^{-2\pi\lambda t}\sin((2\pi/T)t + \alpha) \quad , \qquad (3\text{-}13)$$

where

$$\alpha = \sin^{-1} f/\sqrt{\lambda^2 + f^2}$$

and λ is the damping constant, T is the period and δ_0 is a constant. An example of the calculated oscillation is shown in Fig. 3-5, for λ = 0.2 GHz and T =1nsec. The envelope (shown by dotted lines) of the damped free oscillation is;

$$\delta(t) = \pm\delta_0 e^{-2\pi\lambda t}. \quad , \qquad (3\text{-}14)$$

This envelope is tangent to the oscillation at points where

$$\frac{2\pi}{T} t'_m + \alpha = m + \frac{\pi}{2} \; (m = 0,1,2, \ldots) \quad ,$$

i.e.

$$t'_m = \frac{T}{2} m + \frac{T}{2}\left(\frac{1}{2} - \frac{\alpha}{\pi}\right) \quad . \qquad (3\text{-}15)$$

The frequency can then be calculated as

$$f = \frac{1}{T} = \frac{1}{(t_{m+2} - t_m)} \quad . \qquad (3\text{-}16)$$

However, the calculation of the frequency by this method lacks accuracy since the tangential points are difficult to locate experimentally.

The frequency can also be calculated using the oscillation peaks. The peak positions are;

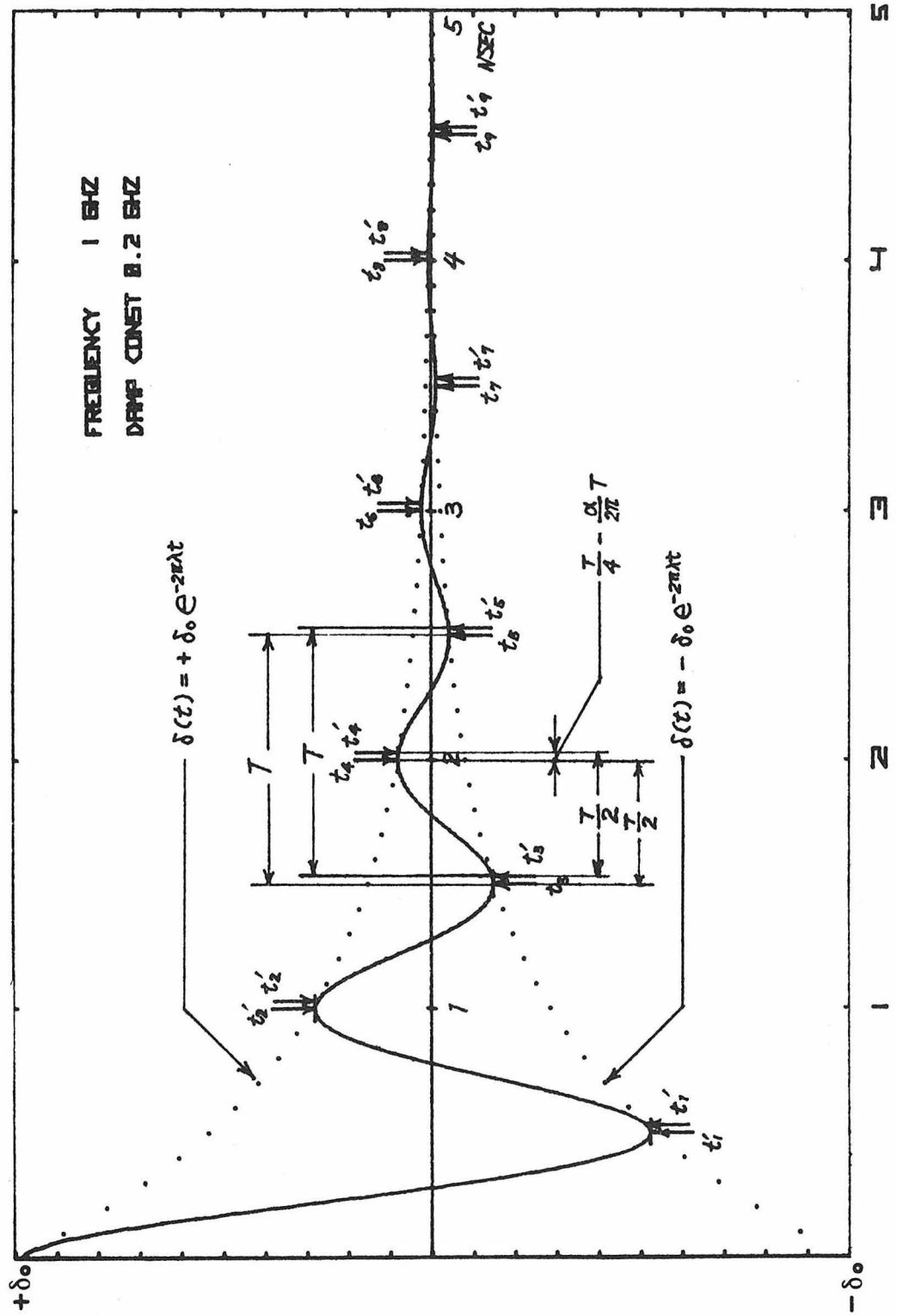

FIG. 3-5
OCILLATION PERIOD AND DAMPING CONSTANT

$$\frac{2\pi}{T} t_m = m \qquad (m = 0,1,2, \ldots) \quad , \qquad (3\text{-}17)$$

i.e.

$$t_m = \frac{T}{2} m \quad . \qquad (3\text{-}18)$$

Therefore, the frequency is the inverse of the time interval between adjacent peaks. Experimentally, this method of measurement is easier than the previous method involving the tangential points.

Since Eq. (3-13) was derived from the linearized equation (3-2), it applies only to small angle oscillation. The half period is calculated exactly from Eq. (2-21) for the oscillation along the easy axis. The calculated half period is plotted as a function of oscillation angle with the applied field as a parameter in Fig. 3-6. The half period is shown rather than the period so that the frequency can be inspected even within a cycle. It can be seen that the half period is an increasing function of the angle. Nevertheless, it is within 4% of the final value if the oscillation angle is less than 57°. There, the convenient analytical expression (3-13) can be used to investigate the oscillation with high accuracy.

When the base line drifts or the oscillation is superposed on a slow flux change, an error exists in the measurement of period. Let the shift of the base line be

$$\delta(t) = At \quad , \qquad (3\text{-}19)$$

where A is a drift of the base line per sec. A typical damped oscil-

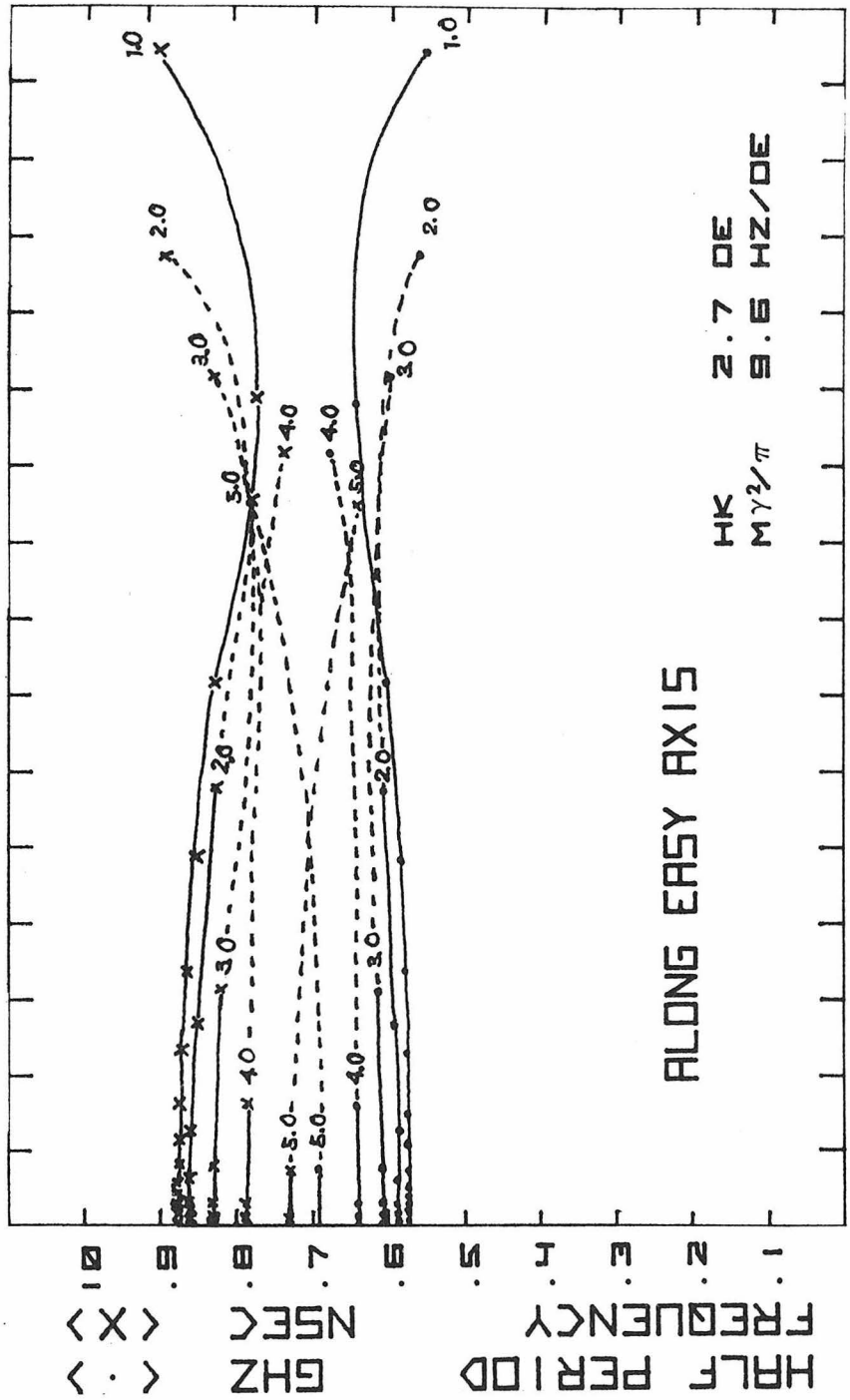

FIG.3-6 CALCULATED HALF PERIOD AS A FUNCTION OF OSILLATION ANGLE

lation superimposed on this drift is shown in Fig. 3-7 for A = -0.2 δ_o, 0, and +0.2 δ_o ($nsec^{-1}$). The peak positions of the oscillations without the drift are shown by vertical dotted lines. The peak positions of the oscillation with the drift are given by

$$\sin \omega t = \frac{A}{2h\delta_o\sqrt{\lambda^2 + f^2}} e^{2\pi\lambda t} \quad , \qquad (3\text{-}20)$$

and are shown by arrows. When the drift is positive, the period measured between adjacent minimum points (T_1) is shorter than without the drift; or, between adjacent maximum points, it is longer. The peak position of the oscillation with the negative drift shows a similar shift but in opposite direction.

The relative change of the period due to the drift can be calculated as a function of the ratio of the drift rate to the oscillation peak value. The resultant curve is shown in Fig. 3-8 for f = 1 GHz and $\lambda = 2 \times 10^8$ Hz. The curve shows the compensation to be used for the period measurement. For example, the period T measured on the curve C of Fig. 3-5 contains a 16% relative change at time $t_1 = 3$.

3.2.1.3 Measurement of Damping Parameter

The damping parameter for the free oscillation can be obtained from its decay time. The envelope of the oscillation can be expressed as;

$$\delta_e(t) = \pm\delta_o e^{-2\pi\lambda t} \quad , \qquad (3\text{-}14)$$

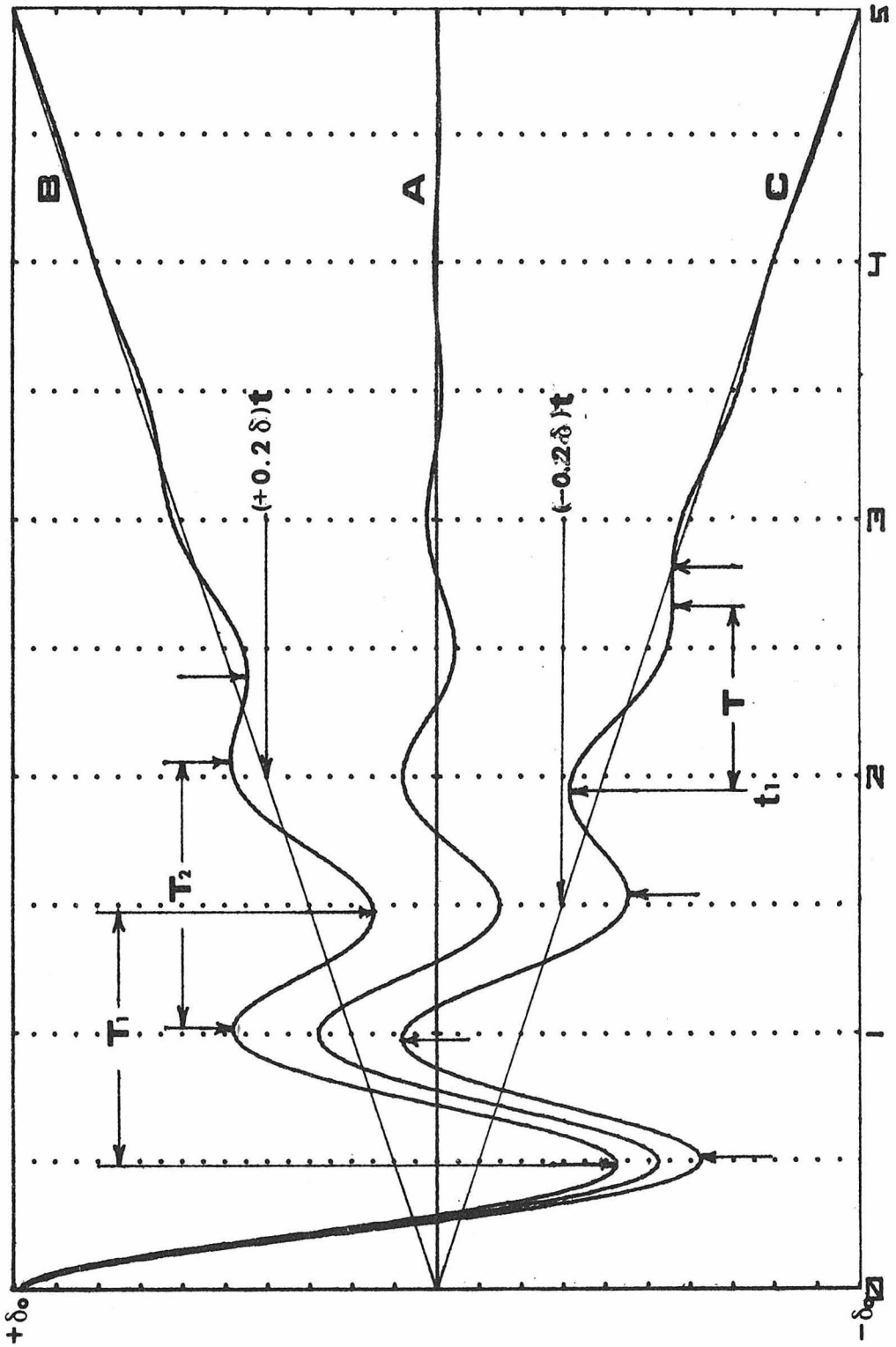

FIG. 3-7 DAMPED FREE OSCILLATION WITH BASE LINE DRIFT

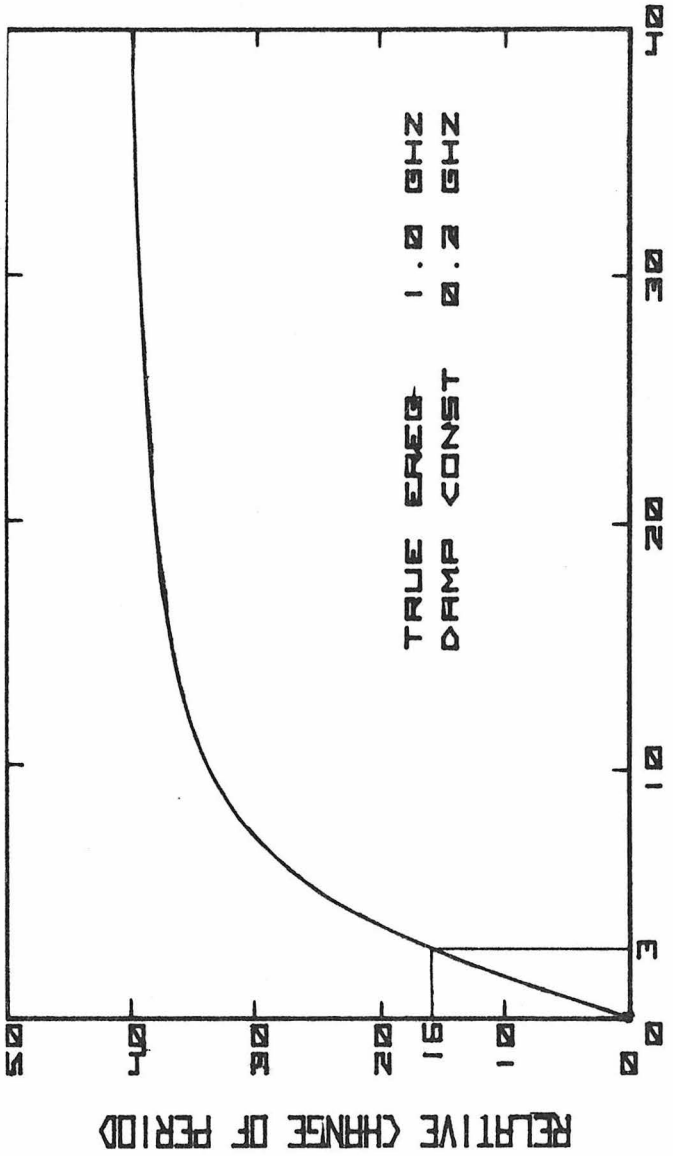

FIG.3-8 PERIOD CHANGE
DUE TO BASE LINE DRIFT

or in an experimentally useful form;

$$\log|\delta_e(t)| = \log \delta_o - 2\pi\lambda t \ (\log e) \quad . \quad (3\text{-}21)$$

The damping constant is proportional to the slope of the line expressed by this equation. Fortunately, the calculation of the damping parameter is not sensitive to the existence of base line drift, since the amplitude of oscillation is obtained from the difference of the upper and lower envelope.

3.2.2 The In-plane Resonance

Ferromagnetic resonance excited in the film plane can be observed by two methods. One is to detect the microwave power absorbed by the film. The other is to detect the transverse flux change caused by the microwave using a pick-up loop. The power generated at the loop is proportional to the power absorption (Appendix II) so that these methods are equivalent. In both methods, a stripline is used to apply a uniform microwave field over the film placed between the flat strip conductor and the ground plane. A uniform constant field is applied perpendicular to this microwave field. For the resonance along the easy or the hard axis, the respective film anisotropy axis is aligned along the static field. In the power absorption method, the power transmitted through the stripline is measured as a function of the constant field. This transmitted power is the input power minus the power absorbed by the film. In the pick-up loop method, the same equipment is used as for the reversal experiment (Sec. 2.2.1); except that the pick-up loop is oriented to detect the flux change in

the direction along the microwave field. An additional loop is used to cancel the voltage induced by the microwave field. For convenience of measurement, the derivative of the resonance curve can be used in both methods by modulating the constant field with an alternating field and using a lock-in amplifier. This allows the resonance half-power linewidth to be measured as $\sqrt{3}$ times the field separation between the peaks of the derivative curve. The damping parameter λ can then be calculated from this linewidth using Eq. (3-12).

3.3 Results and Discussion

3.3.1 Oscillation Frequency

Damped free oscillation was observed at the completion of 180° flux reversal in Ni-Fe thin films both along the easy and hard axis of the film. Typical transverse flux waveforms for easy axis reversals are shown in Fig. 3-9 with applied field pulse as a parameter. The sample (18-19-4) has H_k = 2.7 Oe, H_c = 2.2 Oe, and α_{90} = 3.5°. A constant field of 0.1 H_k was always applied along the hard axis. The initial direction of the magnetization is 5.7° from the easy axis. The flux level corresponding to the initial angle is shown by a short bar as in Fig. 3-9. Magnetization rotation is theoretically expected to be oscillatory for all fields larger than the reversal threshold of 0.7 H_k. Curve A shows the waveform for an applied field of 0.96 H_k. It can be seen that no oscillation is evident. Oscillation can just be observed with the field of 1.2 H_k as shown by the curve B. The oscillation does not occur around the final level of the waveform as expected but starts to oscillate before the transverse flux reaches the final level. The oscillation becomes clear as the field is increased to 1.4 H_k and 2.8 H_k. The oscillation is observed around the final level for the field of 2.8 H_k as shown by the curve D. Here the oscillation can be clearly seen and the amplitude decreases exponentially with time as predicted by the coherent rotation theory.

The frequency of the damped free oscillation was observed to increase as the magnetic field pulse increased. Two transverse flux waveforms for different values of the applied field are shown in Fig. 3-10. Curve A is the waveform for an applied field of 2.8 H_k and

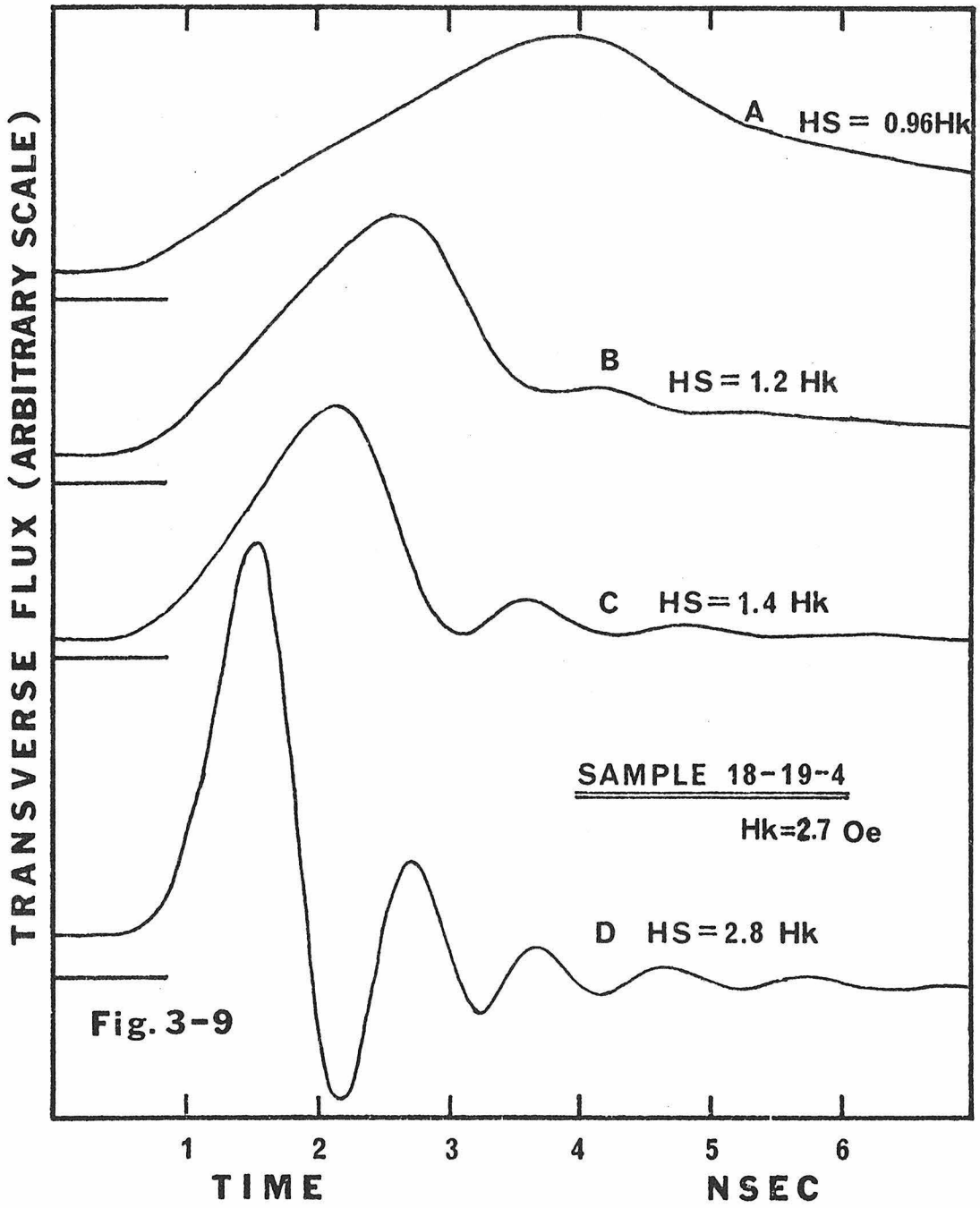
TRANSVERSE FLUX (ARBITRARY SCALE)
A HS = 0.96Hk
B HS = 1.2 Hk
C HS = 1.4 Hk
SAMPLE 18-19-4
Hk=2.7 Oe
D HS = 2.8 Hk
1
2
3
4
5
6
TIME
NSEC

Fig. 3-9

curve B is the waveform for an applied field of 3.9 H_k. Both curves show clear oscillation lasting for several cycles. It can be seen that the oscillation period, T_a, in curve A is longer than the period, T_b, shown by curve B; the frequency of the damped free oscillation increases as the applied field increases.

The transverse flux waveform was observed also for reversal along the hard axis. Typical examples of hard to hard axis transverse flux waveforms are shown in Fig. 3-11 with magnetic field pulse as a parameter. Curves A, B and C are for the field pulse of 2.9 H_k, 3.1 H_k and 3.5 H_k, respectively. A constant magnetic field of 0.04 H_k is always applied along the easy axis. The initial direction of the magnetization is 16.2° from the hard axis. The flux level corresponding to this initial angle is shown by a short bar. The calculated reversal threshold is 1.2 H_k since the constant field of 1.2 H_k is always applied along the hard axis. All reversals along the hard axis are expected to be oscillatory. Curve A shows an oscillation superposed on another slowly decreasing flux component. This same effect can be seen for the reversals along the easy axis shown by curves B and C in Fig. 3-9. With larger fields, the oscillation can be clearly seen around the final level of the waveform for several cycles. The amplitude of the oscillation decreases exponentially with time.

The frequency of the oscillation for reversal along the hard axis is lower than that for reversal along the easy axis when the same magnetic field is applied. This difference can be seen in Fig. 3-12. Two transverse flux waveforms are shown in this figure for the

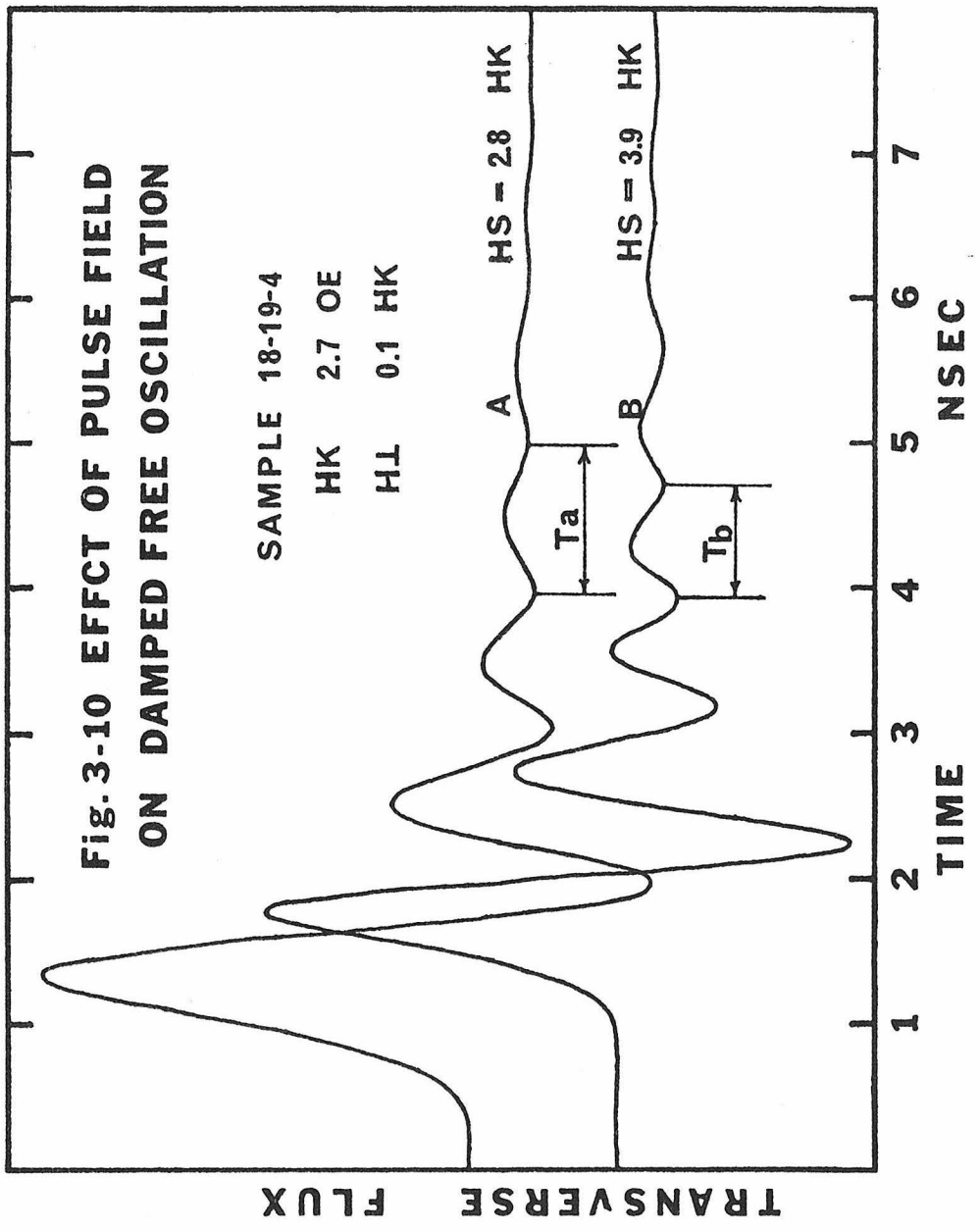
Fig. 3-10 EFFCT OF PULSE FIELD
ON DAMPED FREE OSCILLATION
SAMPLE 18-19-4
HK 2.7 OE
H⊥ 0.1 HK
A
HS = 2.8 HK
B
HS = 3.9 HK
Ta
Tb
TRANSVERSE FLUX
TIME
NSEC
1
2
3
4
5
6
7

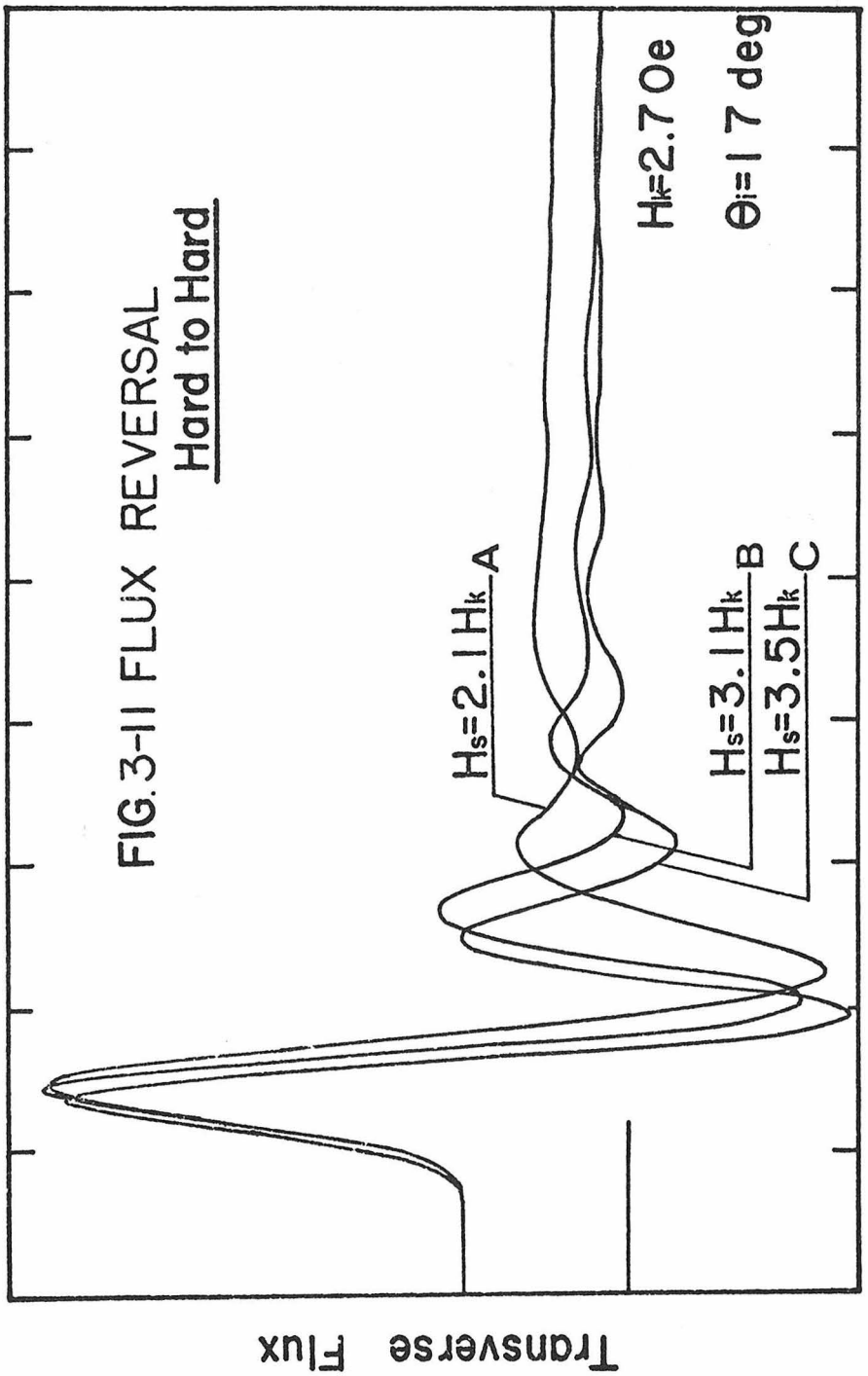
FIG. 3-11 FLUX REVERSAL
Hard to Hard
Hs=2.1Hk A
Hs=3.1Hk B
Hs=3.5Hk C
Hk=2.7 Oe
θi=17 deg
Transverse Flux
Time nsec/div

reversal along the respective axis. The applied field pulse is 2.5 H_k for both cases, and the bias field of 0.1 H_k is applied normally to this field. Both curves show a clear oscillation at the completion of the reversal. The waveform for the easy axis shows a higher frequency than that for the hard axis. This difference is the effect of the uniaxial anisotropy. The motion of the magnetization, near the easy axis, is affected by the anisotropy in such a way that an effective field of H_k exists along this axis. Therefore, the total effective field along the easy axis is the sum of the externally applied field H_s and this anisotropy field H_k, i.e., $H_s + H_k$. On the other hand, the motion of the magnetization, near the hard axis, is affected by the anisotropy in such a way that an effective field of $-H_k$ exists along this axis. Therefore, the total effective field along the hard axis is the difference of the externally applied field and the anisotropy field, i.e., $H_s - H_k$. This difference in the total effective field accounts for the different frequency of oscillation along the easy and hard axis.

Oscillation at the same frequency can be observed for flux reversal along both the easy and hard axis if the total effective field is the same in each case. An example is shown in Fig. 3-13. For reversal along the easy axis, the sum of the applied field and the anisotropy field is 2.4 H_k; and for reversal along the hard axis, the difference of these fields is 2.5 H_k. It can be seen that the frequencies of these reversals are practically identical.

The frequency of the damped free oscillation is not constant but depends on where in the oscillation the frequency is measured. A

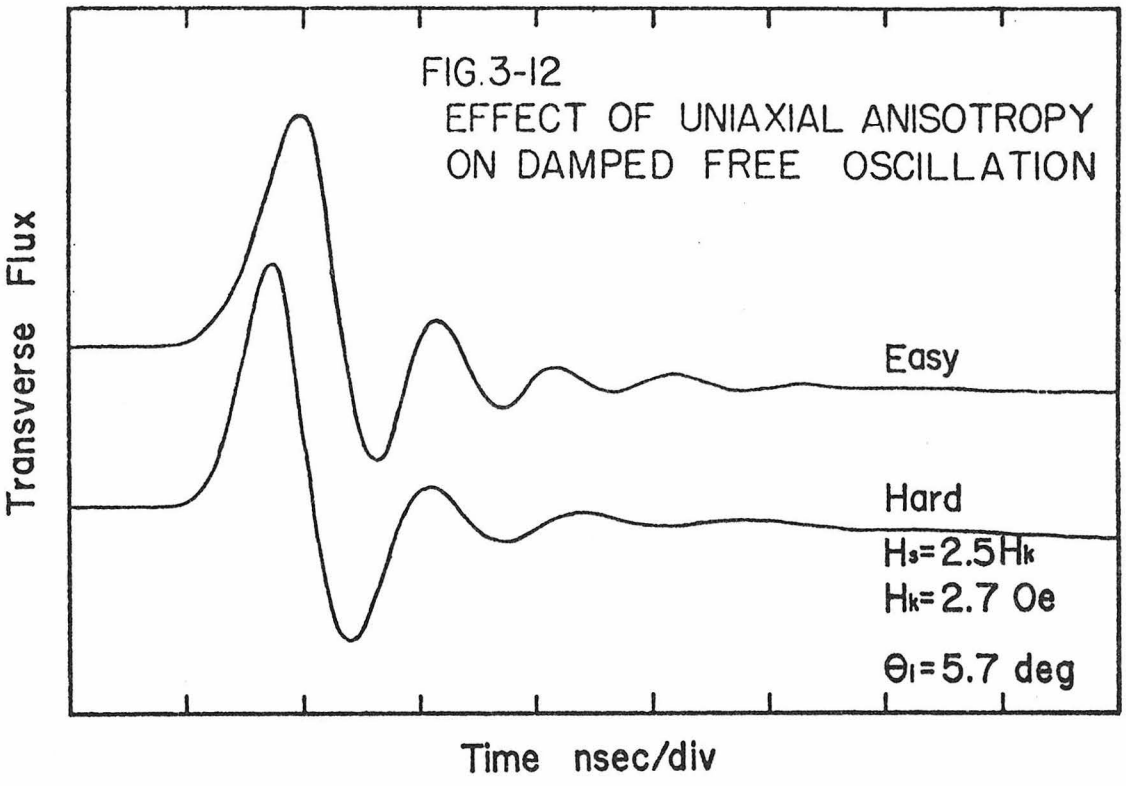

FIG.3-12
EFFECT OF UNIAXIAL ANISOTROPY
ON DAMPED FREE OSCILLATION

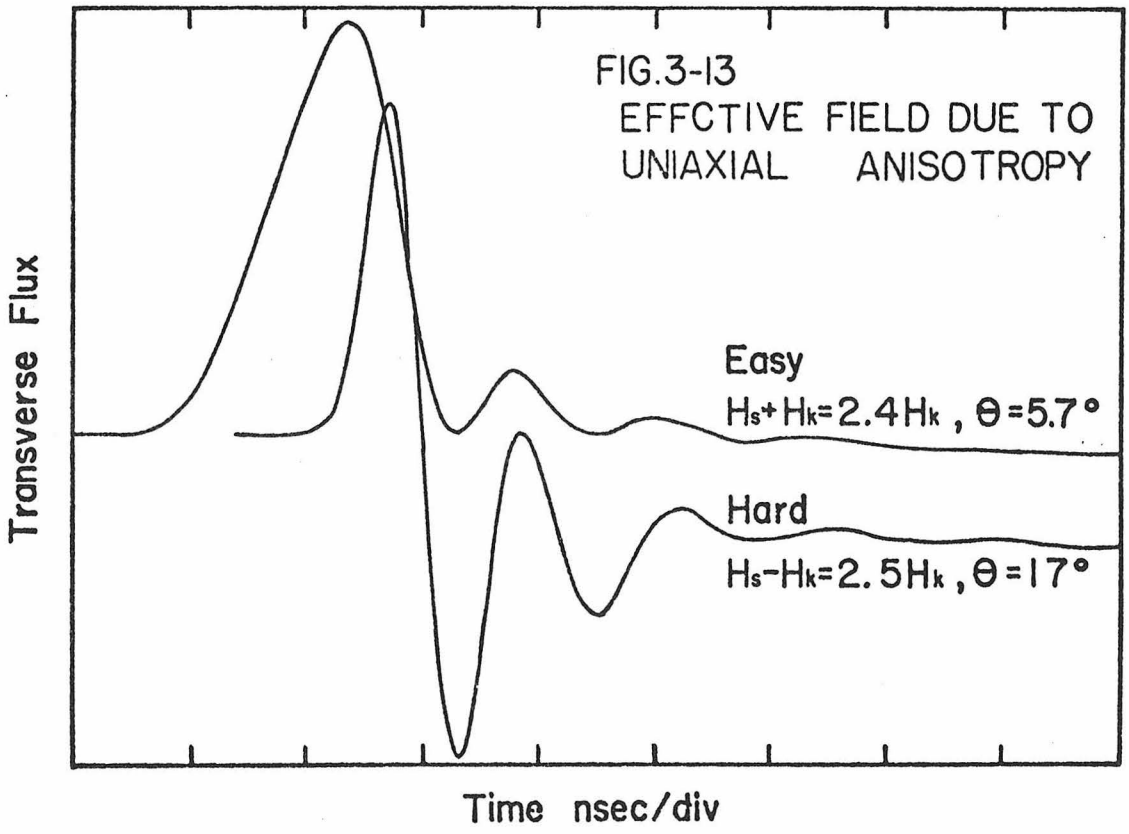

FIG.3-13
EFFCTIVE FIELD DUE TO
UNIAXIAL ANISOTROPY

frequency obtained from the early part of the oscillation is higher than that measured on a later part of the oscillation. A typical example, for reversal along the easy axis, is shown for the sample 18-19-4 in Fig. 3-14. A magnetic field pulse of 2.75 H_k is applied along the easy axis and a bias field of 0.1 H_k is applied along the hard axis. The flux rotates from its initial angle of 5.7° to its final angle 179.8°. Several cycles of oscillation can be seen around the final flux level. Nine periods measured along the oscillation are indicated by numbers 0,1,2 .... The frequency calculated from each period is shown in Fig. 3-15 in order of these period numbers. The experimental error is shown by short horizontal lines attached to the data points. It can be seen that the frequency increases during the periods 1 ~ 3 and then decreases during the following periods. The frequency reaches a final value, which is the same as the resonance frequency corresponding to that effective field. The frequency approaches a final value of 0.95 GHz during the latter part of the oscillation. The data points scatter around this fixed value about 13% due to a slight change of the base line of oscillation. To see if the nonlinearity of the flux reversal accounts for this change, the frequency change calculated from Eq. (2-21) is also shown by the dotted line in Fig. 3-15. It can be seen that the frequency is lower in the early part of the oscillation, where the oscillation angle is large. The frequency gradually approached the same final value as the oscillation proceeds. The change observed experimentally is quite different from this change theoretically expected and indicates some other mechanism.

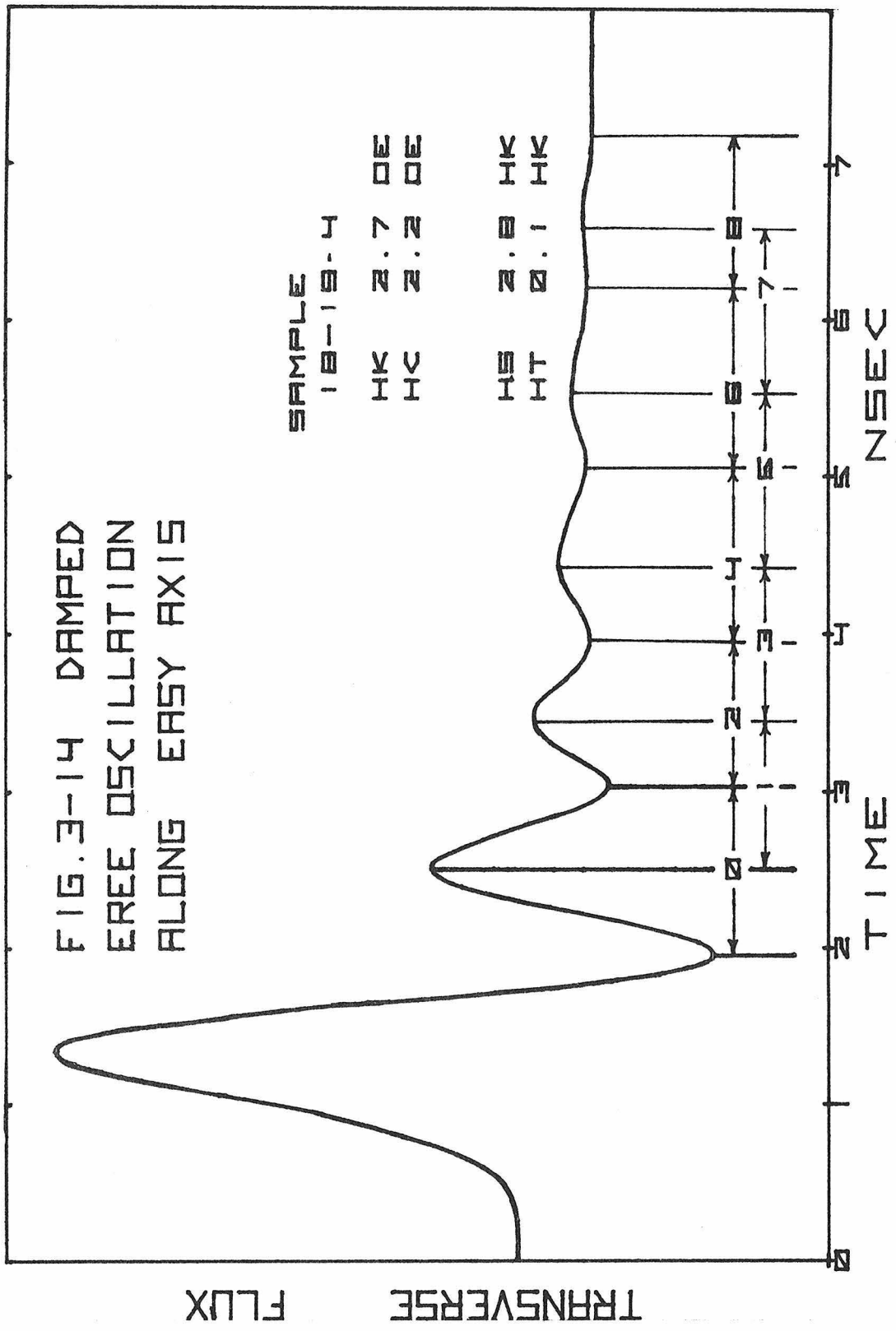

FIG. 3-14 DAMPED FREE OSCILLATION ALONG EASY AXIS

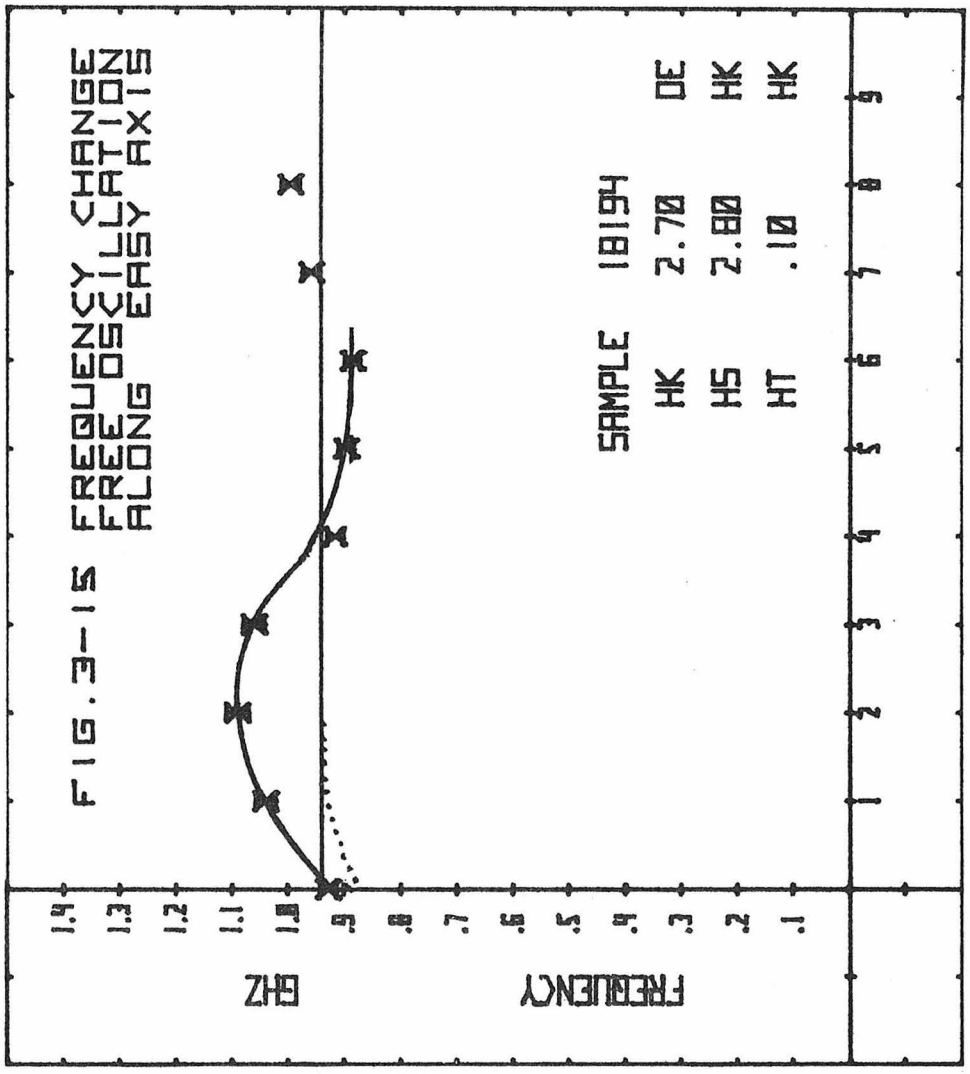
FIG.3-15 FREQUENCY CHANGE
FREE OSCILLATION
ALONG EASY AXIS
SAMPLE 18194
HK 2.70 OE
HS 2.80 HK
HT .10 HK
FREQUENCY
GHZ

A similar frequency change is also observed after flux reversal along the hard axis. A typical example is shown in Fig. 3-16. A total magnetic field of 3.17 H_k is applied along the hard axis and a bias field of 0.04 H_k is applied along the easy axis. The flux rotates from its initial angle of 7.8° from the hard axis to its final angle of 179°. Several cycles of oscillation can be seen around the final flux level. Seven periods measured on this oscillation are indicated by the numbers 0,1,2.... The frequency obtained is shown by the solid line in Fig. 3-17, in order of these periods. The experimental error is shown by short horizontal lines attached to the data points. A frequency change similar to that observed for oscillation along the easy axis can be seen. The frequency increases in the early part of oscillation and then decreases to a final value. The average of the last three data points is 0.71 GHz; this is equal to the corresponding resonance frequency 0.71 GHz. The frequency change calculated from Eq. (2-21) is also shown in Fig. 3-17 by the dotted line. The calculated frequency is almost constant during the oscillation. A slight increase is almost constant during the oscillation. A slight increase of about 0.6% can be seen at the beginning. This change is quite different from that experimentally observed. The observed frequency change suggests some other mechanism.

For the same sample, the square of frequency as a function of pulse field is shown in Fig. 3-18. The frequency was obtained from the latter part of the oscillation. A least square straight line was drawn through the data points. For the oscillation along the easy axis, it has a slope of 0.085 GHz^2/Oe and a field axis intersection of

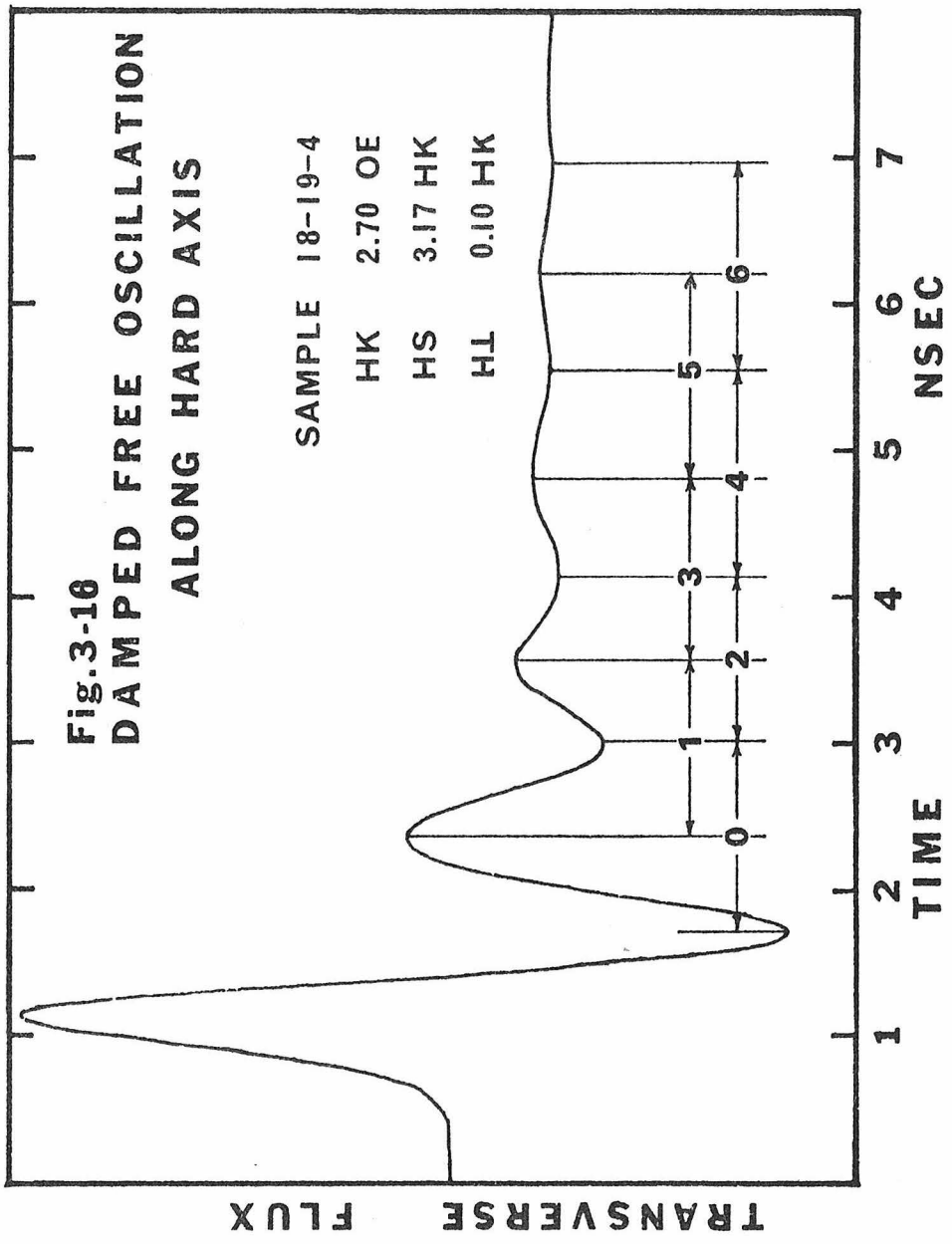
Fig.3-16
DAMPED FREE OSCILLATION
ALONG HARD AXIS
SAMPLE 18-19-4
HK 2.70 OE
HS 3.17 HK
HL 0.10 HK
0
1
2
3
4
5
6
TRANSVERSE FLUX
1
2
3
4
5
6
7
TIME
NSEC

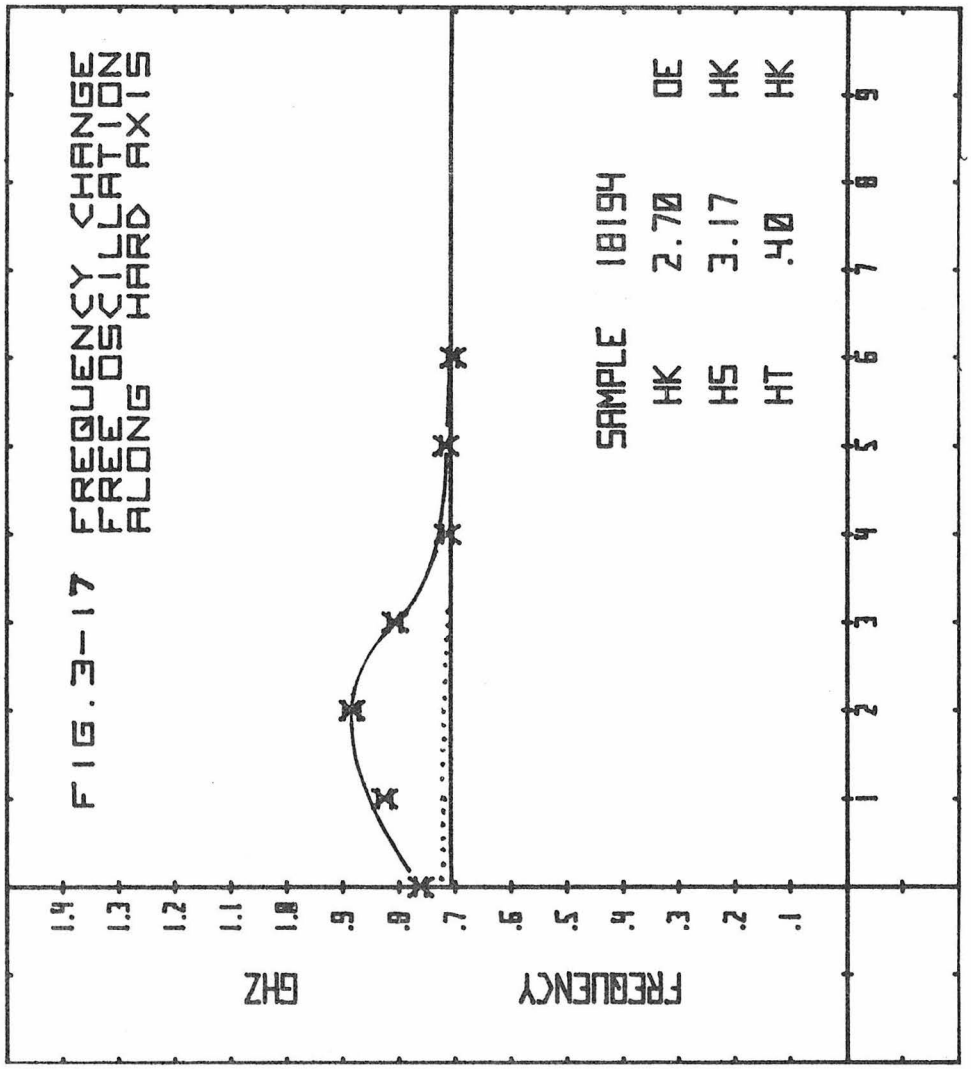
FIG. 3-17 FREQUENCY CHANGE
FREE OSCILLATION
ALONG HARD AXIS
SAMPLE 18154
HK 2.70 OE
HS 3.17 HK
HT .40 HK
FREQUENCY
GHZ
1.4
1.3
1.2
1.1
1.0
.9
.8
.7
.6
.5
.4
.3
.2
.1
1
2
3
4
5
6
7
8
9

$-1.15\ H_k$. For the hard axis, it has a slope of 0.085 GHz^2/Oe and an intersection of $+0.81\ H_k$. According to Eqs. (3-4) and (3-6), these straight lines should have the same slope $M\gamma^2/\pi$; and the respective intersections should be at $-H_k + \frac{\pi}{M\gamma^2}\lambda^2 (\sim -H_k)$ and $+H_k + \frac{\pi}{M\gamma^2}\lambda$ $(\sim +H_k)$. These slopes obtained experimentally agree within 5%. The intersectional values for the easy and hard axis oscillation is within 15 and 19% of H_k, respectively.

Similar f^2 vs. Hs curves were obtained for in-plane resonance and are shown in Fig. 3-19. The curves are straight lines as predicted by Eq. (3-10). The respective slopes are 0.087 GHz^2/Oe and 0.085 GHz^2/Oe; and the respective field axis intersections are $-1.02\ H_k$ and $+0.77\ H_k$. The slope of the f^2 vs. Hs curves for resonance and free oscillation agree within 2%. Their intersections agree within 12%. These agreements are quite good considering the difficulties of the frequency measurements associated with the free oscillation.

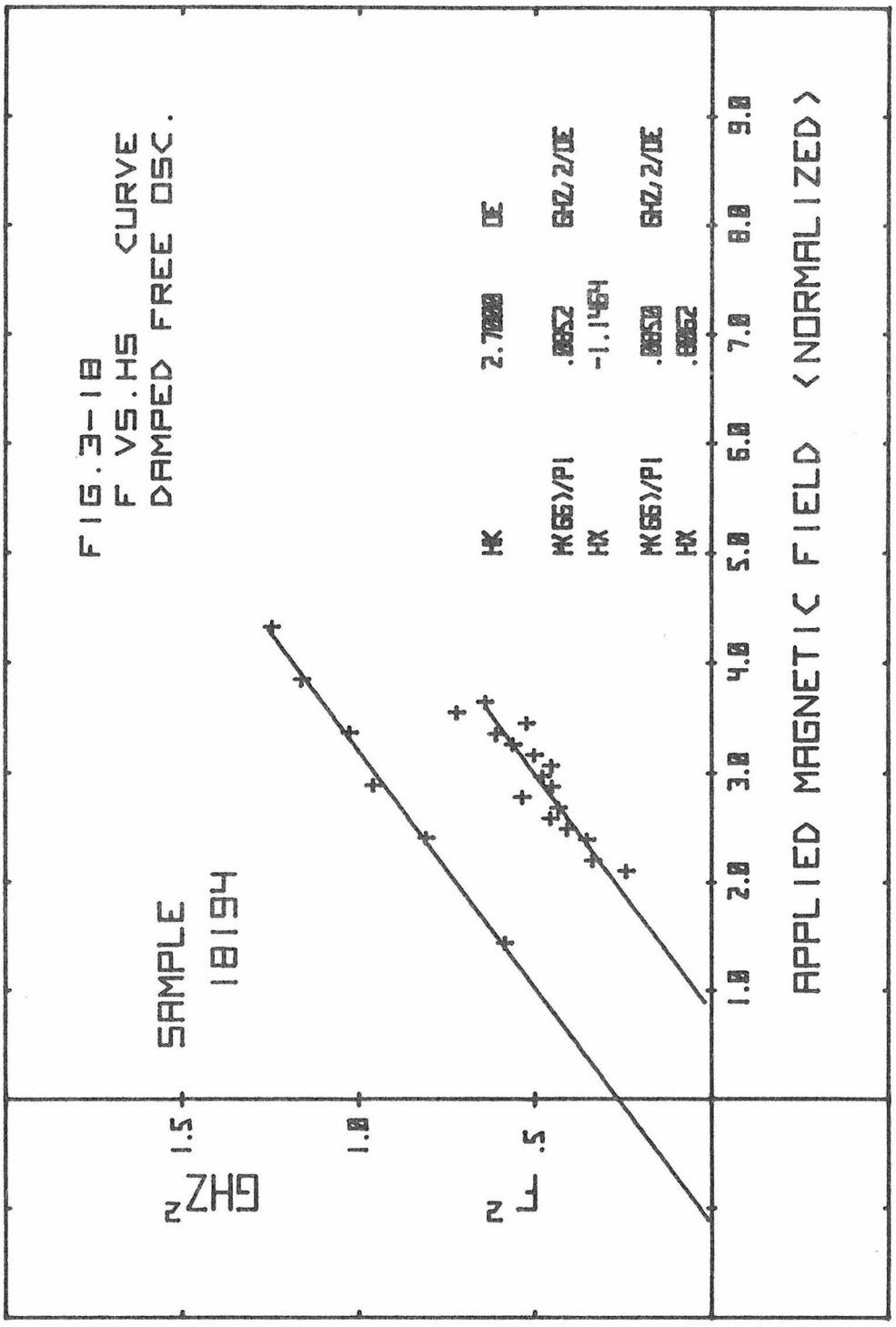
FIG.3-18
F VS.HS CURVE
DAMPED FREE OSC.
SAMPLE
18194
GHZ²
1.5
1.0
.5
1.0
2.0
3.0
4.0
5.0
6.0
7.0
8.0
9.0
APPLIED MAGNETIC FIELD <NORMALIZED>

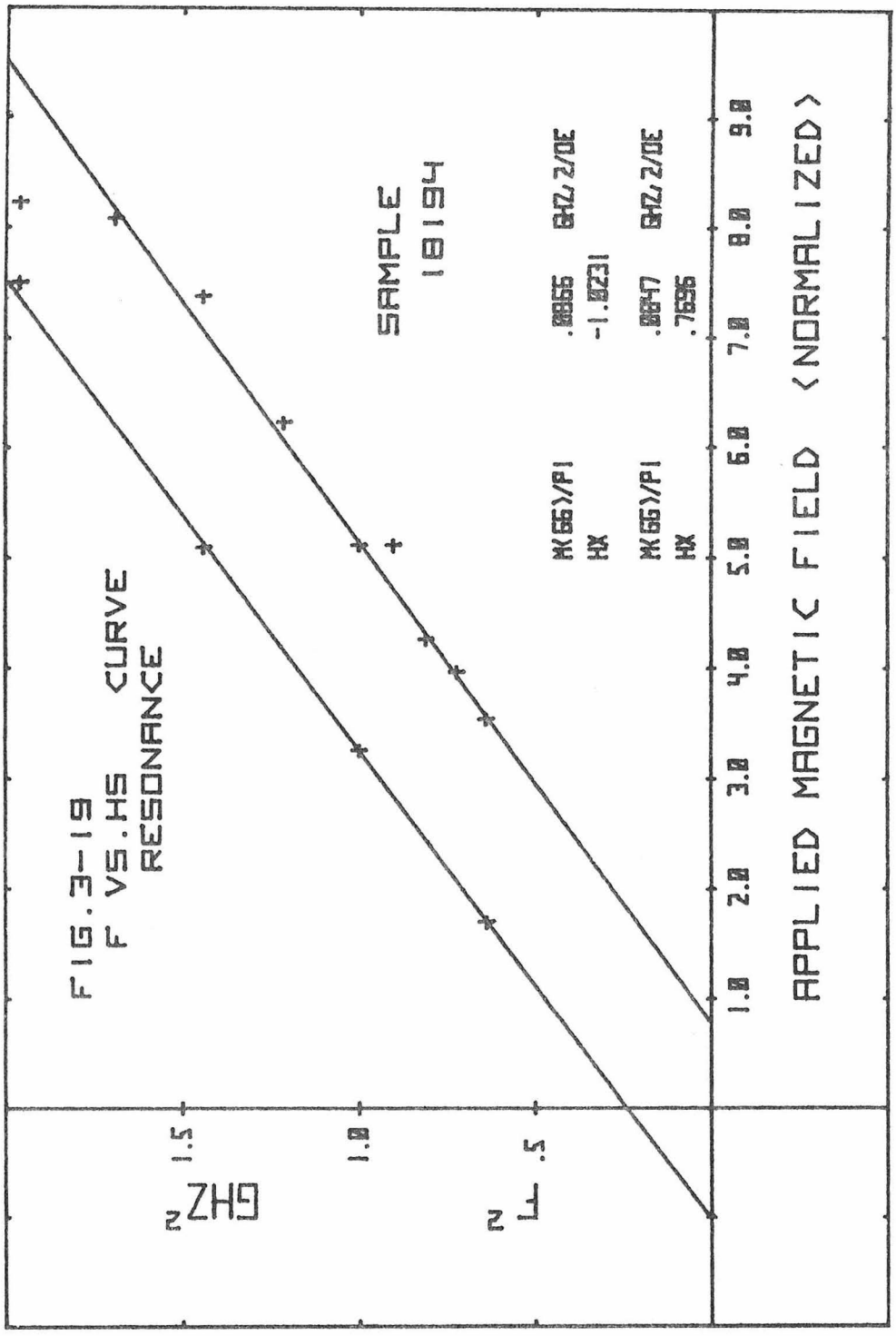
FIG.3-19
F VS.HS CURVE
RESONANCE
SAMPLE
18194
MK(66)/PI .0865 GHZ/KOE
HK -1.0231
MK(66)/PI .0847 GHZ/KOE
HK .7696
GHZ
F
1.0
1.5
.5
1.0
2.0
3.0
4.0
5.0
6.0
7.0
8.0
9.0
APPLIED MAGNETIC FIELD <NORMALIZED>

3.3.2 Damping Parameter

The damping parameter, λ, was obtained from the decay time of the damped free oscillation using Eq. (3-14). Typical results are shown in Fig. 3-20 a and b. In Fig. 3-20a, a transverse flux waveform is shown for the reversal along the easy axis of sample 18-19-4. A magnetic field pulse of 2.89 H_k is applied along the easy axis; and a bias field of 0.1 H_k is applied along the hard axis. Oscillation can be clearly seen around the final level of the waveform. The envelope of this oscillation is shown by dotted lines. In Fig. 3-20b, the logarithm of the oscillation amplitude is plotted as a function of time. The damping parameter obtained from the slope of this line is 0.14 GHz. This value agrees with the one obtained from resonance within 7%.

Damping parameter was obtained even when the oscillation was superposed on a slow flux change. Two kinds of damping parameter were obtained separately for the oscillation and the slow flux change. A typical example is shown in Fig. 3-21a and b. In Fig. 3-21a, a transverse flux waveform is shown for the reversal along the easy axis. For this case, the applied field pulse is 1.2 H_k and the bias field is 0.1 H_k. Oscillation can be seen for two cycles as the flux approaches its final level. The envelope of this oscillation is shown by dotted lines. In Fig. 3-21b, two kinds of semi-logarithmic plottings are shown. One is the oscillation amplitude as a function of time. The other is the average value between the envelopes as a function of time. Both show straight lines; and their slopes are different. The damping parameter obtained from the amplitude decay is

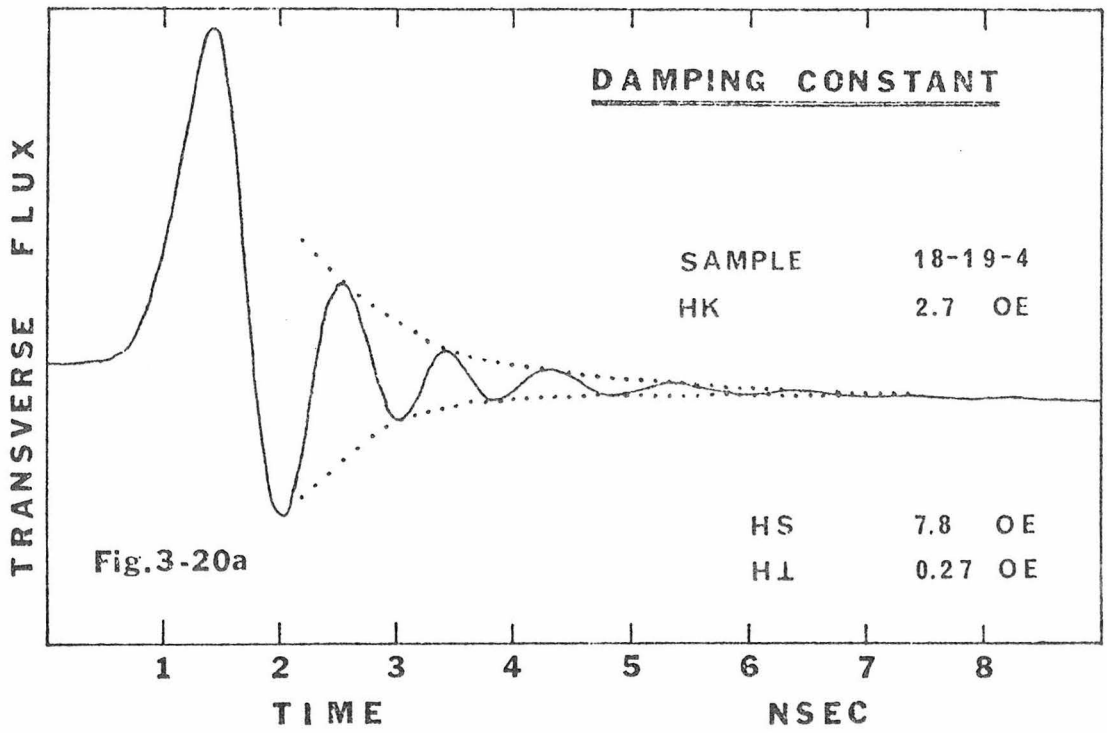

Fig.3-20a

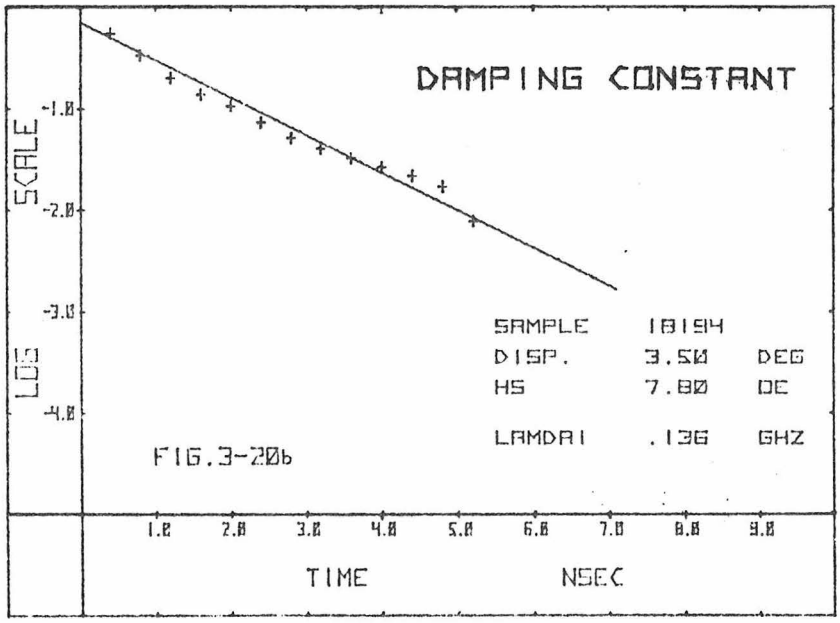

FIG.3-20b

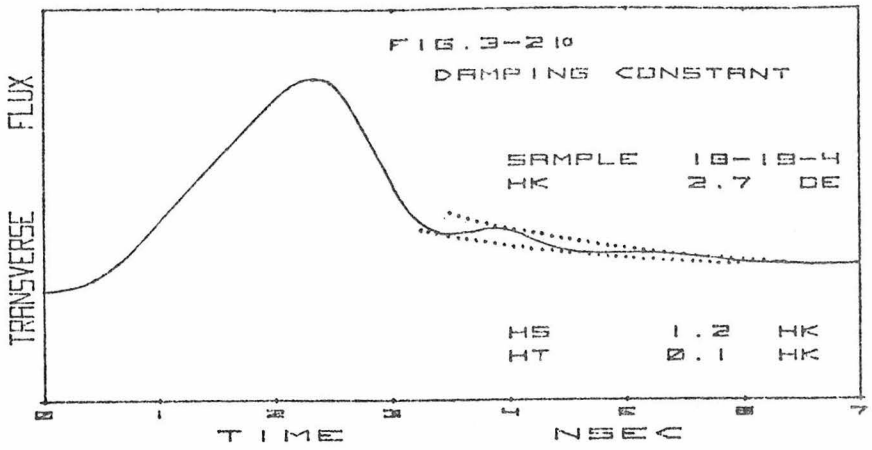
FIG. 3-21a
DAMPING CONSTANT
SAMPLE 18-19-4
HK 2.7 DE
HS 1.2 HK
HT 0.1 HK
TRANSVERSE FLUX
TIME NSEC

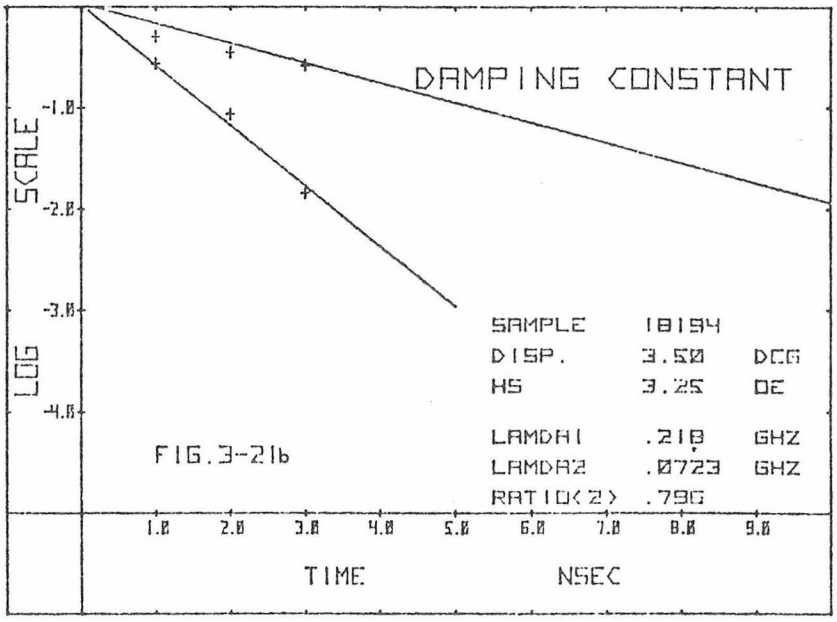
DAMPING CONSTANT
SAMPLE 18194
DISP. 3.50 DCG
HS 3.25 DE
LAMDA1 .218 GHZ
LAMDA2 .0723 GHZ
RATIO(2) .796
FIG. 3-21b
LOG SCALE
-1.0
-2.0
-3.0
-4.0
1.0 2.0 3.0 4.0 5.0 6.0 7.0 8.0 9.0
TIME NSEC

0.22 GHz. This value is 47% larger than the corresponding value obtained from resonance. When an oscillation is superposed on another slow flux change, its decay time should be independent of this change. Therefore, the difference of 47% is not due to the slow flux change. It can be shown that the frequency response of the pick-up loop does not effect the measurement of damping parameter; but its effect appears only as a slow change of the waveform (Sec. 2.2.4.4). Therefore, the difference of the damping parameters is not due to the effect of the frequency response, either. The decay time obtained for the slow flux change is 2.2 nsec ($=1/2\pi\lambda_2$). The decay time calculated using the pick-up loop's frequency response is 0.7 nsec. Apparently, the response is not an effective cause for the slow flux change.

The damping parameter for the free oscillation is plotted as a function of frequency in Fig. 3-22. The damping parameter is a decreasing function of frequency. The decrease is more or less linear for the frequencies higher than 0.8 GHz. At about 0.7 GHz, a rapid change can be seen. The average of damping parameter is 0.13 GHz for the frequency higher than 0.95 GHz. The damping parameter was also calculated from the half-power linewidth of the in-plane resonance curve. The resonance was observed along the easy axis. The damping parameter was plotted as a function of frequency also in Fig. 3-22. The damping parameter for the in-plane resonance seems to be constant around 0.15 GHz. The damping parameter for the resonance and free oscillation agree within 15%. The rapid increase of the damping parameter at 0.7 GHz is due to the noncoherency of reversal, since it is about this reversal speed that the observed waveform starts to

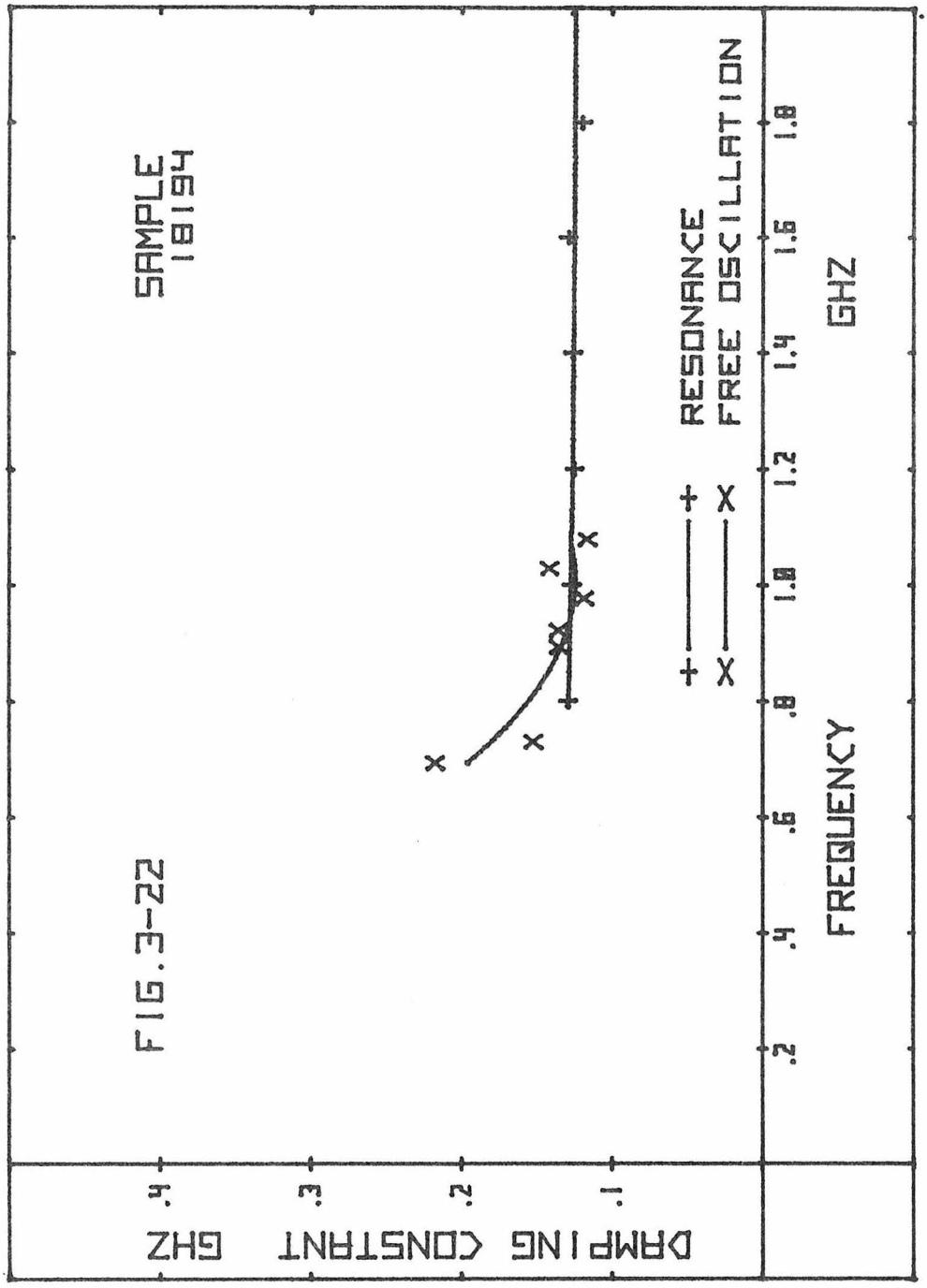
SAMPLE
18194
FIG.3-22
DAMPING CONSTANT GHZ
.4
.3
.2
.1
.2
.4
.6
.8
1.0
1.2
1.4
1.6
1.8
FREQUENCY
GHZ
RESONANCE
FREE OSCILLATION

deviate from that expected from the coherent rotation theory.

3.4 Summary

Oscillation has been clearly observed at the completion of 180° flux reversal along both the easy and, for the first time, hard axes of the film. This oscillation has been studied in detail for the first time. Oscillation along both axis decays exponentially as the flux approaches a new equilibrium. As the oscillation angle reduced, the oscillation frequency approached a constant value. This value was equal to the corresponding resonance frequency. The damping parameter, λ, was obtained from the decay time of the oscillation. It was found that the damping is equal to that for the corresponding resonance if the frequency is high. This agreement between damped oscillation and resonance is well described on the basis of the coherent rotation theory. It is concluded that the oscillation is a free oscillation around the new equilibrium. It was also found that, for large oscillation angle, the frequency is higher than the corresponding resonance frequency. For a slow reversal, the damping parameter is found to be larger than that obtained from the corresponding resonance. These differences cannot be explained by the coherent rotation theory.

APPENDIX

In-Plane Resonance Experiment by Pick-Up Loop Method and Power Absorption Method

A continuous oscillation of magnetization around a constant magnetic field can be excited by a microwave magnetic field. (Sec. 3.1.2.) When the microwave field of

$$h(t) = h_o \cos \omega t \quad , \qquad \text{(A-1)}$$

and the constant field of, H_s, are applied to the magnetization, M, the oscillation is;

$$\delta = \delta_o \cos(\omega t - \alpha) \quad , \qquad \text{(A-2)}$$

where

$$\delta_o = \frac{4\pi\gamma^2 M}{\left[(\omega_o^2 - \omega^2)^2 + (4\pi\lambda\omega)^2\right]^{1/2}} h_o \quad , \qquad \text{(A-3)}$$

$$\alpha = \tan^{-1} \frac{4\pi\lambda\omega}{\omega_o^2 - \omega^2} \quad , \qquad \text{(A-4)}$$

$$\omega_o^2 = 4\pi\lambda^2 M(H_s \pm H_k) \quad , \qquad \text{(A-5)}$$

and λ is the damping constant and γ is the gyromagnetic ratio and + or - corresponds to the constant field applied along the easy or hard axis, respectively.

The microwave power is generated in the pick-up loop due to the

magnetic flux change. The power is:

$$P_{\ell} = \frac{1}{T} \left[\frac{d(KM\delta)}{dt} \right]^2 / Z_o dt \quad (T = \frac{2\pi}{\omega})$$

$$= \frac{C^2 H_o{}^2 M^2}{2Z_o} \cdot \frac{(4\pi\gamma^2 M\omega)^2}{(\omega_o{}^2 - \omega^2)^2 + (4\pi\lambda\omega)^2} \quad , \qquad \text{(A-6)}$$

where Z_o is the characteristic impedance of the transmission line and C is the coupling constant between the magnetic flux and the pick-up loop. The power absorbed in the film is:

$$P_a = \frac{1}{T} \left(-\vec{M} \cdot \vec{dh}\right)$$

$$= -\frac{1}{T} \int M\delta_o \cos(\omega t - \alpha) \cdot -h_o \sin \omega t \, \omega dt$$

$$= \frac{1}{2} M\delta_o h_o \omega \sin \alpha$$

$$= \frac{1}{2} \frac{h_o{}^2 \lambda}{\gamma^2} \frac{(4\pi\gamma^2 M\omega)^2}{(\omega_o{}^2 - \omega^2)^2 + (4\pi\lambda\omega)^2} \quad . \qquad \text{(A-7)}$$

Comparing Eqs. (A-12) and (A-13), the generated power and the absorbed power can be related to each other as,

$$P_{\ell} = \frac{C^2 M^2 \gamma^2}{\lambda Z_o} P_a \quad . \qquad \text{(A-8)}$$

The generated power is proportional to the absorbed power, since $C^2M^2\gamma^2/\lambda Z_o$ is constant for a given thin film. Therefore, the observation of resonance by pick-up loop method is equivalent to that by power absorption method.

REFERENCES

F. Bloch, Phys. Rev. 70, 460 (1946).

N. Bloembergen, Phys. Rev. 78, 572 (1950).

M. S. Blois, Jr., J. Appl. Phys. 26, 975 (1955).

J. T. L. Brown and C. E. Pollard, Electrical Engng. 66, 1106 (1947).

H. B. Callen, J. Phys. Chem. Solids 4, 256 (1958).

S. B. Cohn, IRE Trans. MTT-2, No. 2, 52 (1954).

R. L. Conger and F. C. Essig, Phys. Rev. 104, 915 (1956).

T. S. Crowther, MIT Lincoln Lab Report 51-2 (1959).

W. Dietrich, W. E. Proebster and P. Wolf, IBM Journal 4, 189 (1960).

A. L. Frumkin, Soviet Phys. - Solid State 14, 1373 (1972).

K. Fuchs, Proc. Camb. Phil. Soc. 34, 100 (1938).

R. L. Garwin, Rev. Sci. Instrum. 21, 903 (1950).

T. L. Gilbert, Phys. Rev. 100, 1243 (1955).

K. J. Harte, MIT Lincoln Lab. Tech. Report No. 364 (1964)

K. J. Harte, J. Appl. Phys. 36, 960 (1965).

K. J. Harte, J. Appl. Phys. 38, 1341 (1967).

T. E. Hasty and L. J. Boudreaux, J. Appl. Phys. 32, 1807 (1961).

B. R. Hearn, J. Electronics and Control 16, 33 (1964).

F. B. Humphrey, J. Appl. Phys. 29, 284 (1958).

F. B. Humphrey and E. M. Gyorgy, J. Appl. Phys. 30, 935 (1959).

F. B. Humphrey, J. Appl. Phys. 38, 1520 (1967).

J. H. Hoper, IEEE Trans. on Mag. MAG-2, 566 (1966).

C. Kittel, Phys. Rev. 70, 965 (1946).

V. V. Kobelev, Fitz. Metal. Metalloved. 13, 467 (1962).

M. H. Kryder and F. B. Humphrey, Rev. Sci. Instrum. 40, 829 (1969).

M. H. Kryder and F. B. Humphrey, J. Appl. Phys. 40, 2469 (1969).

M. H. Kryder, "Flux Reversal in Ferromagnetic Thin Films" (Ph.D. Thesis, California Institute of Technology, 1970).

M. H. Kryder and F. B. Humphrey, J. Appl. Phys. 41, 1130 (1970).

M. H. Kryder and F. B. Humphrey, IEEE Trans. on Mag. MAG-7, 725 (1971).

L. D. Landau and E. M. Lifshitz, Phys. Z. Sowjet 8, 153 (1935).

A. F. Mayadas, J. F. Janak and A. Gangulee, J. Appl. Phys. 45, 2780 (1974).

C. D. Olson and A. V. Pohm, J. Appl. Phys. 29, 274 (1958).

Y. Sakurai, T. Kusuda, S. Konishi and S. Sugatani, IEEE Trans. on Mag. MAG-2, 570 (1966).

D. O. Smith, J. Appl. Phys. 29, 264 (1958).

D. O. Smith, Magnetism 3, Chapter 10, 506 (1963) (Academic Press, Ed. by G. T. Rado and H. Shul).

K. U. Stein, "Impulsummagnetisierung dunner Speicherschichten" (Dissertation, 1965).

K. U. Stein, Z. Angew. Phys. 18, 528 (1965).

K. U. Stein, Z. Angew. Phys. 20, 36 (1965).

K. U. Stein, Z. Angew. Phys. 20, 323 (1966).

Y. Suezawa and F. B. Humphrey, IEEE Trans. on Mag. MAG-8, 319 (1972).

H. Suhl. J. Phys. Chem. Solids 1, 209 (1957).

E. Tatsumoto, M. Nomura and M. Goto, Japan J. Appl. Phys. 2, 254 (1963).

R. V. Telesnin, E. N. Ilicheva, O. S. Kolotov, T. N. Nikitia, and V. A. Pogozhev, Phys. Stat. Sol. 14, 371 (1966).

C. H. Wilts, "Basic Problems in Thin Film Physics" 422 (1966). (Vandenhoeck and Ruprecht, Goettmgen, Ed. by R. Niedermayer and H. Mayer)

P. Wolf, Z. Physik 160, 310 (1960).

P. Wolf, J. Appl. Phys. 32, 95S (1961).